PALYNOSTRATIGRAPHIC CONSTRAINTS ON THE UPPER TANEZZUFT AND AKAKUS FORMATIONS IN THE GHADAMIS BASIN OF LIBYA

A Dissertation

by

MOHAMED N. IMSALEM

Submitted to the Graduate and Professional School of
Texas A&M University
in partial fulfillment of the requirements for the degree of

DOCTOR OF PHILOSOPHY

Chair of Committee,	Anne Raymond
Committee Members,	Mike Pope
	Christina Belanger
	Daniel Thornton
Head of Department,	Julie Newman

December 2021

Major Subject: Geology

ABSTRACT

The Ghadamis Basin in northwest Libya has generated a tremendous amount of oil and gas, sourced primarily from the lower Silurian anoxic black shales (aka 'hot shales') at the base of the Tanezzuft Formation. These dark grey, fissile shales contain substantial amounts of organic matter, as well as radioactive minerals. The Silurian System in the Ghadamis Basin consists of both the Tanezzuft and the overlying Akakus formations. Cores and outcrops are difficult to correlate across the basin but can be improved using chitinozoans biostratigraphy. Eighty samples from three wells that collectively cover the entire Silurian in the northeastern Ghadamis Basin yielded a diverse group of marine chitinozoans. Identified species include *Ancyrochitina ancyrea, A. fragilis, Sphaerochitin concava, S. sphaerocephala, Fungochitina spinifera, Pseudoclathrochitina carmenchui,* and *Eisenackitina cylindrica*. These species along with others could allow for robust age determination and enhanced stratigraphic correlation between the three wells, which can increase our understanding of the Ghadamis Basin's paleogeography and paleoenvironments.

DEDICATION

I would very much like to devote my dissertation to my mother and father, whom I love profoundly. As I finish my PhD, I feel so lucky to be with my mother, who has devoted her life to her children, especially me. I am eager for her to attend my graduation. My life would never be happier than if I could hear her voice praying and wishing the best for me. And now I'd like to talk about my father, the man behind the scenes. Words could never be enough to thank him for all of his support. He has always been there for me. Every day, I thank Allah for my father being there throughout my doctoral studies. My mother blessed me far beyond what I could ever have hoped for in a mother. She has taught me so much in my 37 years of life, and I appreciate every lesson offered to me. I'd like to dedicate my PhD to my family, my uncles, and my only child, Owais Mohamed N. Imsalem. To you all, I admire both your hard work and love; you've always trusted in me and pushed me to be a stronger man and better geologist. Words could never express how thankful I am. Phrases couldn't describe how much you mean to me. Thank you for your patience while I pursued my dream.

I would also like to thank my brother and sisters, who love me and guide me in everything I pursue. To my wonderful mother, your encouragement when times have been rough is very much valued and acknowledged.

ACKNOWLEDGEMENTS

I would like to recognize a few individuals who have volunteered their time and effort, bringing their wisdom to the successful completion of my dissertation. Every one of these individuals were available to give me whatever was required to complete my work.

This research would not have been possible without the support of my committee chair, Dr. Anne Raymond, and committee members, Drs. Christina Belanger, Mike Pope, and Daniel Thornton, who provided me with enormous personal and professional supervision and taught me so much about scientific research and life in general. Their comments and advice were always welcome when I had a question. As paleontologists and scientists, Drs. Anne Raymond and Christina Belanger offered me important feedback on my research. I appreciate you both having faith in me and for being such awesome leaders. I would also like to convey my appreciation to the members of my committee, Drs. Mike Pope and Daniel Thornton, for continuously offering suggestions, whenever needed.

I would very much like to thank Dr. Mohamed Zobaa for providing valuable information on palynology tools, processing samples, and generally supporting me. He always addressed my questions whenever I faced issues with Paleozoic palynology techniques. Thank you very much for your help and guidance. During my doctoral adventure, you were indeed a wonderful and indispensable guide.

I would also like to thank Dr. Adewale Amosu, who accompanied me on my academic journey from the start, through to this final level. Dr. Ade has given me

invaluable feedback and guidance to support me throughout my research. I very much appreciate your help and encouragement.

Special thanks go to Dr. Ahmed M. Elsarawy, who has never hesitated to help me and inspire me to continue. You have always been there when I needed support. You are one of the best people I've met in my life. And to my colleagues, I could never have found better cooperation than what you offered me during my degree. Also, special thanks to my supervisor in Libya, Dr. Ali D. El-Mehdawi, who always encouraged me and offered important advice throughout my academic journey.

Special thanks go out to my country of Libya, and in particular the University of Garyounis (Benghazi) and Ministry of Higher Education, whose financial resources have supported me throughout my academic journey.

The authors thank Mr. Mohamed Elsteil, Walied El khufaifi, and Khalifa. H. Ashahomi in the Arabian Gulf Oil Company (AGOCO) and everyone involved in collecting and organizing the data at the headquarter and core store division in Ganfouda, Benghazi, Libya. The authors also thank Dr. Harry Rowe (formerly of the Bureau of Economic Geology, now at Premier Oilfield Laboratories) for making his mudrock calibration samples available for calibrating the XRF device.

The authors want to acknowledge Dr. Juan Carlos Laya for access to the Rigaku Miniflex 600 benchtop X-ray diffraction analyzer in his lab at Texas A&M University and his graduate student, James Teoh, for showing the lead author how to do the XRD analysis. We also thank Dr. Mohamed K. Zobaa of the University of Texas at Permian

Basin (UTPB) for his numerous contributions, ranging from advice about sample preparation to discussing palynomorphs' systematics. Finally, a particular thanks to Dr. Gil Machado for the personal communication during the 2020 palynology online workshop.

CONTRIBUTORS AND FUNDING SOURCES

Contributors

This research was supervised by a dissertation committee composed of Drs. Anne Raymond [advisor] of the Department of Geology and Geophysics, Christina Belanger [first committee member], also of the Department of Geology and Geophysics, Mike Pope [committee member], also of the same department, and Daniel Thornton [committee member] of the Department of Oceanography. The doctoral candidate otherwise independently performed the work for this dissertation.

Funding Sources

I would like to acknowledge my profound gratitude to the Ministry of Higher Education and Scientific Research of Libya, through the University of Garyounis (Benghazi), for providing financial assistance during my doctoral work at Texas A&M University.

NOMENCLATURE

Aka	Akakus First potential Formation
Tan I, II, III	Tanezzuft Formation units
dt (μs/ft)	Sonic-log
pefz (b/e)	Photoelectric log
rhoz (g/cc)	Density-log

TABLE OF CONTENTS

Page

LIST OF FIGURES

Page

LIST OF TABLES

Page

1. INTRODUCTION

1.1. Economic Significance of Silurian strata in the Ghadamis Basin

The Ghadamis Basin has generated abundant amounts of gas-rich hydrocarbon, especially from the early Silurian ‘hot shale’, a unit at the base of the Tanezzuft Formation, which contains a significant amount of organic matter and a high proportion of radioactive elements that can be detected by x-ray diffraction analysis (XRD) and x-ray fluorescence analysis (XRF). Silurian ‘hot shale’ is a potential source rock for oil and gas generation in the Ghadamis Basin in northwest Libya, especially in the Akakus and Tanezzuft formations (Figure 1.1). Although palynological research has been conducted in the Ghadamis Basin, few studies reported palynogical assemblages of the subsurface divisions from the Tanezzuft and Akakus formations (Tekbali et al., 1991; Steemans et al., 2000; Le Héron et al., 2013; Richardson and Ioannides, 1973; Daniels et al., 1990; Elfigih, 2000). Because of this, the biostratigraphy of the Akakus and Tanezzuft formations has yet to be resolved.

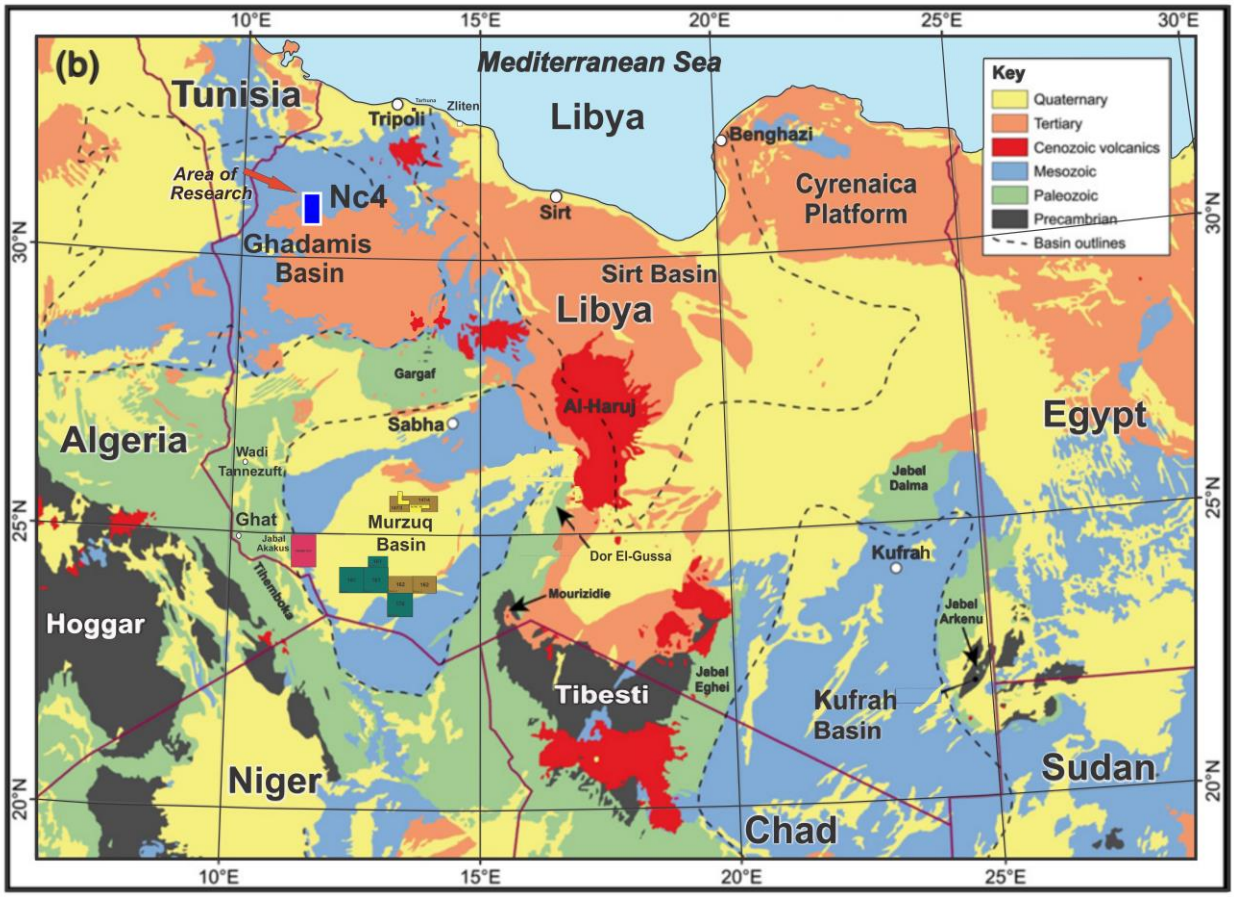

Figure 1.1: The NC4 Block is located in the Ghadamis Basin in northwestern Libya, as depicted on this simplified geologic map modified from (Meinhold et al., 2011).

1.2. Dissertation Organization

The second chapter of this dissertation presents an integrated three-dimensional model of the reservoir characteristics and paleoenvironments of the Silurian Lower Akakus formation in the Ghadamis Basin, based on an interpretation of the petrophysical logs. This chapter is in revision in the Gulf Coast Association of Geological Sciences (GCAGS) Journal, with co-authors.

The third chapter of my dissertation presents a reservoir quality assessment of the Lower Akakus and Lower Tanezzuft formations, based on geophysical well logs and petrophysical

composition. This chapter is based on an extended abstract published in Transactions of the GCAGS with co-authors. However, I have included an additional section describing the data and methodology used in these analyses for the dissertation.

The fourth chapter of this dissertation focuses on identifying chitinozoans and other palynomorphs from the Silurian in the Ghadamis Basin and establishing a biostratigraphic zonation and the likely paleoenvironments of the subsurface units of the Silurian Tanezzuft and the Akakus formations (Tan III of the Tanezzuft Formation, and the lower, middle and upper units of the Akakus Formation: (Daniels et al., 1990; Elfigih 2000). This project is of special importance because once the stratigraphic zonation is established and we made also thin sections from the core samples (Figure A-1), the shale beds can be correlated laterally. This research will result in a better understanding of source rock in the Ghadamis Basin and will improve our ability to locate possible sources of oil. I plan to submit this chapter to the journal, Palynology, with co-authors.

1.2.1. Geological setting of the Ghadamis Basin

During the Late Ordovician and Silurian, the Ghadamis Basin lay on the northern coast of Gondwana (see Figure 2.2; Figure A-2), 70° S paleolatitude at the end of the Ordovician, and 60° to 70° S paleolatitude in the early Ordovician (Llandovery), 425 million years ago (Stampfli, 2013: Table A-1). Today, the Ghadamis Basin (Figure 1.1) straddles the boundaries of Libya, Algeria, and Tunisia. The present-day margins of the basin are marked by structures uplifted during the Hercynian in the Carboniferous: the Qarqaf Arch to the south, Djeffara - Nufusa Arch to the northeast, and Amguid Spur and El Biod Arch (also known as the Tihimboka Arch) to the west (Klitzsch, 1970; Mamgain, 1980; Selley, 1997b; Figure 1.1). These structures do not define

the extent of the Early Paleozoic depocenters, which were open towards the north and formed part of the regionally extensive Gondwanan continental shelf, including the peri-Gondwanan terranes, which today form parts of Europe and the Middle East (Dewey et al., 1973; Klitzsch, 1981; Selley, 1997b; Boote et al., 1998; Stampfli et al., 2013; Le Héron et al., 2018; Table A-1).

Silurian sediments in the Ghadamis Basin are quite thick, spanning a depth interval from 7,612 ft to 9,1295 ft, corresponding to most of the Silurian (Llandovery to Pridoli) (Imsalem et al., 2018). The Silurian shale and sand of the Tanezzuft Formation in the Ghadamis Basin accumulated after the Late Ordovician glaciation of Gondwana (Le Héron et al., 2013). During deposition of the Tanezzuft Formation, sediment prograded across the shelf from the southeast to the northwest, forming a progradational system tract. The base of the Tanezzuft Formation consists primarily of shale, some of which is rich in U^{+4} and organic carbon; this is referred to as Silurian 'hot shale' (Arduini, 2003). As the shoreline continued to prograde across the basin, shale and discontinuous sand beds accumulated in the upper part of the Tanezzuft Formation (Adruini, 2003). The Akakus Formation has interfingering sandstones and shales in the three wells of Ghadamis Basin.

1.3 Study Rationale

Mr. Thodhoraq Shteto, the geologist in the Arabian Gulf Oil Company (AGOCO), is responsible for Ghadamis Basin concessions. Based on observations of Silurian sediments from the Ghadamis Basin in cores and well logs, he and his team realized that the interlayering of shale and sand in the Ghadamis Basin, and the tendency of sand layers to pinch out, makes correlation almost impossible. To solve this problem, AGOCO collected as many shale cores as they could from three wells to make a composite columnar section that would include all of the

Silurian shales in the basin. Understanding the distribution of palynomorph assemblages from these wells will provide an additional correlation tool, poetentially enabling correlation of most of the wells that AGOCO owns in the Ghadamis Basin. This work also will contribute to our understanding of Silurian biostratigraphy and paleobiogeography.

1.4 References

Arduini, M., M. Barassi, A. Golfetto, A. Ortenzi, E. Serafini, E. Tebaldi, E. Trincianti, C. Visentin, 2003, Silurian–Devonian sedimentary geology of the Libyan Ghadamis Basin: example of an Integrated Approach to the Acacus Formation Study. In: Salem, M.J., Oun, K.M. (Eds.), Symposium on the Sedimentary Basins of Libya II.

Boote, D. R., D. D. Clark-Lowes, and M. W. Traut, 1998, Palaeozoic petroleum systems of North Africa: Geological Society, London, Special Publications, v. 132, no. 1, p. 7–68, doi:10.1144/gsl.sp.1998.132.01.02.

Carr, I. D. 2002, Second-order sequence stratigraphy of the Palaeozoic of North Africa: Journal of Petroleum Geology, v. 25, n. 3, p. 259-280.

Daniels, HJ, B. Thusu, and S. Abushaala, 1990, Sedimentological and palynological facies analysis of Acacus and Tanezzuft formations in Concession NC7A, northwest Libya: AGOCO internal report.

Klitzsch, E., 1970, Die Strukturgeschichte Der Zentral Sahara: Geologische Rundschau, v. 59, no. 2, p. 459–527, doi:10.1007/bf01823806.

Elfigih, OB., 2000, Regional diagenesis and its relation to facies change in the Upper Silurian, Lower Acacus Formation, Hamada (Ghadames) Basin, northwestern Libya [dissertation]: St. John's (NL, Canada): Memorial University of Newfoundland.

Le Héron, D. P., G. Meinhold, A. Page, and A. Whitham, 2013, Did lingering ice sheets moderate anoxia in the Early palaeozoic of Libya?: Journal of the Geological Society, v. 170, no. 2, p. 327–339, doi:10.1144/jgs2012-108.

Mamgain, V. D., 1980., The Pre-Mesozoic (Precambrian to Palaeozoic) Stratigraphy of Libya. Industrial Research Centre, Tripoli.

Page, A., G. Meinhold., D. P. Le Heron, and M. Elgadry, 2013, Normalograptus Kufraensis, a new species of graptolite from the western margin of the kufra Basin, Libya: Geological Magazine, v. 150, no. 4, p. 743–755, doi:10.1017/s0016756812000787.

Richardson, J. B., and N. Ioannides, 1973, Silurian Palynomorphs from The Tanezzuft and Acacus Formation, Tripolitania, North Africa: Micropaleontology, v. 19, no. 3, p. 257, doi:10.2307/1484881.

Steemans, P., 2000, Annotations to the Devonian Correlation Table, b501di00: Miospore Palynology, Western Europe: Senckenbergiana lethaea Journal, v. 80, no. 2, p. 759–760, doi:10.1007/bf03043378.

Selley, R. C., 1997, Chapter 3 The Sirte basin of Libya: Sedimentary Basins of the World, p. 27–37, doi:10.1016/s1874-5997(97)80006-8.

Tekbali, A. O., and G. D. Wood, 1991, Silurian spores, acritarchs and chitinozoans from the Bani Walid Borehole of the Ghadamis Basin, Northwest Libya. (In: The Geology of Libya. M.J. Salem et al, editors) The Geology of Libya. Third Symposium on the Geology of Libya. (M.J. Salem, O.S. Hammuda and B.A. Eliagoubi, editors). Amsterdam; New York: Elsevier v. 4. p. 1243- 1273.

2. RESERVOIR QUALITY ASSESSMENT OF THE LOWER AKAKUS AND LOWER TANEZZUFT FORMATIONS IN THE NC4 BLOCK, GHADAMIS BASIN, LIBYA[1].

2.1. Introduction and Geological setting of the Hamada (Ghadamis) Basin.

The Ghadamis Basin is classified as a sizeable intra-cratonic sag basin that began in the Paleozoic (Bora and Dubey, 2015). The first major orogenic event to influence the basin history was the Hercynian Orogeny. The basin is bounded by Nafusa Arch and Zamzam Depression on the east side and the Tihemboka Uplift on the westside. In the north-south direction, the Hamada (Ghadamis) Basin, which is in the northwest region of Libya, is bounded by Dahar Arch on the north and the Al-Qarqaf Arch in the south.

The Paleozoic succession in North Africa has five sequences bounded by significant unconformities (Carr, 2002). The Silurian sequences is bounded by the late Ordovician Unconformity at the base and the Caledonian Unconformity at the Silurian/Devonian boundary (Carr, 2002; Underdown et al., 2007). In west Libya, the three Late Ordovician and Silurian-aged formations, Mamuniyat, Tanezzuft, and Akakus, make up Carr's second sequence; Carr (2002) identified these three formations respectively, as lowstand, transgressive, and highstand. While the Mamuniyat Formation generally underlies the Tanezzuft Formation, there is a discontinuous unit called Bi'r Tlakshin, which is thought to infill topographic lows on top of the exposed and eroded Ordovician Mamuniyat Formation. The Bi'r Tlakshin unit was first described from the C1 well (Hallett, 2016). A disconformity separates the Tanezzuft Formation from the Bi'r Tlakshin unit. The literature describes the contact between Tanezzuft and Akakus formations as

[1] Reprinted with permission from Reservoir Quality Assessment of the Lower Acacus and Tannezuft Formations in the NC4 Block, Ghadames Basin, Libya by M. Imsalem, A. Amosu, M. Wehner, A. Raymond, and Y. Sun, Gulf Coast Association of Geological Sciences (GCAGS) Journal, 68, pp.255-268.

conformable, but another disconformity lies at the top of the Akakus Formation (Aissaoui et al., 1996; Bosnina et al., 2017).

Stratigraphically, the Tanezzuft Formation can be divided into two or three units, and the Akakus Formation has generally been divided into three lithostratigraphic units. The lower Tanezzuft unit consists of ‘hot shale’ (laminated, organic rich mudstone), while the upper units are more silt-prone, gray, micaceous, with occasional thin, meter-scale sandstone units. Lithologically, the Akakus Formation is more complex than the Tanezzuft Formation, and consists of interbedded sandstones and shales. The shales within the Akakus Formation are dark, silty, and micaceous (Aissaoui et al., 1996), while the sandstones are typically fine to very fine grained, dominated by detrital quartz grains. Other reported detrital components (generally the accessory component of the sandstones) of the Akakus sandstones include glauconite, micas, feldspars, Fe-chlorite ooids, and phosphatic bioclasts (Aissaoui et al., 1996). The authigenic mineralogic components include silica overgrowths, calcite cement, siderite, and kaolinite.

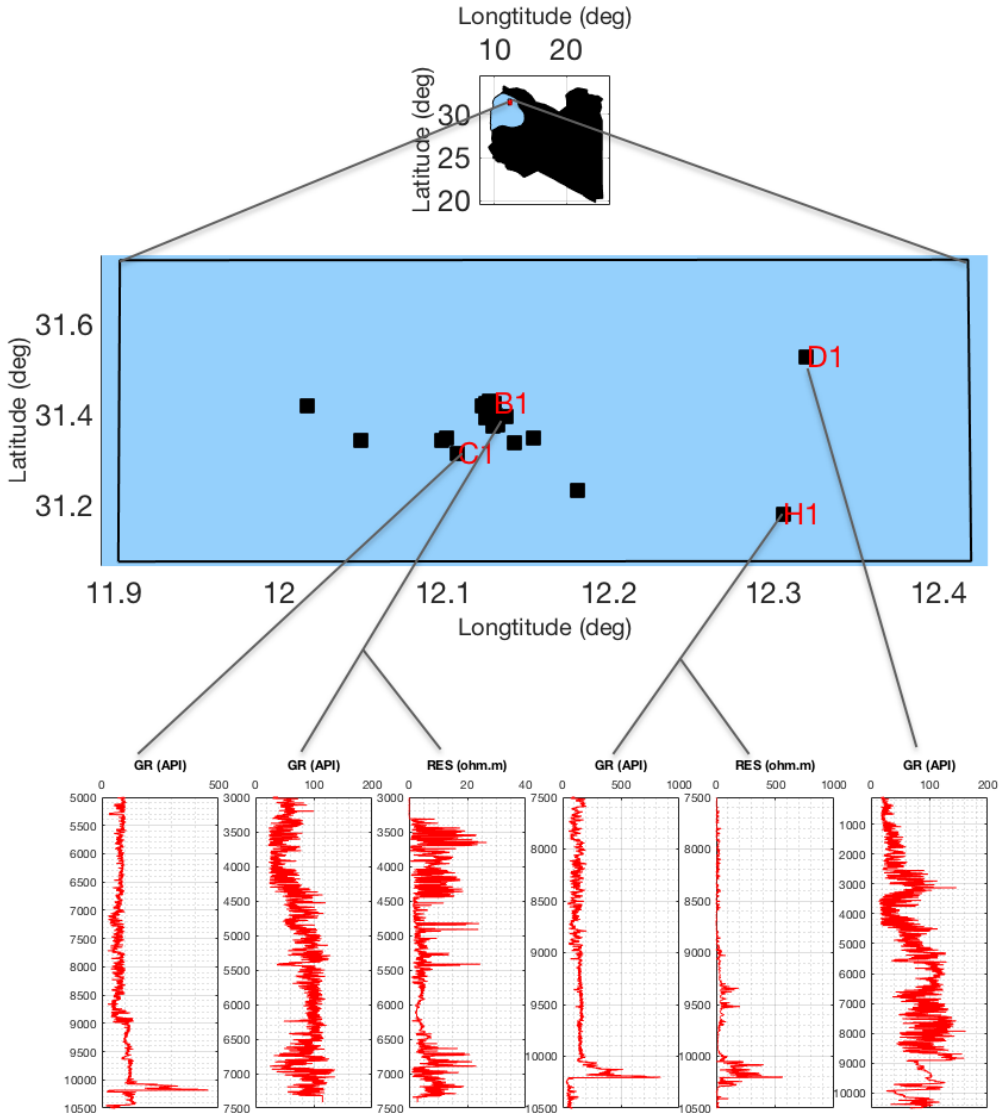

Figure 2.1: Location map of the Ghadamis basin in Libya. Available Gamma-ray (GR) and resistivity show the lithological variation. High values of GR (>450 American Petroleum Institute gamma-ray units, or gAPI) in the C-1 and H-1 wells indicate the presence of the 'hot shale' in these wells. The GR log shown for the B-1 well ends above 7500 feet and is too shallow to record the 'hot shale' at approximately 10,000 – 10,500 ft. (Imsalem, 2018).

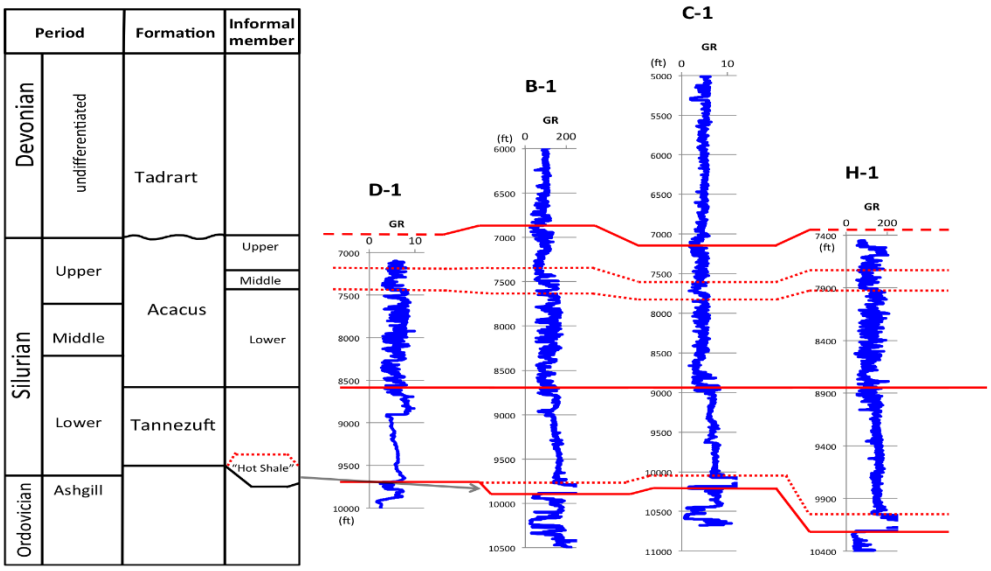

Figure 2.2: A stratigraphic correlation of four wells in the NC4 concession in Ghadamis Basin primarily based on gamma-ray logs. All the gamma-ray values (GR) are in units of American Petroleum Institute gamma radiation units (gAPI). Missing GR data in the B-1, C-1 and H-1 wells indicate too much gamma radiation to record. The Silurian Tanezzuft Formation is divided into two units; the overlying Silurian Akakus Formation is divided into three units.

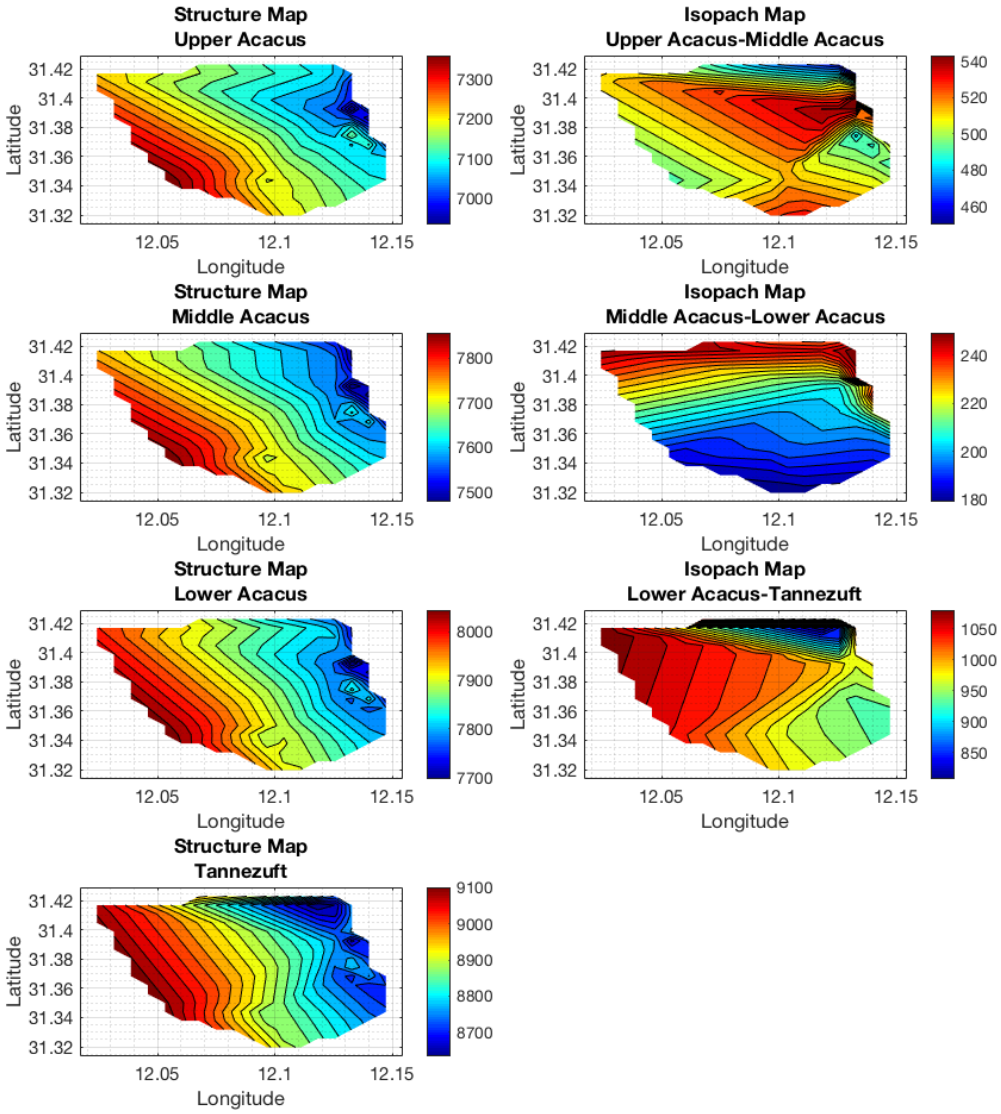

Figure 2.3: Structure maps (subsurface map) and isopach maps of the Upper Akakus, Middle Akakus, Lower Akakus and the three members of the Tanezzuft Formations. Colors in the structure map correspond to thickness that is a thickness differences within a chart unit. of overburden sediment (blue thin, red thick); colors in the isopach map indicate the relative thickness of the unit (blue thin, red thick).

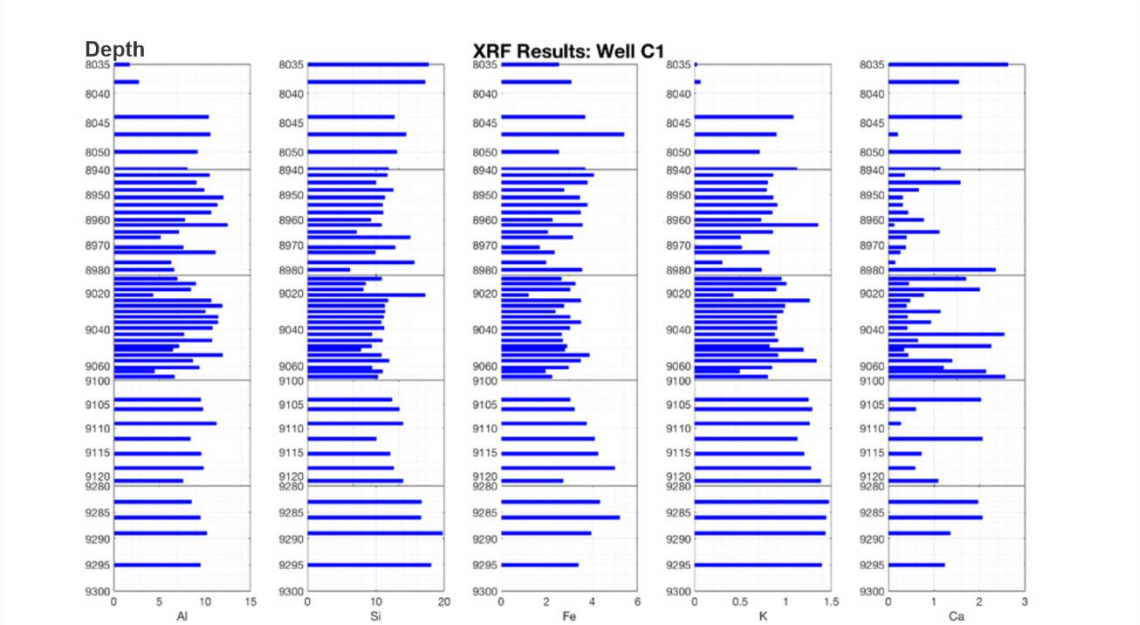

Figure 2.4: XRF analysis results from well C1 for major elements that are associated with the bulk minerals in feet. Numbers on the left side of each chart indicate depth in the core in feet.

Figure 2.5: XRF analysis results from well H1 for major elements that are associated with the bulk minerals in feet. Numbers on the left side of each chart indicate depth in the core in feet.

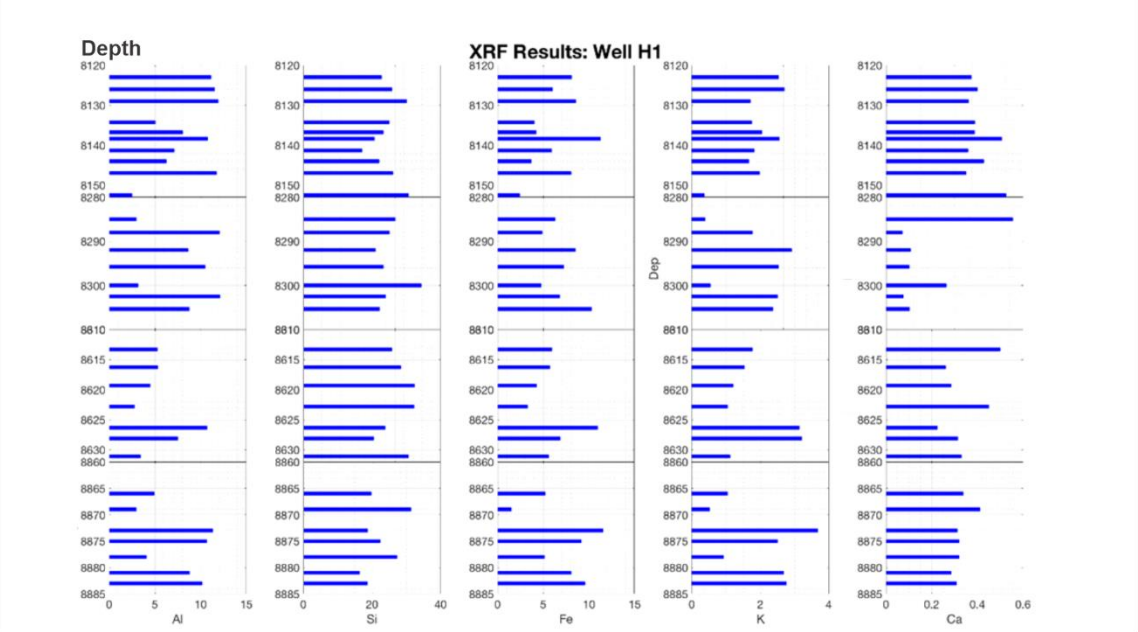

Figure 2.6: XRF analysis results from well B1 for major elements that are associated with the bulk minerals in feet. Numbers on the left side of each chart indicate depth in the core in feet.

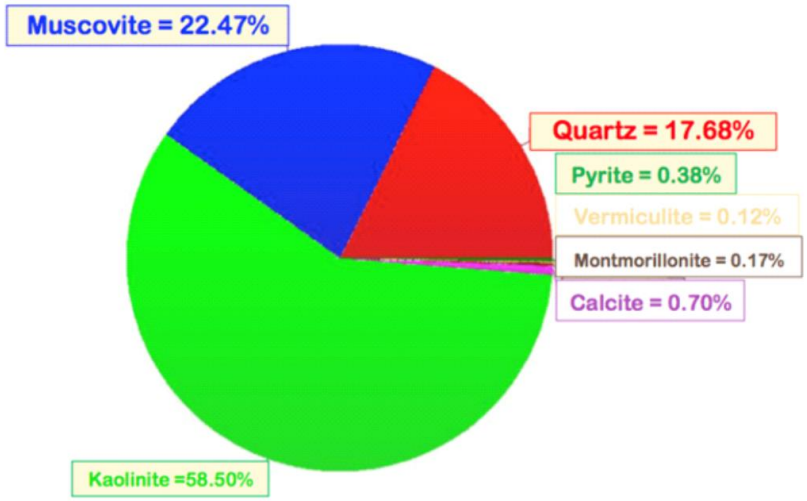

Figure 2.7: Pie diagram based on XRD Peak analysis of four subsurface rock samples from well C1.

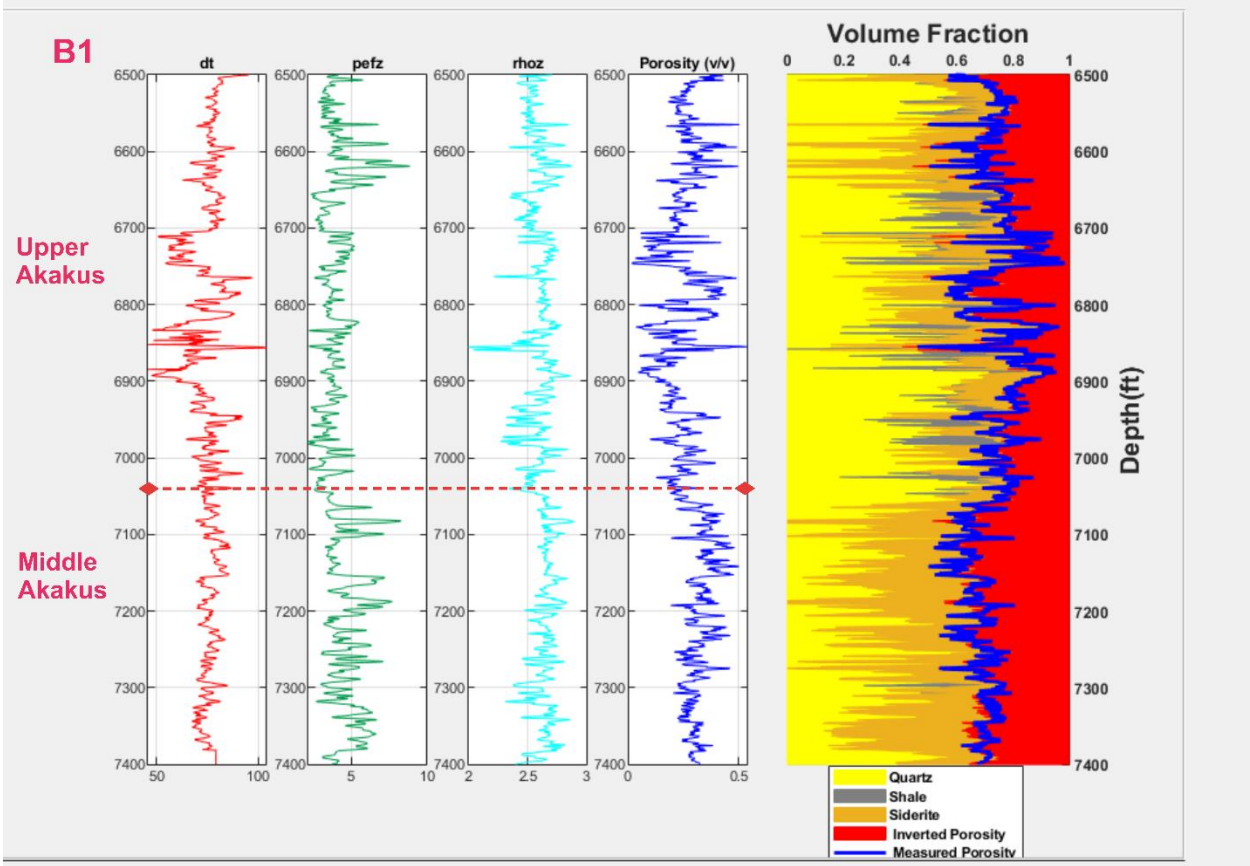

Figure 2.8: Petrophysical composition analysis of geophysical well-logs from well B1 in the NC4 concession, Ghadamis Basin. This notation of Tan = Tanezzuft Formation, and Aka = Akakus Formation.

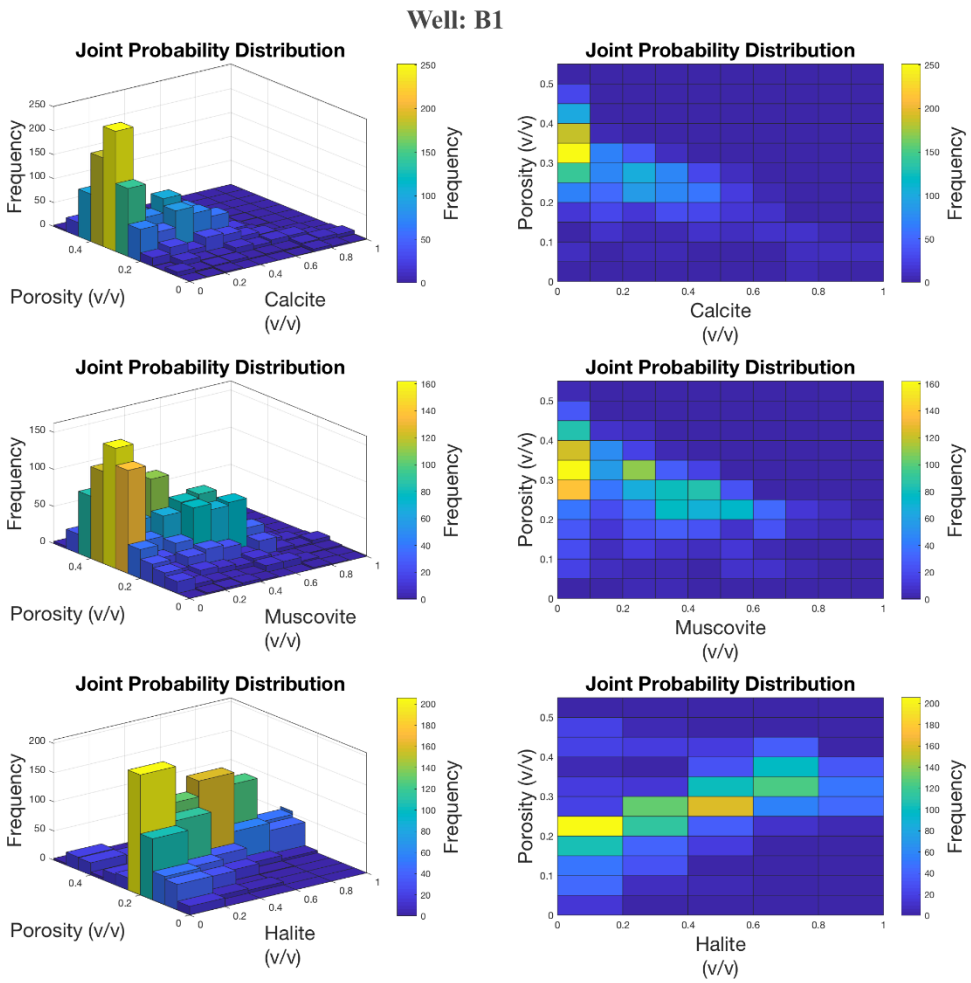

Figure 2.9: Joint probability distribution trends of porosity with calcite, muscovite and halite.

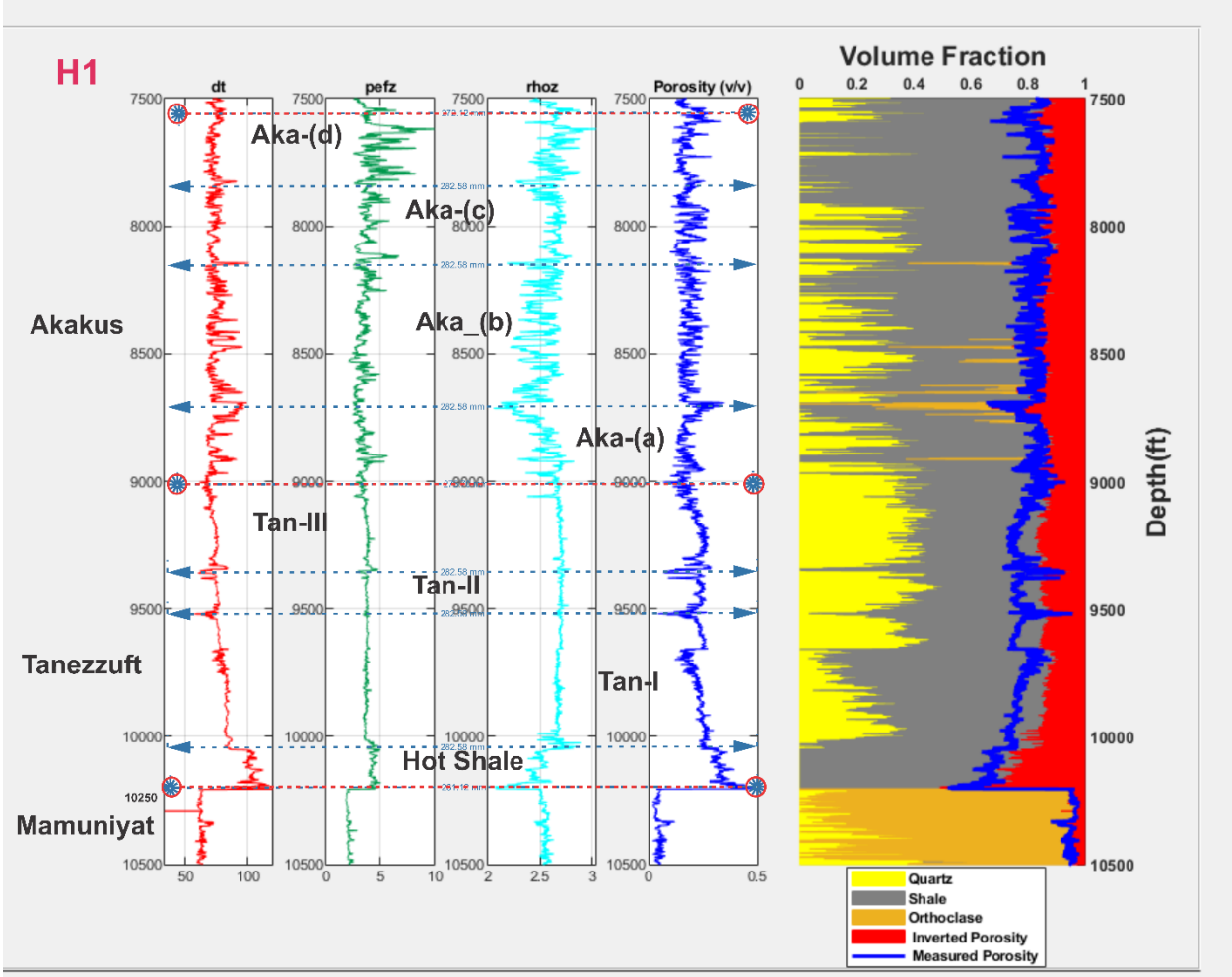

Figure 2.10: Petrophysical composition analysis of geophysical well-logs from well H1 in the NC4 concession, Ghadamis Basin.

2.2. Data and Methodology

In the regional geologic context, the boreholes of this study are located at the center of the Ghadamis Basin. Subsurface samples were collected from three wells (Figure 2.1): one at the Tunisian-Libyan border on the west (C1 borehole), one in northern Libya (B1 borehole), and one in the eastern part of the Ghadamis Basin (H1 borehole, a recently drilled well in 2014). Samples were taken from three cores (H1, B1, C1) for geochemical analysis. Of these samples,

147 were used for (XRF) analysis and three for X-ray diffraction (XRD) analysis. The X-ray fluorescence (XRF) data was acquired with a Thermo Scientific Niton XL3t 950 GOLDD+ Analyzer (for most sedimentary rocks detects up to 36 elements) using the Cu/Zn filter and calibrated with mudstone standards, courtesy of Dr. Harry Rowe (then at Bureau of Economic Geology), based on the methodology laid out by Rowe et al. (2012). XRD spectra were acquired for 4 samples from the wells: C1, B1, and H1. Based on the spectra, the following bulk minerals were identified: quartz, muscovite, and kaolinite. Accessory minerals include calcite, pyrite, halite, shale, orthoclase, chlorite, clay, quartz, montmorillonite, vermiculite, and siderite.

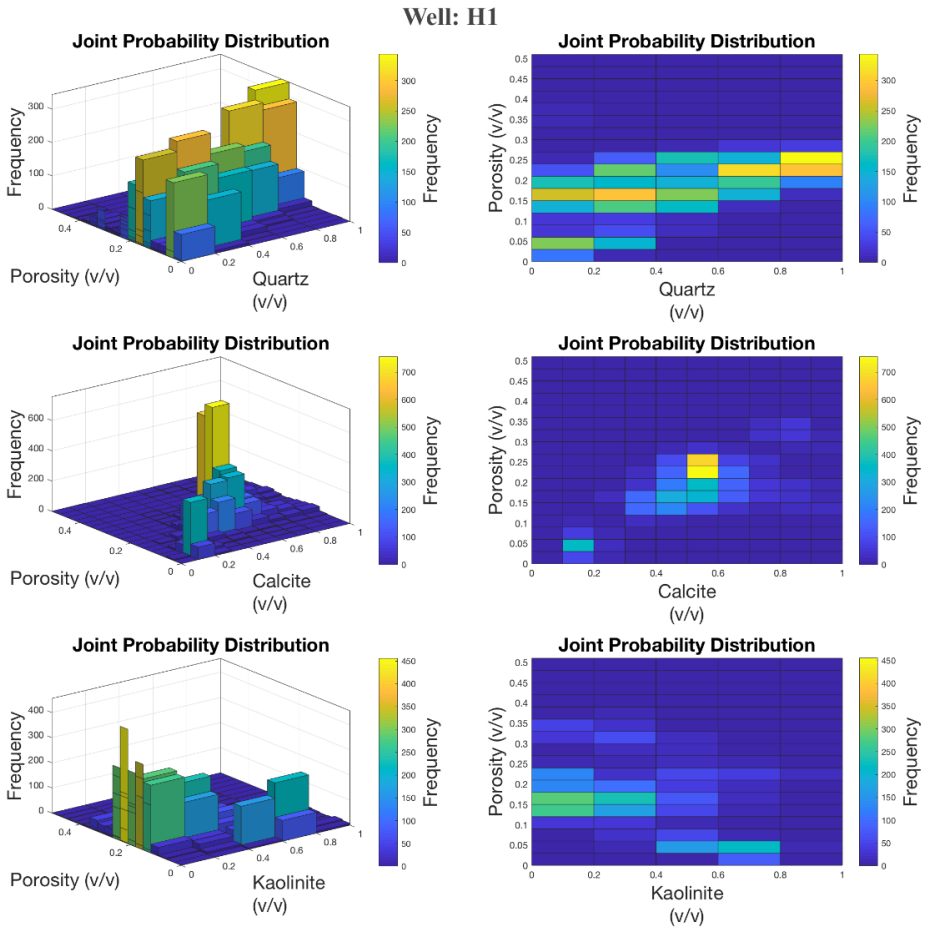

Figure 2.11: Joint probability distribution trends of porosity with quartz, calcite, and kaolinite.

Petrophysical composition analysis is carried out using a special class of geophysical logs including bulk density, photoelectric factor, acoustic slowness, and neutron porosity. For each depth point, a linear system of equations is constructed and solved as an inverse problem. The systems of equations can be simply expressed as:

$$\mathbf{CV = L \ldots (1)}$$

where C is a matrix of the petrophysical properties of the rock constituents, V is a vector of the unknown proportions of the rock constituents and L is a vector of geophysical log measurement which represents the bulk petrophysical properties of the rock formation. An additional equation that makes the sum of mineral and fluid proportions unity is included (see Doveton et al., 2014; Amosu and Sun, 2018a, b). We make use of a new software program, MinInversion (Amosu and Sun, 2018) in implementing equation (1). The program also computes the joint probability distribution between porosity and the mineral components.

2.3. Result and Discussion

The results of XRF and XRD analysis are used to inform the choice of mineral components used in the inversion; however, the number of logs available limits the number of mineral components for which inversions can be done. Figure 2.8 shows the petrophysical composition analysis of geophysical logs from wells B1 in the NC4 concession, Ghadamis Basin. The zone spans a section of the upper Akakus (see also Figure A-3). The minerals inverted for are calcite, muscovite and halite. The inversion reveals the variation of the mineral volumes with depth. Figure 2.9 shows the joint probability between porosity and mineral

volumes. In general, the porosity decreases with increase in calcite and muscovite and increases with the volume of halite. It is possible that the halite is associated with the brines, which may have higher salinity than expected. A complicating factor could be that halite may be precipitated from the brines as the borehole releases pressure in the invaded zone. The modeling result for the presence of halite is partially collaborated by the detection of high chlorine content by XRF, but the results were not quantified due to the lack of standards for chlorine. The sensitivity of XRF to chlorine detection is not known. Figure 2.10 shows the petrophysical composition analysis of geophysical logs from wells H1 in the NC4 concession, Ghadamis Basin. The zone ranges from the lower Akakus to the 'hot shale'. The mineral components inverted for are quartz, calcite, and kaolinite. The lower Akakus contains a larger volume of calcite. The Tanezzuft apparently is divided into three different facies members (Imsalem et al., 2018; see Figure 2.10). The lowermost member is the 'hot shale'. It contains heavy minerals and dark colored shale and is exceptionally rich in organic matter including palynomorphs and paleopalynology fossils such as spores, chitinozoans, acritarchs, scolecodonts and, rarely, graptolites. The middle member contains more calcite cement and low amount of sandstone. It is separated from the upper member by a kaolinite contact. The third member is mostly quartz with fine-grained sandstone and subangular grain shape. The Silurian 'hot shale' has a significant mixture of calcite and kaolinite. Below the Silurian 'hot shale', larger volumes of kaolinite occur. Figure 2.11 shows the relationship between porosity and the inverted mineral volumes. The porosity increases as the amount of quartz and calcite increases, while it decreases as the amount of kaolinite increases. In the lower Akakus and Tanezzuft formations, increases in porosity with increased amounts of quartz may be attributed to interparticle porosity between the quartz grains. In these units, most quartz grains occur concentrates in thin layers, as seen in thin sections (Figure A-1). The increase

in porosity with increased calcite may indicate that the calcite in the two formations has undergone diagenetic processes such as dissolution.

2.4. Summary

Using geophysical well-log data together with XRF and XRD measurements on core samples from wells located in the NC4 concession of the Ghadamis Basin, Libya, we examine the petrophysical composition of the Akakus and Tanezzuft formations and the relationship between the mineral components and porosity. We find that in the Akakus Formation, an increase in the volumes of calcite and muscovite corresponds to a decrease in porosity, while halite volumes increase with porosity. It is possible that at certain depths a large volume of halite is dissolved in brine. In the Tanezzuft Formation quartz, calcite and kaolinite play important roles in determining the bulk properties of the rocks. Increases in quartz content corresponds to an increase in porosity while an increase in kaolinite volumes corresponds to a decrease in porosity. The decrease in porosity may be a result of kaolinite acting to fill some of the pore spaces available. More well-logs data and a comprehensive study of detecting mineral petrophysical composition will be useful in reducing risk in petroleum exploration for instance determining the correct correlations.

2.5. References

Aissaoui, M. N., Bedir, M. and H. Gabtni, 2016, Petroleum assessment of Berkine-Ghadames Basin, southern Tunisia: AAPG Bulletin, v. 100, n. 3, p. 445-476.

Amosu, A., H. Mahmood, and P. Ofoche, 2018, Estimating the permeability of carbonate rocks from the fractal properties OF Moldic PORES using THE kozeny-carman equation: Research Ideas and Outcomes, v. 4, doi:10.3897/rio.4.e24430.

Amosu, A., and Y. Sun, 2018a, Mininversion: A program for petrophysical composition analysis of geophysical well log data: Geosciences, v. 8, no. 2, p. 65, doi:10.3390/geosciences8020065.

Amosu, A., and Sun YF, 2018b, Rock physics based quantification of carbonate pore type effect on permeability heterogeneity: Application to the Wolfcamp Formation, Permian Basin heterogeneity: Application to the Wolfcamp Formation, Permian Basin, AAPG SWS Section, April.

Bosnina, S., Najem, A. and A. Marimi, 2017, High resolution sedimentological interpretation of the lower Paleozoic clastic reservoirs in Ghadames Basin, Libya: AAPG Middle East Region, Geoscience Technology Workshop.

Carr, I. D. 2002, Second-order sequence stratigraphy of the Palaeozoic of North Africa: Journal of Petroleum Geology, v. 25, n. 3, p. 259-280.

Doveton, J.H. 2014, Compositional Analysis of Mineralogy. In Principles of Mathematical Petrophysics; International Association for Mathematical Geosciences: Houston, TX, USA, Volume 9, pp. 94–121.

Hallett, Don., 2016, Petroleum Geology of Libya. Elsevier.

Imsalem M, 2007, Geological Mapping (thin-section description) of Wadi Al-Athrun & Wadi Ain Al-Daboussiah area, sector (4), Northern part of Al-Jabal Al-Akhdar, NE Libya: the thesis submitted to the department of Earth sciences at Garyounis University, Benghazi Libya.

Rowe, H., Hughes, N. and K. Robison 2012, The quantification and application of handheld energy-dispersive x-ray fluorescence (ED-XRF) in mudrock chemostratigraphy and geochemistry: Chemical Geology, v. 324, p. 122-131.

Meinhold, G., A. C. Morton, C. M. Fanning, D. Frei, J. P. Howard, R. J. Phillips, D. Strogen, and A. G. Whitham, 2011, Evidence from detrital zircons for recycling OF

Mesoproterozoic and NEOPROTEROZOIC Crust recorded In Paleozoic and Mesozoic sandstones of Southern libya: Earth and Planetary Science Letters, v. 312, no. 1-2, p. 164–175, doi: 10.1016/j.epsl.2011.09.056.

Sloss, L. L. 1963, Sequences in the cratonic interior of North America: Geological Society of America Bulletin, v. 74, p. 93-114.

Spina, A., Vecoli, M., Riboulleau, A., Clayton, G., Cirilli, S., Di Michele, A., Marcogiuseppe, A., Rettori, R., Sassi, P., Servais, T. and L. Riquier 2018, Application of Palynomorph Darkness Index (PDI) to assess the thermal maturity of palynomorphs: a case study from North Africa: International Journal of Coal Geology, v. 188, p. 64-78.

Underdown, R., Redfern, J. and F. Lisker 2007, Constraining the burial history of the Ghadames Basin, North Africa: an integrated analysis using sonic velocities, vitrinite reflectance data and apatite fission track ages: Basin Research, v. 19, n. 4, p. 557-578.

3. INTEGRATED THREE-DIMENTIONAL RESERVOIR, DEPOSITIONAL ENVIRONMENT, PETROPHYSICAL MODELLING OF THE SILURIAN LOWER AKAKUS FORMATION, GHADAMIS BASIN, NORTHWESTERN LIBYA[2]

3.1. Introduction

The Ghadamis Basin is an intracontinental sag basin in northwestern Libya and is one of the most prolific hydrocarbon basins in North Africa (Figure 3.1). Almost all of the oil is contained in Silurian and Devonian sandstones, with only a small amount of Ordovician, Carboniferous, and Triassic sediment (Hammuda, 1980; Echikh, 1992; Echikh, 1998). The Silurian Lower Akakus Formation is one of the essential reservoirs in the region. Akakus sandstone reservoirs to the northwest are a result of low-displacement faults and unconformity subcrop traps. Recoverable reserves are approximately equivalent to 259 million barrels of oil in a large number of small pools in the towns of Tigi and Tlacsin, and in the NC-2 and NC-100 concessions (Echikh, 1992). The distribution of oil and gas fields in the Libyan Ghadamis Basin is influenced by the stratigraphic architecture of the Silurian-Devonian succession (Dardour et al., 2004). The main source rock in the Silurian of the Ghadamis Basin, the ‘hot shale’ at the base of the Tanezzuft Formation, is overlain by the lower Akakus reservoir; the latter consists of intercalated thin beds and streaks of sand and shale.

[2] In revision in the Gulf Coast Association of Geological Sciences (GCAGS) Journal

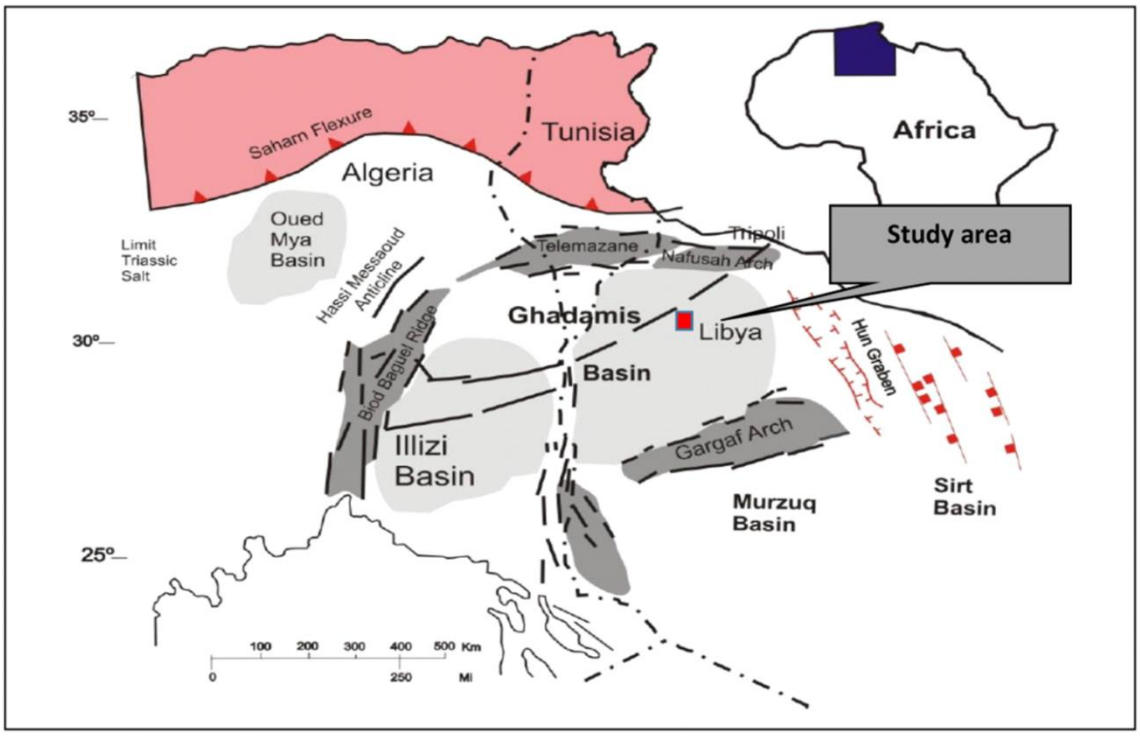

Figure 3.1: General structural setting of the North African Ghadamis region. Location of structural features modified after Acheche et al. (2001).

3.1.1. Tectonic Setting

The Ghadamis Basin is located to the north of the Tebisti Mountains range, part of the stable Saharan Platform. The latter was folded extensively during the Precambrian. Since then, epeirogenic movement produced wide, shallow basins and broad uplifts (Bishop, 1975).

The Cimmerian and the Avalonian Cadomian peri-Gondwanan terranes surrounded the northern part of the Gondwanan passive, shallow shelf margin during the Neoproterozoic and Early Paleozoic. These terranes started to drift northward during the Ordovician (Hallett, 2016). Their collision with Laurentia resulted in the Caledonian orogeny (Hallett, 2004).

The Thimboka High separates the Ghadamis and Illizi basins (Figure 3.1). This essential structural element affects the Ghadamis Basin in many ways, including its sedimentary fill and the maturity of its source rocks. The Thimboka structural terrane formed during the end phase of Pan-African tectonics in the Cambrian (Hallett, 2004). According to Echikh (1998), early Ordovician tectonic instability resulted in uplift and the erosion of sediment, resulting in the absence of the Cambrian strata over the Thimboka area. The same event produced a series of north-south to northwest-southeast uplifts and troughs in the central and southern parts of Libya.

North of the Ghadamis Basin, the Nafusa/Telemazane arch forms its northern boundary (Figure 3.1). Magloire (1968) mentioned that the Telmazane is a Hercynian block, which forms a lineament along the northern boundary of the Saharan platform. However, stratigraphic gaps in the Silurian and Ordovician suggest that the structure may have formed during the Caledonian Orogeny.

To the west, the Hassi Massaoud/Baguel area consists of horst and grabens bounded by local, north-south trending flexures, and faults controlled by Precambrian basement fault zones, (Bishop, 1975).

3.1.2. Stratigraphy and Distribution

The presence of uplifted areas during the early Paleozoic controlled much of the sedimentary basin fill (Figure 3.2). This infill started with the clastic continental deposition that was variable in terms of supply. In addition, climatic variation played a significant role in the determination of lithologies in the basin.

Some geologists interpreted the depositional environment of the lower part of the Akakus Formation to range from fluvial to shallow marine with tidal bars and tempestite deposits (Hallett, 2004). Previously, Bellini and Massa (1980) interpreted the Akakus Formation as

recording a fall in relative sea level during the mid-Silurian, resulting in the deposition of the silts and sandstones in a system of northwards prograding deltas. Dardour et al. (2004) on the other hand, discussed stratigraphic controls on Paleozoic petroleum systems in Ghadamis Basin and described the Akakus Formation as a late highstand systems tracts. Hallett (2004) described the relationship between the Lower Akakus and the underlying Tanezzuft using the palynomorphs and graptolite zones to be strongly diachronous from south to north.

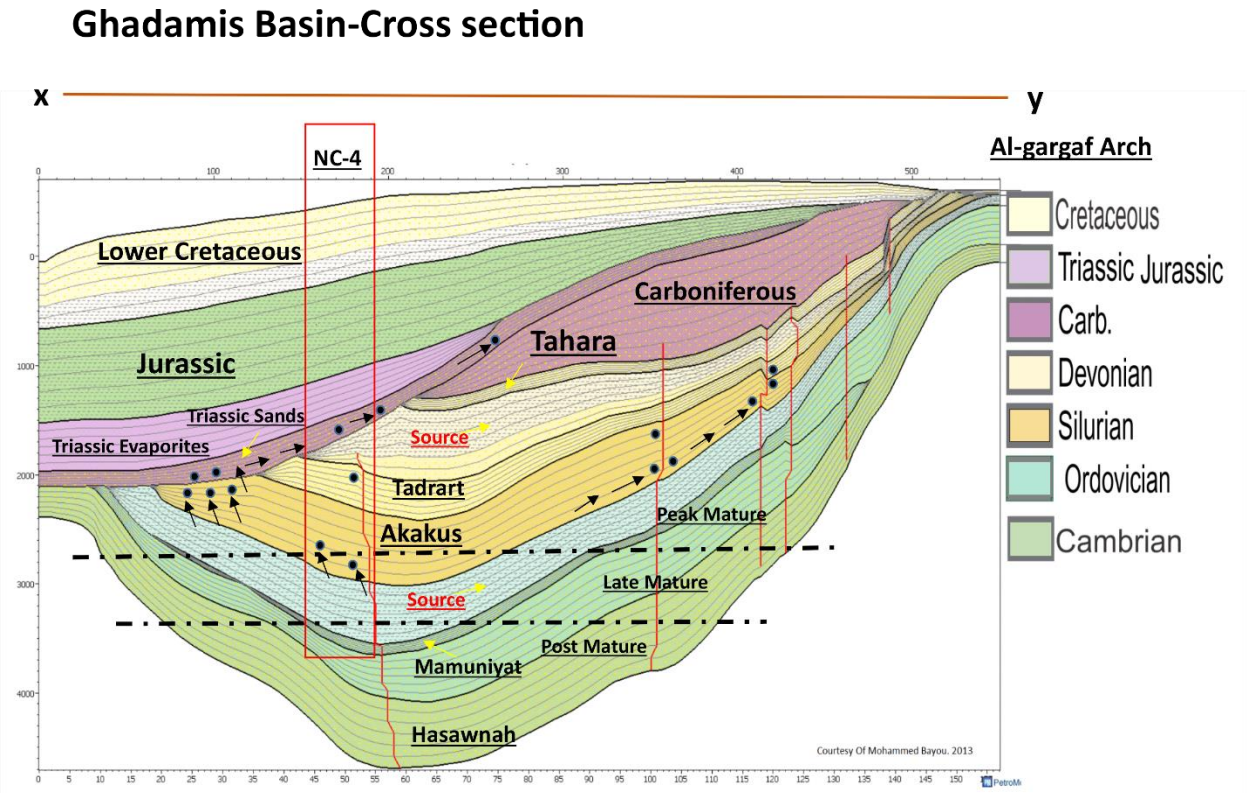

Figure 3.2: Cross-section of the Ghadamis Basin; the study area is located in the central part of the Basin. Courtesy of Baayou (2013). Source reservoir rocks are in both Ordovician and Silurian periods. Red vertical lines are the faults.

Bellini and Massa (1980) studied the Akakus Formation in detail and subdivided it into informal lower, middle and upper units. The formation consists of outcrops along the western flanks of the Murzuq Basin. The Akakus net sandstone thickness ranges from approximately 500 to 1300 ft. The Akakus average porosity is at least 16% (Rusk, 2001). It is still poorly defined in the subsurface of Murzuq Basin, where it has been penetrated by only two wells (A1-76, H1-NC58) with thicknesses of 1100 ft. The formation seems to be missing over the present Idhan depression and on top of the Traghan High (Echikh and Sola, 2000).

Sequence stratigraphic analysis and chronostratigraphic analysis can reveal more details of the depositional history of the basin (Amosu and Sun, 2017).

Lower Akakus sandstone in the study area is divided into sequences of sand and shale intercalation. There is one mega-sealevel regressive phase starting from a blocky sand unit at the bottom of the section, followed by intercalating layers and streaks of sand and shale. Other papers discussing the depositional history of the Ghadamis Basin include Imsalem et al. (2018 a, b).

3.2. Methodology

To assist with the interpretation of the depositional environment of the Lower Akakus Formation in Ghadamis Basin, we have standard well logs (i.e., gamma ray and resistivity), drill core, and Formation Micro-Imager log (FMI). For this study, 3-D geomodeling was performed using Schlumberger's Petrel© software (2016), while the detailed lithology and mineralogy was done with MinInversion (Amosu and Sun, 2018).

The workflow for the geomodelling in Petrel© is as follows. Once all the data is collected and imported into Petrel©, a facies is assigned to each sample depth at 30 cm or 0.5 ft. using a rule-based system. The rule-based facies classification has three classes: shale, siltstone,

and sandstone. This rule-based classification scheme relies mostly on gamma ray (GR) values, so if GR < 95 American Petroleum Institute units (API) the facies is considered sand, while GR between 95 and 105 API is considered silt and any GR > 105 is considered shale. Then effective porosity (ϕ_e) is calculated using the formula: $\phi_e = \phi_t(1 - V_{sh})$. In the formulation for ϕ_e, $\phi_t$is total porosity and V_{sh} is shale volume (calculated from facies class). After effective porosity is calculated, then water saturation (Sw) is calculated using a form of Simandoux's equation (Simandoux, 1963) where *F* is a formation factor for clean sands *($F = a\varphi^{-m}$)*, V_c is the volume fraction of clay in solid matrix, R_c is the resistivity of the clay, and Q_c is the effective clay conductivity (Lee, 2006). $\left(\frac{\emptyset^m}{a.Rw}\right) SW^n + \left(\frac{Vsh}{Rsh}\right)$ SW - $\frac{1}{Rt}$ = 0. Finally, Petrel© has a module for building 3-D models of facies, effective porosity, and water saturation based on the well logs and the calculated values for effective porosity, and water saturation. Furthermore, Petrel© was used to construct cross-sections and flattened 2-D surfaces based on interpreted stratigraphic boundaries (Figure 3.3). In shaly sands the water saturation is calculated following the method of Bardon and Pied (1969), $\frac{1}{Rt} = \left(\frac{\emptyset^m . SW^n}{a.Rw}\right) + \left(\frac{Vsh.SW}{Rsh}\right) = 0$ as shown in Equation 4 of (Simandoux, 1963). Production test data and lithology facies data match with facies derived using the equations. Sedimentary structures, such as cross laminations, and facies analysis are included to get the complete picture of the depositional environment model. FMI data were useful in the determination of the types of sedimentary features and depositional setting of core data as well (Figure 3.5).

The detailed workflow for using MinInversion is described in Amosu and Sun (2018), as well as in Imsalem et al. (2018b). The open-source program, MinInversion, is flexible as it allows the user to select the compositions (minerals and porosity) to be estimated. It is an open-

source program for estimating rock mineralogy from standard digital geophysical wireline logs on a routine basis. In its most basic form, MinInversion is a solver for linear equations and offers a number of matrix inversion methods, such as least squares, LU-decomposition, and Moore-Penrose generalized inverse methods. Generally, MinInversion works well as long as basic well logs like gamma ray, neutron, density, and PE logs are available, which we had for B1 and H1 wells as shown in Imsalem et al. (2018b). Here, we use MinInverstion to predict the porosity, mineralogy and lithology of the B1 and H1 wells from wireline logs.

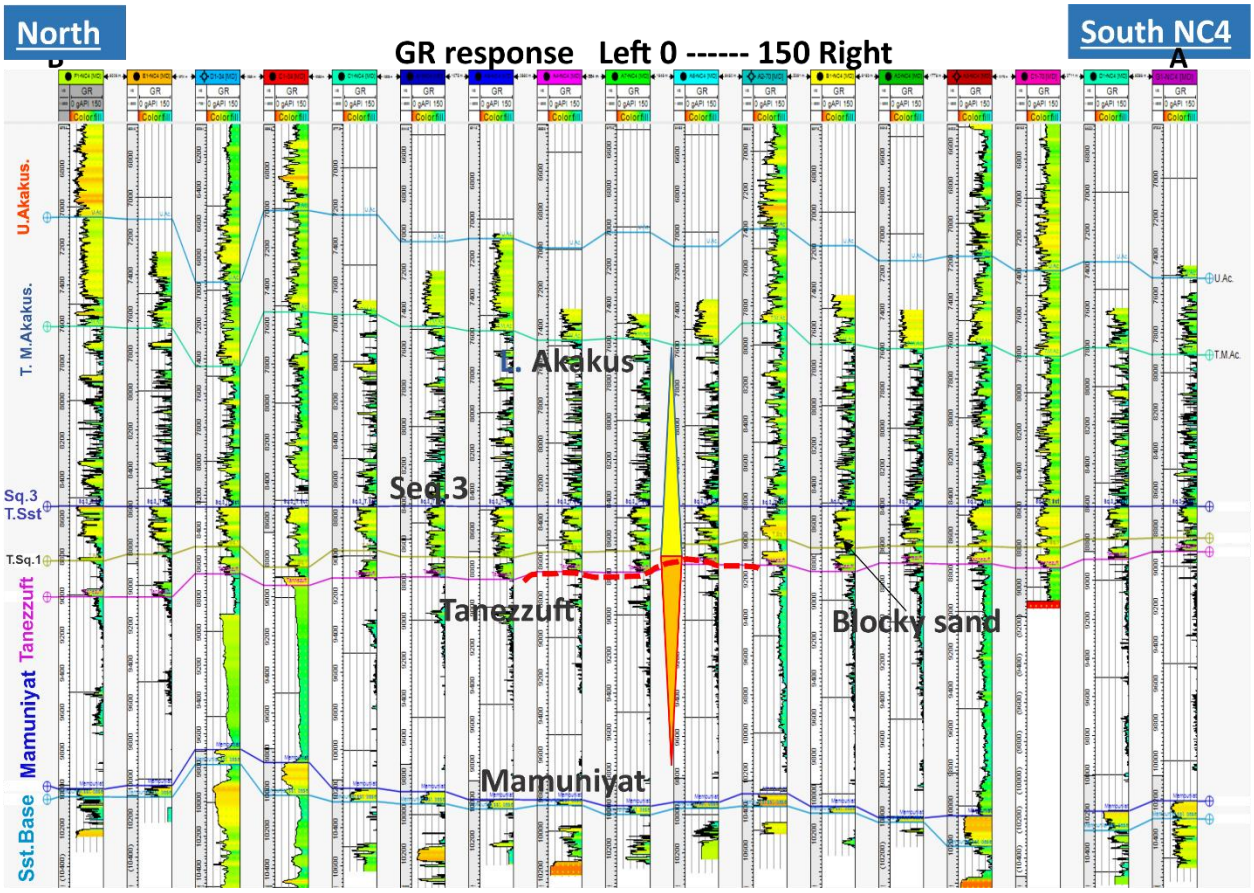

Figure 3.3: A cross-section, consisting of vertical wells, showing the to lateral correlation throughout the area of Ghadamis Basin using gamma-ray log response from South to North.

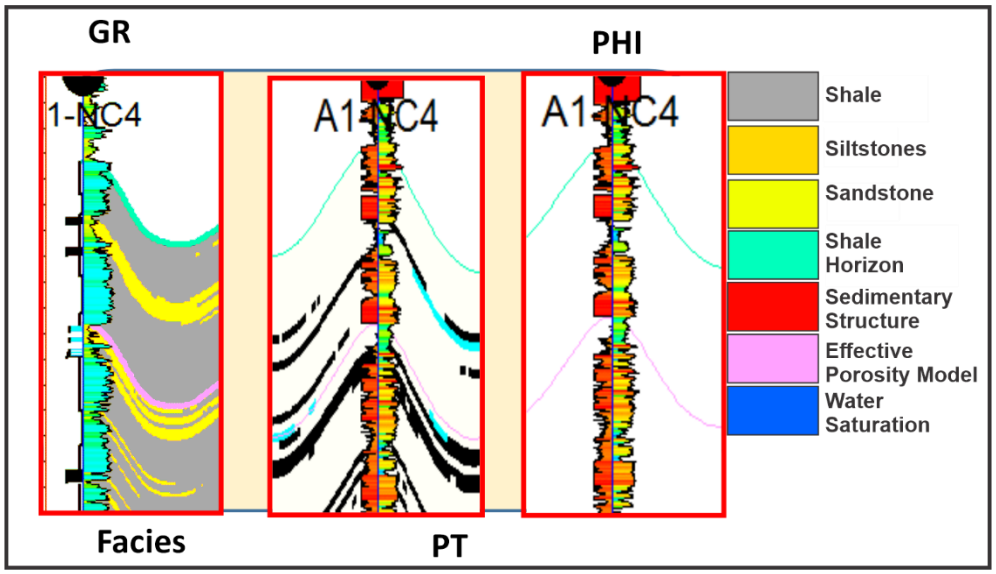

Figure 3.4: Different displays of the same well in the concession. (A) Well log displayed with horizons using gamma ray log (GR); (B) well log with production test (PT) data; (C) well log displayed with facies modeling. Phi is porosity in well-logs.

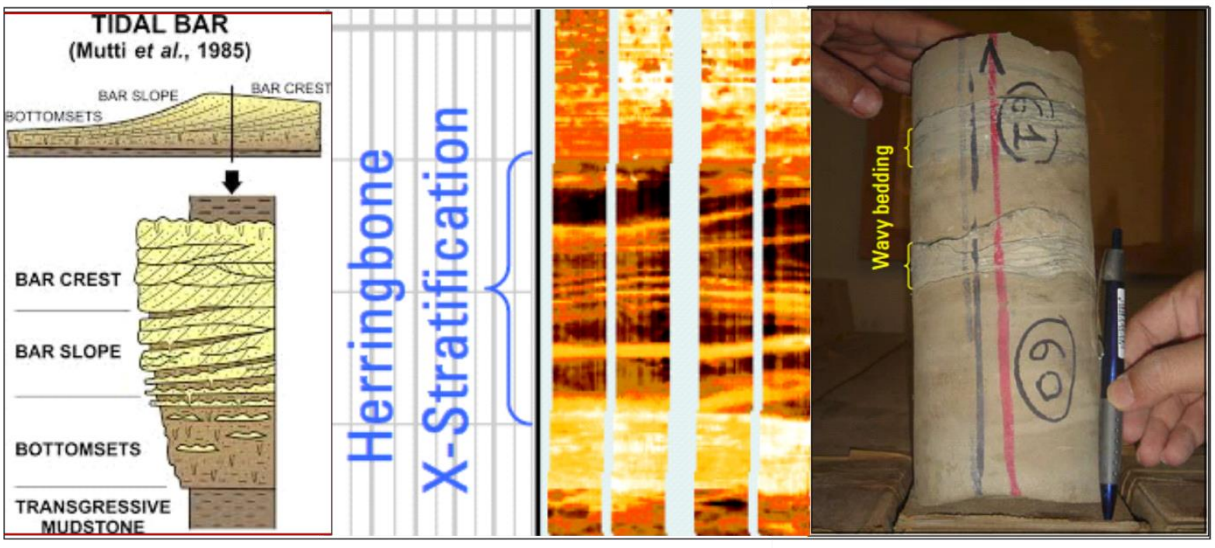

Figure 3.5: Example of sedimentary structures as viewed in FMI well log (left side) and drill core (on the right). The FMI log shows herringbone cross-stratification while the drill

has an example of wavy bedding. Both the drill core data and FMI log were made available courtesy of AGOCO Core Lab.

Some sedimentary structures, such as tidal cross bedding, can be identified from different well localities in the area (Figure 3.8). Tidal sand-waves have morphologies that reflect the imbalance between the two opposing tidal flows. The ripple cross-laminated sand breaks up the pattern by interlaminations and lenses of finer grain sediment (silt and mud). Where sand dominates, this is categorized as flaser bedding, but if there is a continuous gradation in the proportions of sand and finer-grain sediment, the sample is categorized as wavy bedding. Herringbone cross-bedding occurs predominantly in the shallow subtidal zone because of periodic reversals in the current direction due to tidal cycles (Collinson et al., 2006).

Previous production data provides useful information in several ways. First, the data have been used to determine the possible and best-fit perforation design in oil and gas well drilling. Second, results of effective porosity equations using the shale volume, the total porosity and water saturation formula have been used to calibrate available test data, and to model it in Petrel©. Finally, these data have been used in computing 3D reservoir properties (Figure 3.6). It is useful to utilize flattening techniques in Petrel© software at different levels within the model. Different slices reflect different intervals, and in the interim, these intervals depict the vertical changes in the depositional environment.

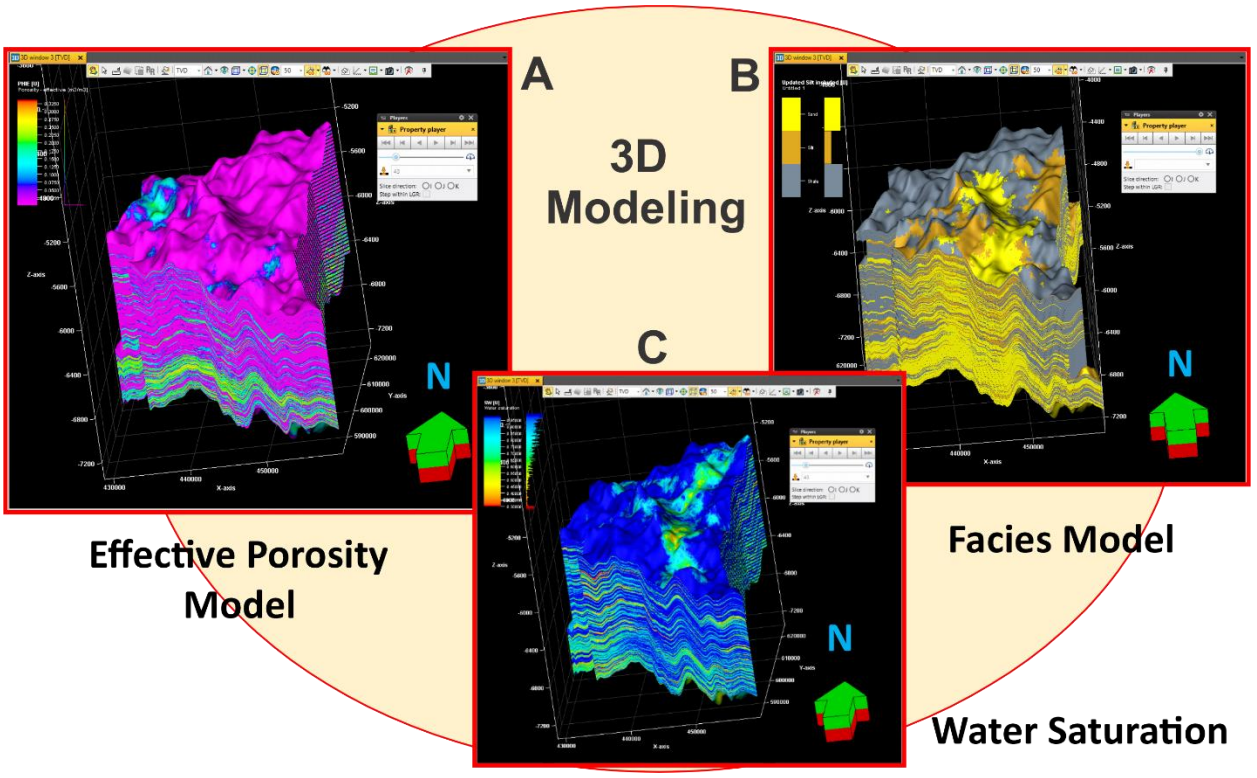

Figure 3.6: The main steps of 3D property modeling, from data generation, using a calculation which includes (A) effective porosity (mostly pink color), (B) facies distribution (gray, orange and yellow colors), and (C) water saturation (SW): blue, green and turquoise colors).

3.3. Results

We perform several iterations of property modeling and structural modeling. This involves dividing the model into numerous layers and zones which requires lots of computer power. The well cross-section is characterized using classical subdivision of the lithofacies in the area. We observe distinct sequences; the lower sequences are thick sand units with minor shale streaks at the top. The upper sequence has more shale with minor sand laminations (Figure 3.8; Figure 3.6).

Figure 3.7: Core showing two shale – sand depositional cycles and examples of cross-bedding from cores. On the left image, the first depositional cycle begins with the lower dark distorted shale layer and middle light sand layer. It ends below the upper dark, distorted shale layer. The second depositional cycle includes the upper dark distorted shale layer and the overlying light sand layer. Wavy to flaser cross-bedding types occur in some wells in the study area.

There are three main sand packages defined in the Akakus reservoir. These types of Akakus packages can be classified into lower, middle, and upper Akakus respectively. These packages can also be observed using petrophysical composition analysis (Imsalem et al., 2018b; Aimen et al., 2020). The lower packages are characterized by high porosity although they are poorly tested and production information is not available. The middle package is classified as a moderately porous section, but it has relatively lower porosity compared to the lower package. The upper package has very little porosity with the exception of some thin streaks with high

porosity. The upper package unexpectedly has a higher production rate than the others, probably due to the imprecision in selecting the proper intervals for the production test.

From property modeling, we generate a facies model, an effective porosity model, a water saturation distribution model (Figure 3.6), and a production test result distribution model. The facies model gives a better understanding of the vertical and lateral facies variations (Figure 3.9). The porosity and water saturation models reveal the 3D distribution of these properties. The models enable the generation of different thickness maps specifically for different facies.

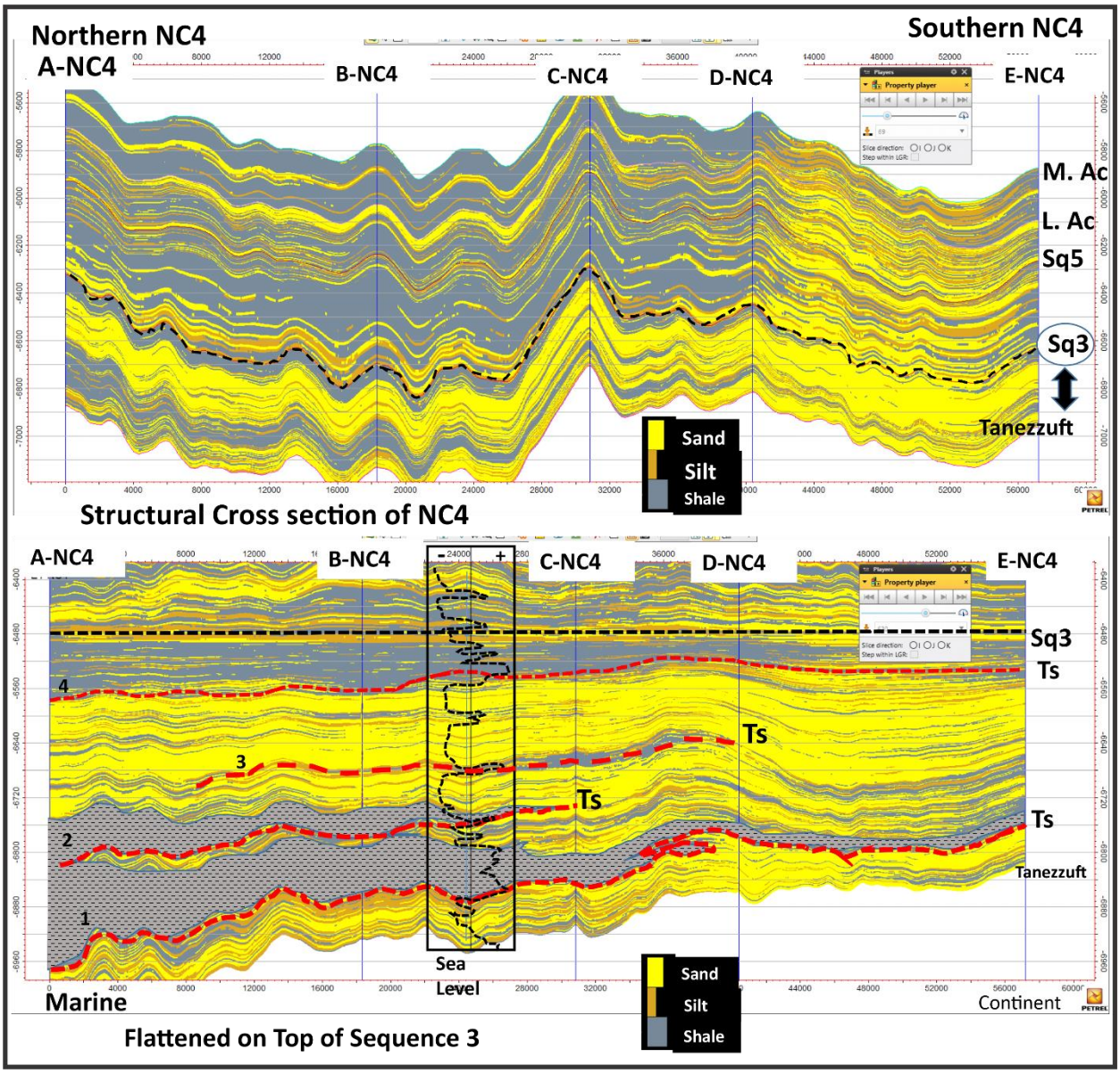

Figure 3.8: Cross-section from south to north of the study area, facies changes displayed in a structural datum, while in the top section the lower part is flattened with exaggerated view. The red lines are the contact lines between facies change. The Petrel software has a feature allowing to flatten any given horizon like in the black dotted line above.

Figure 3.7 shows a net thickness map generated from the 3D property model and preliminary identification of a prospect. Assessing the dangers of oil and gas well drilling connected with the identified petroleum oil and gas prospects will require more research.

3.4. Discussion

The structural cross-section in the area of study reveals scant information about the depositional environment. To understand it better, we subdivide the facies into different categories such as distal mouth bar facies, proximal facies, and channel distributary (Elfigih, 2000), established from preliminary observations of the different sedimentary features from reports, outcrops, and core data. Combining core analysis and FMI interpretation with property modeling gives a better overview of the basin. Property modeling involves creating and filling cells of a 3D grid with discrete or continuous geological properties. The goal is to use all geological information available to build a realistic property model. Depositional environment integration helps in building one complete panoramic view of the area, enabling us to envision larger scale features of the Akakus Formation.

Some wells have very distinct sedimentary structures, including wavy cross-bedding, flaser bedding, herringbone cross stratification, and hummocky cross stratification, suggesting bimodal currents (Elfigih, 2000). Several well reports from the area show that the major trend of the paleocurrent is in the NW-SE direction (Acheche, 2001). Both tidal bundles and bioturbation are present with some reactivation surfaces; all these features indicate a shallow marine depositional setting and tidal influence in the area. There is also evidence of regressive cycles from the lower to the upper part of the section (Bishop, 1975).

Variations observed reflect the changes in time in response to dynamic marine and continental interactions. For example, shale and fine-grained sediments indicate marine deposits while coarse-grained sand units indicate proximal facies. In the area of interest, the shale and fine-grained materials most likely come from the southwest and also from the northwestern part of the area, while on the other hand, the coarse-grained sediments are sourced from the east and northeast of the area (Aiman, 2020).

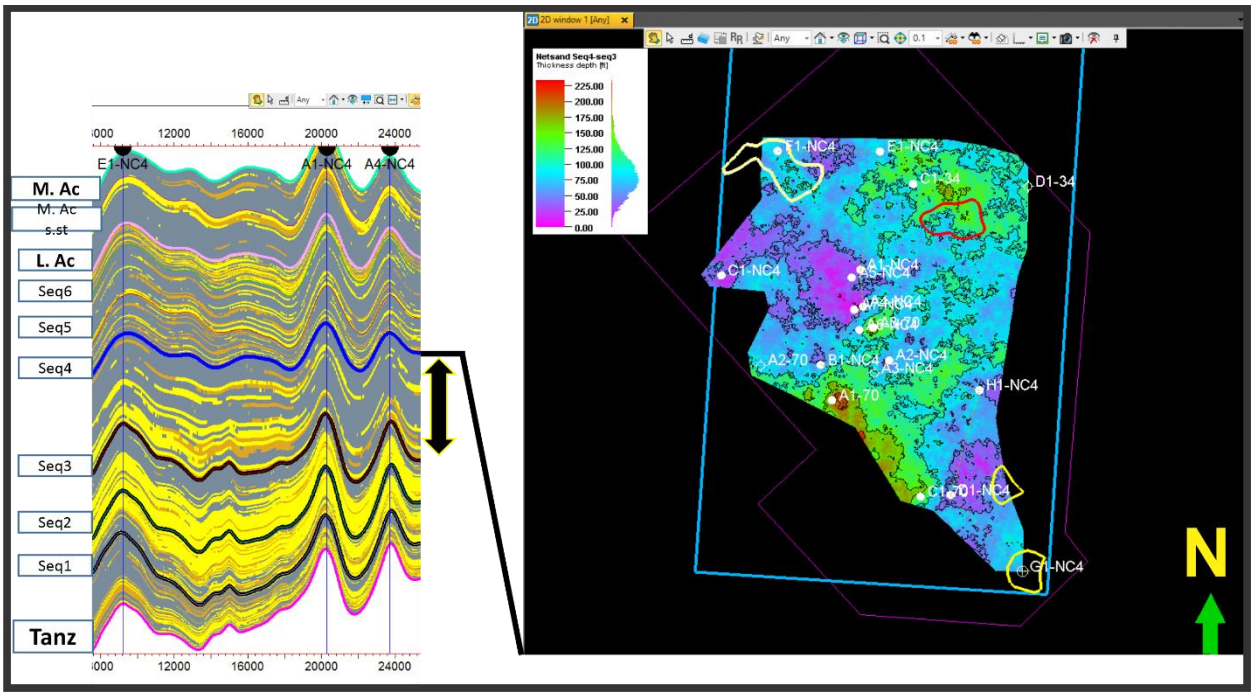

Figure 3.9: Net sand thickness (red color indicates the highest sand thickness and the purple color indicates the lowest sand thickness in the well drilled) at the boundary of sequence 4 and preliminary prospects identification. Color scheme as in Figure 3.6.

Based on facies changes and subdivisions of the section into sand and shale layers, the boundaries of each surface of these layers are considered as localized depositional events,

whereas the change in the layers reflects change in the depositional dynamics of the area. The surfaces between these depositional cycles can be delineated to construct sequence stratigraphic packages or sets (Figure 3.7). The base of the Lower Akakus reservoir is represented by a regressive surface of coarse sand unit that is terminated below by underlying deep marine shale. This scenario of lithological change is repeated throughout the whole section. One of the applied techniques in the property model is to examine the section using horizontal slicing display, which enables visualizing lateral variation of internal facies. This same method can be applied in seismic slicing of the 3D cube as well, but instead of displaying seismic attributes or reflection amplitudes, the property displays the facies with its contents in lateral and vertical view. Horizontal property slicing reveals some lateral facies variation features. One of these features is a NE-SW trending channel. The gradual facies change from proximal into distal delta is also identified. This change is associated with sedimentary structures, including wavy cross-beds, tidal bundles, and reactivation surfaces in some of the core data. All of these features indicate bimodal current activities in the area (Elfigih, 2000).

Well-to-well correlation in the basin shows a change from sand to shale lithology. The blocky GR response at the base of the section represents the highest porosity section. This section was not a target interval before this study. More studies are needed to explain the reason for discordance between high porosity layers and inefficient production test results.

3.5. Summary

The intercontinental Ghadamis Basin in northwest Libya is one of the most prolific hydrocarbon basins in North Africa, and the Silurian Lower Akakus and underlying Tanezzuft

formations represent one of the most productive source rock - reservoir pairs in the region. The primary source rocks of the Silurian system in the Ghadamis Basin is the radioactive, organic-rich shale (the 'hot shale') at the base of the Tanezzuft Formation. Layers of intercalated thin beds or lenses of sand and shale in the overlying Lower Akakus Formation form the reservoir. By integrating well logs and seismic data, we developed a three-dimensional (3D) property model of the Lower Akakus reservoir. This model combines comprehensive depositional environment characteristics with seismic attributes and petrophysical properties for petroleum system interpretation.

The depositional environment of the Silurian Lower Akakus Formation of the Ghadamis Basin represents a transition from a wave-dominated to a tide-dominated delta. Two types of cross-bedded sedimentary structures suggest a tide-dominated delta, clear herringbone structures, and large-scale hummocky cross-stratification. Wavy and flaser bedding also appear. The coarsening upward cycles of the Lower Akakus indicate sea-level regression. However, minor transgression events also occurred in the Ghadamis Basin at that time.

We computed petrophysical properties (porosity, permeability, and saturation) for the three-dimensional (3D) reservoir rock volume of the Silurian Lower Akakus Formation. The finalized model enables us to characterize the petroleum system. This three-dimensional model shows this record of the petroleum system elements as well as the processes of hydrocarbon migration and accumulation. Based on our results, we identify three zones in the modeling analysis for future exploration.

3.6. References

Acheche, H., M., A. M. Rabet, H. Ghariani, A. Ouahchi, and S. L. Montgomery, 2001, Ghadames Basin, southern Tunisia, A reappraisal of Triassic reservoir and future prospectively. AAPG, p. 766-767.

Amosu, A., and H. Mahmood, 2018, PyLogFinder: A Python Program for Graphical Geophysical Log Selection: Research Ideas and Outcomes, v. 4, doi:10.3897/rio.4. e23676.

Amosu, A., and Y. Sun, 2017, WheelerLab: An interactive program for sequence stratigraphic analysis of seismic sections, outcrops and well sections and the generation of chronostratigraphic sections and dynamic chronostratigraphic sections: SoftwareX, v. 6, p. 19–24, http://doi.org/10.1016/j.softx.2016.12.003.

Amosu, A., and Y. Sun, 2018, MinInversion: A Program for Petrophysical Composition Analysis of Geophysical Well Log Data: Geosciences, v. 8, no. 2, p. 65, doi:10.3390/geosciences8020065.

Baayou, M., 2013, basin modeling of selected Libyan basins, Petronas University MSc thesis.

Bardon, C., and B. Pied, 1969, Formation Water Saturation in Shaly Sands. Petroleum Transactions of the SPWLA, p. 19-21.

Bishop, W. F., 1975, Geology of Tunisia and adjacent parts of Algeria and Libya. AAPG bulletin, v. 59, p. 186.

Magloire, P. R., 1970, Triassic gas field of Hassi er R'Mel, Algeria1: Geology of Giant Petroleum Fields, doi:10.1306/m14368c26.

Bellini, E., and D. Massa, 1980, A Stratigraphic Contribution of the Paleozoic of the Southern Basins of Libya, in The Geology of Libya Volume I, Edi, Salem and Busrewil, Academic Press Inc. USA, p. 6-8.

Collinson, J., N. P., Mountney, Thompson D., 2006, Sedimentary Structures, Terra Publishing, third edition, p. 104.

Dardour, A. M., Boote R. D, and Baird A. W., 2004, Stratigraphic Controls on Palaeozoic Petroleum Systems, Ghadames Basin, Libya, Journal of Petroleum Geology, Vol. 27(2), April 2004, p. 141-162.

Echikh, K., 1992, Geology and Hydrocarbon Potential of the Ghadamis Basin. Internal Report, National Oil Corporation of Libya (NOC), Tripoli.

Echikh, K., 1998, Geology and Hydrocarbon Occurrences in the Ghadamis Basin, Algeria, Tunisia, Libya. In: Hallet, D., 2002, Petroleum Geology of Libya. Elsevier B.V. (1st edition, 2nd Impression 2004). p. 113. P. 106.

Echikh, K., and M. A. Sola, 2000, Geology and Hydrocarbon Occurrences in the Murzuq Basin, SW Libya, Elsevier Science, Geological Exploration on Murzuq Basin, M.A. Sola, and D. Worsley, editors.

Hallett, D., 2004, Petroleum Geology of Libya, Elsevier, 2nd impression, p. 52-59, 125, p. 144-172, p. 277-281.

Hammuda, O. S., 1980. Geologic Factors Controlling Fluid Trapping And Anomalous Freshwater Occurrence In The Tadrart Sandstone, Al Hamadah Al Hamra Area, Ghadames Basin. In : Salem M. J. and Busrewil, M.T.(Eds) 2nd Symp. The Geology of Libya. Al-Fatah Univ., Fac. Sci., Tripoli, II, 501-507.

Imsalem, M., Olszewski T, Raymond A. 2018a. Pollen and Multivariate Analysis from Ecological and latitudinal gradients in Morocco. Poster presented at: 52nd Annual Meeting of the Geological Society of America; March 12-13; Little Rock Marriott, Arkansas, AR.

Imsalem, M., Zobaa M. K, Raymond A. 2018b. Palynomorph identification and Preliminary Palynostratigraphy of the Silurian Tanezzuft and Akakus Formations in the Libyan Ghadames Basin. Poster presented at: 130th Annual Meeting of the Geological Society of America; 2018; 4-7 November; Indianapolis, IN.

Imsalem, M., A. Amosu, M. Wehner, A. Raymond, and Y. Sun, 2018c, Reservoir Quality Assessment of the Lower Acacus and Tannezuft Formations in the NC4 Block, Ghadames Basin, Libya, GCAGS Transanctions, Vol. 68, Pages 255-268.Magloire, L., 1968, Étude Stratigraphique Par La Palynologie Des Dépôts Argilo-Gréseux Du Silurien Et Du Dévonien Inférieur Dans La Région Du Grand Erg Occidental (Sahara algérien), in: International Symposium on the Devonian System, Volume 3, Calgary, 1967, Proceedings, p. 473–491.

Magloire, P. R., 1968, Triassic Gas Field of Hassi er R'mel, Algeria: Abstract: AAPG Bulletin, v. 52, doi:10.1306/5d25c375-16c1-11d7-8645000102c1865d.

Rusk, D. C., 2001, Libya: Petroleum potential of the underexplored basin centers—A twenty-first-century challenge, in M. W. Downey, J. C. Threet, and W. A. Morgan, eds., Petroleum provinces of the twenty-first century: AAPG Memoir 74, p 440.

Selley, R. C., 1997, Chapter 3 The Sirte basin of Libya: Sedimentary Basins of the World, p. 27–37, doi:10.1016/s1874-5997(97)80006-8.

Simandoux, P., 1963, Dielectric measurements on porous media, application to the measurements of water saturation: study of behavior of argillaceous formations, Revue de l'Institut Français du Pétrole, v. 18, p. 93-215.

Lee, M. W., and T. S. Collett, 2006, A method of Shaly sand correction for estimating gas hydrate saturations using Downhole Electrical Resistivity Log Data: Scientific Investigations Report, doi:10.3133/sir20065121.

4. NEW CHITINOZOANS AND PALYNOSTRATIGRAPHY OF THE SILURIAN TANEZZUFT AND AKAKUS FORMATIONS IN THE GHADAMIS BASIN, LIBYA

4.1. Abstract

Silurian sediments in the Ghadamis Basin of northwest Libya accumulated after glacial melting in the Late Ordovician, and consist of both the Tanezzuft and the overlying Akakus formations. Due to the repetitive lithology of the middle and upper parts of the Tanezzuft Formation and the Akakus Formation, cores and outcrops are difficult to correlate across the basin. In this contribution, we use AGOCO (Arabian Gulf Oil Company) correlations to assign sediments from three Ghadamis Basin cores to the upper part of the Tanezzuft Formation (Tan III) and to the lower, middle and upper units of the Akakus Formation, and investigate the palynoflora of 73 sediment samples from Tan III and the Akakus Formation. Of these, 22 samples yield marine chitinozoans, acritarchs and spores. The presence of *Cingulochitina* cf. *bouniensis* and *Ephanisporites protophanus* in Tan III suggests a middle Silurian (Wenlock) age for this unit. *C.* cf. *bouniensis* indicates a Wenlock age and *E. protophanus* indicates a late Wenlock (Homerian) age. Based on palynomorphs, the lower Akakus unit appears to be Wenlock or later in age. We can not date the middle Akakus unit, however the based of the upper Akakus unit may range into the Ludlow. Using AGOCO well-log data for the C1-34 core, we tentatively place samples 22 and 23 of Richardson and Ioannides (1973) at the base of Tan II, the middle unit of the Tanezzuft Formation. These samples appear to be late in the early Silurian (Telychian) or middle Silurian (Wenlock). We tentatively place samples 21 -19, of Richardson and Ioannides (1973) in Tan III. These samples appear to be late Wenlock (Homerian) in age, slightly younger than our Tan III samples. We confidently place samples 13 – 18 from the C1-34

core, the middle assemblage of Richardson and Ioannides (1973), in the lower Akakus unit. These samples appear to be late Wenlock (Homerian) through early Ludlow (Gorstian) in age. Although Richardson and Ioannides (1973) identified samples 1 – 12 of the C1-34 core as coming from close to the Akakus/Tadrart boundary, these samples come from the base of the upper Akakus unit and indicate a late Silurian (Ludlovian) age. Samples 18 a-c of Richardson and Ioannides (1973) from the B2-34 core could be late Wenlock (Homerian) to latest Silurian (Pridoli) in age. These samples appear to come from the upper Akakus unit, however their position relative to the Akakus/Tadrart boundary remains unknown.

Keywords — Silurian; Palynomorphs; Chitinozoans; Ghadamis Basin; Tanezzuft; Akakus Formations; and Well-Logs.

4.2. Introduction

The Ghadamis Basin is an intracratonic sag basin in Libya, on the northern coast of Africa (Figure 4.1). During the Ordovician and Silurian, the Ghadamis Basin, which formed on the paleocontinent of Gondwana, lay in the southern high latitudes, at approximately 60 to 70 degrees South paleolatitude, where it may have remained through the mid-Silurian (Stampfli et al., 2013; Scotese, 2014), or moved northward to approximately 45 degrees South paleolatitude by the mid-Silurian (Cocks and Torsvik 2020; Torsvik and Cocks, 2013; Domeier, 2016; Appendix Table A-1). Today, the Ghadamis Basin lies close to the coast of Africa. However, in the Early Paleozoic, crust that is now part of the Mediterranean Sea as well as the Iberian Peninsula, Italy, Sicily, most of France, southern Germany, the Czech Republic (Bohemia), and the Balkans was attached to the North coast of Gondwana, separating the Ghadamis Basin from the Rheic Ocean (Scotese, 2014; Torsvik and Cocks, 2013; Stampfli et al., 2013; Figure 4.2).

During the late Mid-Late Ordovician, glaciers covered much of Gondwana and many peri-Gondwana terranes have glacio-marine sediments (Pope and Steffan, 2003; Le Héron et al., 2018). Le Héron et al. (2018) placed the boundary between glaciated and unglaciated shelf near the Ghadamis Basin and interpreted the Late Ordovician Mamuniyat Formation, which outcrops around the rims of in the Murzuq and Ghadamis Basins of Libya, as glacio-marine. In western Gondwana (South America), glaciation continued into the early Silurian (Rhuddanian). Using stable isotopic data, Finnegan et al. (2011) suggested that the late Ordovician sea-level rise represents only partial deglaciation of Gondwana (Figure 4.2). However, by this time, glaciers had disappeared from North Africa and the associated peri-Gondwanan terranes, and organic-rich 'hot shale', which serves as major petroleum source rocks, accumulated in the Ghadamis Basin (Lüning et al., 2000).

The mudstones beds of the Ghadamis Basin contain a diverse assemblage of organic-walled microfossils, including chitinozoans, and spores of early land plants (both cryptospores and vascular land plant spores). However, correlation of these strata within the Ghadamis Basin and between the Ghadamis Basin and Silurian strata from other parts of Gondwana, the peri-Gondwanan terranes, and other paleo-continents has proven difficult due to their repetitive lithologies and the absence of distinctive sedimentary beds. Chitinozoan species have distinctive morphologies, short stratigraphic ranges, and wide paleogeographic distributions independent of facies, as well as the potential for retrieval even with small sample quantities, making them ideal for Silurian biostratigraphic correlation (Verniers et al., 1995). Here, we present the geological and palynological results of a study of chitinozoans in 22 core samples recovered from the Silurian Tanezzuft and Akakus formations of three oil wells (C1, B1, and H1) drilled in the Ghadamis Basin in northwest Libya (Figure 4.1). While this study focuses on chitinozoans, we

also use acritarchs, cryptospores and land-plant spores to determine the stratigraphic age of the Tanezzuft and Akakus formations. In addition, we provide the taxonomy of the chitinozoan taxa encountered in Ghadamis Basin sediments as a result of this study.

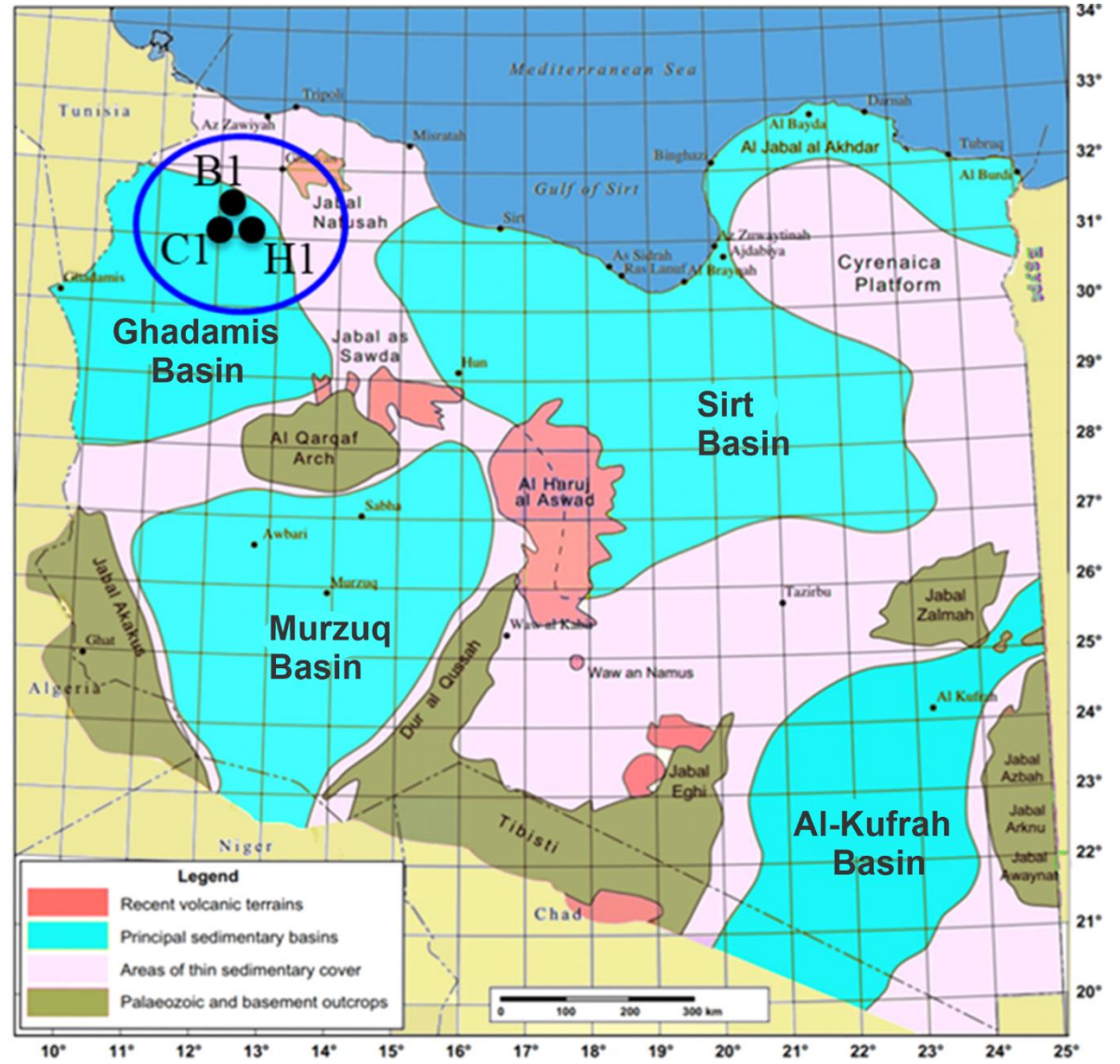

Figure 4.1: Map that shows the Ghadamis Basin (blue circle) in the northwestern flank of Libya as well as the other famous Libyan Basins. The large black dots are for the wells

used in this study and are contained within the concession block, NC4. Modified from Hallett (2016).

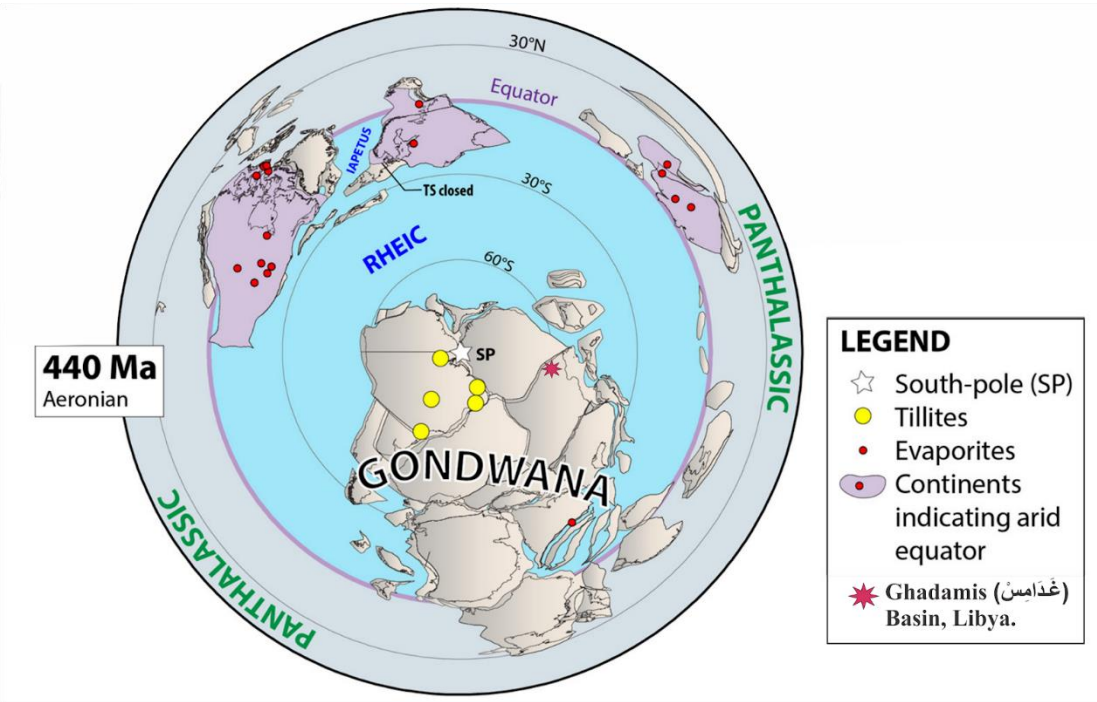

Figure 4.2: The Silurian Paleogeography during the Aeronian epoch (~440 Ma) was a cold period that included remnant glaciation from the end of the Ordovician. Yellow dots designate Silurian tillite deposits. The Ghadamis Basin of Libya lay at 60º South. Modified from Cocks and Torsvik (2020).

4.3. Background – Stratigraphy

The Ghadamis Basin lies close to the Mediterannean coast, to the north of the Al-Qarqaf arch, which separates it from the Muzurq Basin, and to the east of the Sirt Basin (Figure 4.1). Sediment accumulation in the basin began during the Cambrian and continued into the Ordovician. The Late Ordovician Mamuniyat Formation contains glacio-marine sediments (Le Héron et al., 2010; Moreau, 2011). The exact relationship of the Mamuniyat Formation to

glaciation and deglaciation remains ambiguous, but (Le Héron et al., 2018) interpreted Mamuniyat sediments as either tunnel valley or interfluival deposits. In the Ghadamis Basin, paleo-valleys, filled with sediments not preserved elsewhere, occur in the Mamuniyat Formation (Le Héron et al., 2018). These localized sediment bodies, which date to the latest Ordovician, are listed under a number of different stratigraphic formations in North Africa (Hodairi, 2012; Hallet, 2016). In the Ghadamis Basin, the Ordovician "Bi'r Tlacsin" unit, referred to as the "Argile Microconglomeratic" unit in Algeria, is one of these units (Hodairi, 2012). The Iyadar Formation near Ghat, Libya in the Murzuq basin might be equivalent (Mass and Jaeger, 1971; Hallet, 2016). The C1 well in our study is the type well for the "Bi'r Tlacsin" unit in the Bi'r Tlakshin field, which consists mostly of conglomeratic mudstones with occasional sandstone beds; we consider the B'ir Tlacsin unit to belong to the Mamuniyat Formation (Hallet, 2016: Figure 4.3; Figure 4.4).

Following deposition of the "Bi'r Tlacsin" unit of the Mamuniyat Formation, the Tanezzuft and Akakus formations, including the 'hot shale' at the base of the Tanezzuft Formation, accumulated in the Ghadamis Basin, beginning in the Rhuddanian (early Silurian) and continuing into the Pridoli (Late Silurian; Le Héron et al., 2013; Imsalem et al., 2018b; Figure 4.3, Figure 4.4). The Tanezzuft Formation consists of a thick sequence of mudstones and sandstones up to 463 m thick (1510 ft thick), sourced primarily from the southeast, which records progradation of a delta that migrated from the southeast to the northwest during the Silurian (Hallet, 2016). Whereas the Tanezzuft Formation consists primarily of prodeltaic mudstone, the overlying Akakus Formation is sandstone-prone and records various shallow marine sediment, deltaic, and fluvial deltaic depositional environments with increased terrestrial

input of Akakus Formation compared to the Tanezzuft Formation. The contact between the Tanezzuft Formation, which consists primarily of mud- and siltstone, and the Akakus Formation, which has more sandstone than the Tanezzuft, is gradational and reflects the time transgressive nature of the deltaic progradation of sands and mudstones (Lüning and Fello, 2006). The Ordovician sequence containing "Bi'r Tlacsin", and the Silurian sequence containing Tanezzuft and Akakus formations, is bounded at the top by a regional unconformity near the Silurian-Devonian boundary, which may reflect sea-level fall due to Late Devonian glaciation (Underdown et al., 2007; Hallet, 2016). However, the Silurian sequence is mostly complete in the center of the basin based on core samples, well-logs, and seismic data (Aimen et al., 2020). The lowest Devonian stratigraphic unit, the Tadrart Formation, consists mostly of sandstone.

The stratigraphy of the Tanezzuft and Akakus formations has been described, and a number of different stratigraphic schemes proposed based primarily on drill cores and well-log data (Elfigih, 2000; Dardour et al., 2004). Based on drill cores, Daniels et al. (1990) suggested dividing the Tanezzuft Formation into three units. We retain the divisions proposed by (Daniels et al. (1990) for the Tanezzuft Formation. However, we use the nomenclature of BEICIP (Bureau d'Études Industrielles et de Coopération de l'Institut Français du Pétrole) for the Akakus Formation. In their 1973 report, BEICIP subdivided the Akakus Formation into three members (see also Echikh, 1998 and Elfigih, 2017). Finally, although many variants exist (e.g., Tannezuft and Acacus), we use the spellings Tanezzuft and Akakus for these formations.

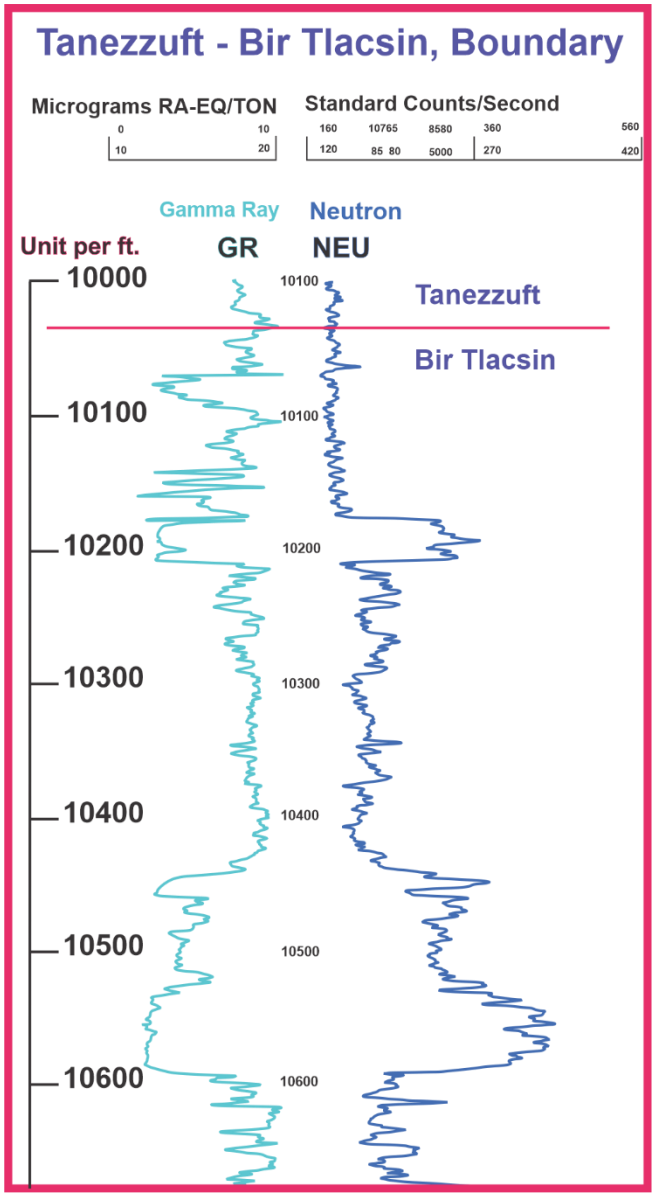

Figure 4.3: Well log showing the "Bi'r Tlacsin", or UO5 in Algeria, and its boundary with 'hot shale' of Tanezzuft Formation in the C1 well. This unit is approximately 100 m (330 ft) in and is reported to contain conglomerates, sandstones, and shales. The vertical scale is in feet.

4.4. Materials and Methods

4.4.1. Wells and Geologic Samples

We use core samples from three wells from the NC4 block of the Ghadamis Basin (Figure 4.1), currently on loan from the Arabian Gulf Oil Company (AGOCO) repository in Benghazi, Libya. These wells, referred to here as C1, B1, and H1, have well logs available for stratigraphic analysis and have been discussed in previous publications (Amosu and Mahmoud, 2018; Imsalem et al., 2018c; Figure 4.4, Figure 4.5). The data and samples supplied by AGOCO included original depth measurements recorded in feet, which we retain for accuracy, although we also report depths and thicknesses in meters. AGOCO provided well logs in LAS format, which is a file format designed for the interchange and archiving of lidar point cloud data, except for the C1 well logs, which had to be digitalized by the authors using Neuralog and exported to LAS format. We visualize well-logs using python version (3. 7. 8) and the *triple combo_plot* function, which allows us to select the top and bottom depths of the graph.

We collected 73 samples from the three wells, from the stratigraphic interval between 8123 - 8883 ft (2476.5 - 2708 m) in well H1, between 8035 - 9295 ft (2450 - 2834 m) in well C1, and between 9750 - 10500 ft (2973 -3200 m) in well B1. Of the 73 samples, 58 come from depth intervals corresponding to the Akakus Formation, and 15 from depth intervals corresponding to the Tanezzuft Formation based on stratigraphic picks from AGOCO (Figure 4.4, Figure 4.5). Figure 4.4 shows the relative position of samples within each well, and Figure 4.5 gives an example of a stratigraphic column with well logs for the H1 well. On average, we selected core samples at intervals of approximately 1 meter (3.28 ft). However, following Vodička (2019) when sandstone was the dominant lithology, we sampled from the adjacent shale layers.

To assist with stratigraphic and facies analysis, we prepared eight 46 x 27 mm thin sections (Figure A-1), discussed in detail in Imsalem et al. (2018). In addition, we analyzed 57

samples from the C1 well with XRD, and four samples semi-quantitatively with a Rigaku Miniflex 600 benchtop X-ray diffraction analyzer in the Department of Geology & Geophysics at Texas A&M University (Figure A-3). Twenty-two of the original 73 samples contained chitinozoans and form the basis for this biostratigraphic study. We also obtained SEM images for a sample from the C1 well (sample S5, 9282 ft). Phytoclast is an organic particle that is very small in size (1 to 1.5) μm. amorphous organic matter (AOM) is a brownish organic matter that is an important material of palynodebris.

4.5. Palynological Methods

4.5.1. Modified preparation Method using Zinc bromide and Centrifuge.

We processed palynological samples following Doher (1980) with two modifications. The first step in both modified processing protocols involved using a mortar to pulverize about 15 grams of each sample. After grinding, all subsequent processing occurred in a clean lab environment with filtered air, a fume hood, and polypropylene tubes.

For the first seven samples, instead of zinc chloride (ZnCl), we used zinc bromide (ZnBr) in 10% HCl with a specific gravity of 2.5 to separate chitinozoans (Imsalem et al., 2018c). Zinc bromide in HCl aqueous acid solution enables users to adjust the specific gravity as desired by means of sterile water and a hydrometer (approximately 2.5 for floating chitinozoans). In using ZnBr in 10% HCl, the two most important parameters are the solution's acidity and precise density. A density of 2.5 successfully separated chitinozoans, which varied between 20 and 2,000 μm in size. Using the centrifuge for a short interval (1,500 rpm for 10 min) concentrated this mixture and avoided any loss associated with a possible density shift in the dense liquid. We

repeated this step twice. Following concentration of the residue in the centrifuge, we rinsed the residue, first in water and finally in alcohol. We observed microfossils attached to framboidal pyrite with the residue at the base of the tube as predicted by Staplin (1960). Users should not discard the heavy portion without a thorough examination. We blended the resulting pellet with a few drops of 40% formaldehyde before preparing a glass slide with coverslip and mounted the slides using Canada Balsam as a natural mounting medium (Imsalem et al., 2018a). This method yielded usable spore assemblages and fragmented chitinozoans. Thus, we reprocessed all samples originally processed with this method using the second modified method, discussed below.

4.5.2. Modified preparation Method without zinc bromide or centrifuge.

Use of the centrifuge caused extensive damage to the chitinozoan microfossils in the first few samples, preventing identification of specimens that we probably could have identified before centrifuging the samples. Furthermore, use of zinc bromide for heavy liquid separation eliminated perfectly good microfossils and organic debris from the sample because they were attached to pyrite. Thus, we processed the remaining 66 core samples using the Doher (1980) technique but eliminated heavy metal separation and use of the centrifuge.

Following this method, the first treatment, a hot potassium hydroxide bath at 95˚C (10% KOH) deflocculated the heavy minerals and organic particles. To remove the large particles, we filtered the deflocculated material through a 300 μm mesh Nitex screen, which is a polycarbonate membrane made from synthetic nylon. We rinsed the samples in water, which is followed by a hot hydrochloric acid bath at 100˚C (40% HCl). This removes the carbonate cement and rock

fragments. After this, we again rinsed the sample in water and left it to settle for 4-5 hours to eliminate the carbonate rock. Next, we used a solution of 50% HF to dissolve the silicates and then allowed the solution to sit for 4-5 hours to allow the particles to settle by gravity. We homogenized the residue remaining using a manual stirrer. We retained this material in vials. In order to mount the 66 samples prepared using this method, we added P.V.A (Polyvinyl alcohol solution) to disperse palynomorphs, protect the residue from fungal attack, and keep the organic residue on the slide from coagulating. We spread the resulting residue on large glass microscope slides for examination and used Canada Balsam as a mounting medium for the slides. All 73 slides made for this study will be deposited into Benghazi University and the most significant slides stored in Halbouty 161 office at Texas A&M University.

4.5.3. Data Collection and Analysis

We made a preliminary scan of all 73 samples to identify the 21 samples that contained chitinozoans. For these 21 samples, we estimate the percentages of palynomorphs and different types of palynodebris, i.e. amorphous organic matter (AOM), generally interpreted as marine in origin, and phytoclasts, generally interpreted as terrestrial plant debris. We estimate percentages by scanning one mounted slide from each sample and counting the number of palynomorphs, AOM masses and phytoclasts in each field of view (FOV) at magnification of 50x using a Zeiss Axioplan 2 microscope with attached AxioCam HRC digital camera. At this magnification, each FOV is 440 µm wide. To make these estimates, we scan slides three times, one each to determine the the number of palynomorphs, pieces of phytodebris and clusters of AOM.

To determine the relative percentage of palynomorphs that belonged to terrestrial organisms (land plants and cryptophytes) and marine organisms (chitinozoans, acritarchs,

scolecodonts), we scan the slides a fourth time, and count the number of palynomorphs belonging to each category (land-plant spore, cryptospore, chitinozoan, acritarch, scolecodont) in each FOV at 50x. We identify the acritarch taxa present in each sample during this scan, but do not tally the relative abundance of acritarch taxa. We determine the relative abundance and identification of chitinozoans in a fifth scan of each slide.

Early Paleozoic palynomorphs tend to be sparse, sometimes yielding fewer than 10 to 20 palynomorphs in 15 grams of shale. Total palynomorph counts using our modified processing method without zinc bromide or centrifuging ranged from 14 to 137 palynomorphs in samples of approximately 15 grams (Table 4.1). For purposes of comparison, a rich modern sample produced by processing 15 grams of sediment generally yields more than 100 palynomorphs (Richardson and Rasul, 1990).

The terrestrial/marine index (t/m index) of each sample is the ratio of the percentage of terrestrial palynomorphs to the percentage of marine palynomorphs, in this case chitinozoans, acritarchs and scolecodonts (Prauss, 2001). We also report the terrestrial phytodebris/marine AOM index (phyto/AOM index), which is the ratio of the percentage of phytodebris to the percentage of AOM clusters for each sample. The marine percentage combines both the relative abundance of marine palynomorphs and marine AOM into the same statistic (Machado, pers. com. 2020). To obtain the marine percentage, we added the number of marine palynomorphs to the number of AOM clusters and divided by the total number of palynomorphs, AOM clusters and pieces of phytodebris in each sample (Machado, pers. com. 2020).

4.6. Results - Stratigraphy

4.6.1. Stratigraphic units of the Tanezzuft and Akakus formations

We subdivide the Tanezzuft Formation into three units, Tan I (which contains the 'hot shale'), Tan II, and Tan III (Daniels et al., 1990; Lüning et al., 2000; Figure 4.4). We subdivide the Akakus Formation into three units: lower Akakus, middle Akakus, and upper Akakus (Echikh, 1998; Elfigih, 2017; Figure 4.4; Figure 4.5). In our study area, we did not obtain any samples from Tan I and cannot assign any samples to Tan II conclusively. We use well logs and observations of core samples in hand specimens and thin sections, and XRD data to distinguish stratigraphic units from the upper part of the Tanezzuft (Tan III), and the Akakus formations. We describe Tan I and Tan II in minimal detail since we could not study the palynology of these units.

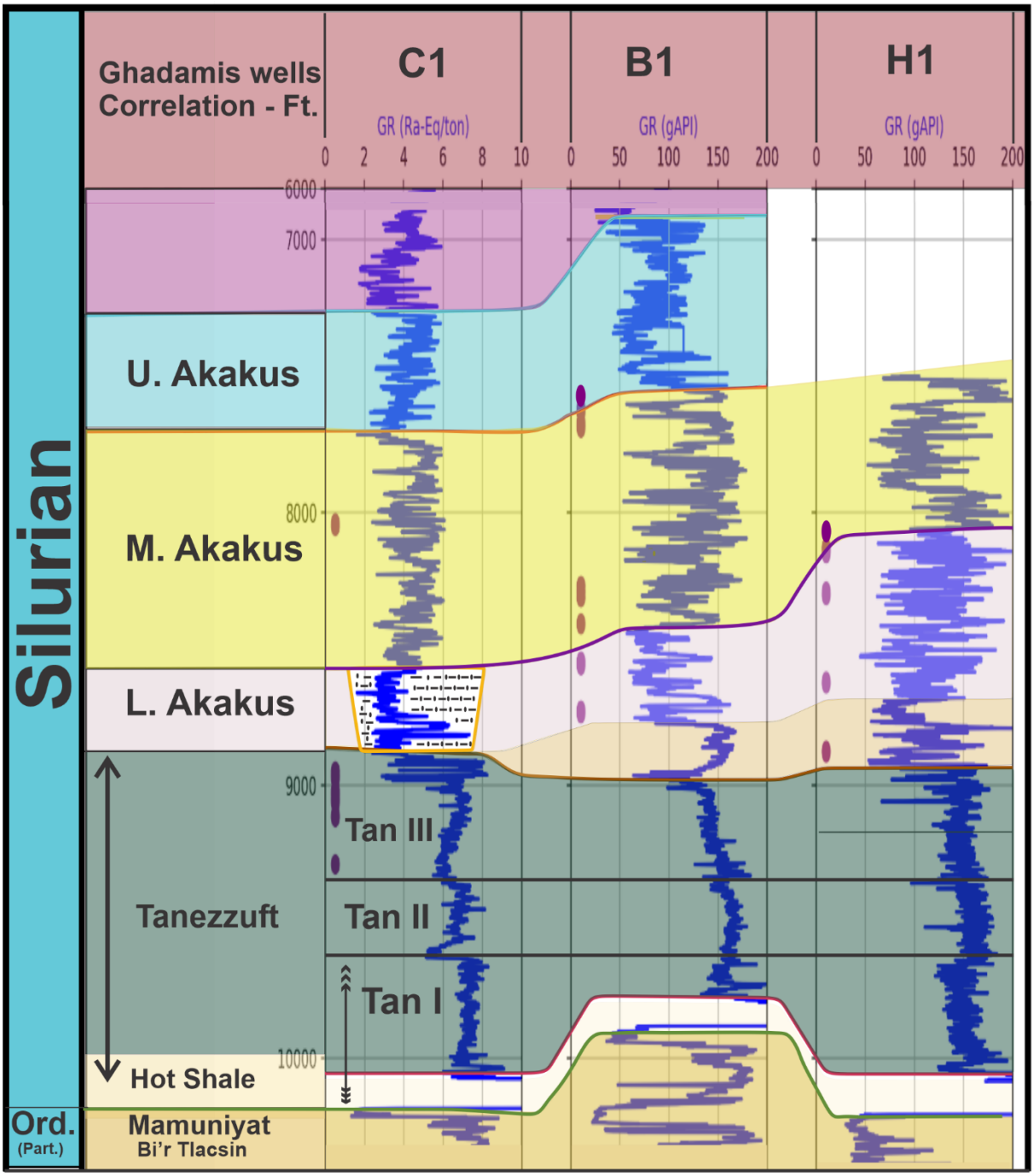

Figure 4.4: A stratigraphic correlation of four wells in the NC4 concession in Ghadamis Basin using Python Programming Language and primarily based on gamma-ray logs. All the gamma-ray values are in units of gAPI. Ghadamis correlation depicts the spatial similarity of stratigraphical samples taken for this study.

4.6.1.1. Lower part of the Tanezzuft Formation (Tan I)

Tan I includes the ‘hot shale’ at the base of the Tanezzuft Formation and the overlying dark grey to black, fissile, carbonaceous silty shales (Daniels et al., 1990; Imsalem et al., 2018c). The ‘hot shale’, consists of gray black, thinly laminated carbonaceous shale, exceptionally rich in pyrite with extremely high TOC (up to 17 wt %) and high uranium content, detectable in gamma-ray logs (Lüning et al., 2000; Figure 4.4, Figure 4.5), but does not occur throughout the basin (Hallet, 2016). The overlying carbonaceous shales have lower TOC (1 - 5 wt %, or 5 wt %) and less pyrite (Lüning et al., 2000). Tan I includes strata from 10215 - 9980 ft (3113 - 3041 m) in the C1 well, 9980 - 9883 ft (3012 - 3041 m) in the B1 well, and 10206 - 9695 ft (3110 - 2955 m) in the H1 well (Figure 4.4, Figure 4.5).

Although Daniels et al. (1990) described the basal ‘hot shale’ unit of the Tanezzuft Formation as part of Tan I, this unit, which is readily identifiable in gamma-ray logs, could be defined as a separate stratigraphic unit. A targeted study of the palynoflora of the ‘hot shale’ and of the overlying ‘cold’ shales with lower Ur content and gamma-ray values assigned to Tan I may help to resolve the status of the ‘hot shale’ as a separate stratigraphic unit (see Bucher, 2013).

4.6.1.2. Middle part of the Tanezzuft Formation (Tan II)

Above Tan I, Tan II consists of slightly fissile mudstone interbedded with sandstone layers (Daniels et al., 1990; Figure 4.4). Well-log gamma-ray signiture suggest that this unit occurs in all three wells; Figure 4.5 shows the log for the H1 well. Tan II has gamma-ray responses typical of shales in well-logs. Meinhold et al. (2016) described this unit as a “cold”

shale which has low gamma-ray values unlike the high gamma-ray values of the ‘hot shale’ at the base of Tan I. We could not assign any of the hand specimens to this unit with certainty. According to Daniels et al. (1990), Tan II includes Tanezzuft Formation strata from 9980 - 9610 ft (3041 - 2929 m) in the C1 well, 9883 - 9610 ft (3012 - 2929 m) in the B1 well, and 9695 - 8750 ft (2955 - 2667 m) in the H1 well (Figure 4.4).

4.6.1.3. Upper part of the Tanezzuft Formation (Tan III)

Tan III (Figure 4.6) consists of a mixture of well-sorted siltstone and fine-grained sandstones (Daniels et al., 1990). The siltstone layers have two different colors, medium to dark, gray-brown, and light to medium gray. Based on well-logs, Tan III occurs in all three wells; however, all Tan III samples in this study come from the C1 well. There are 15 hand specimens for palynofacies analysis, 14 of which have XRD data. The XRD results suggest an abundance of illite, kaolinite, quartz, and siderite. At least one hand specimen may contain significant muscovite, supported by the visual observation of silt-sized muscovite in some hand specimens. The XRD spectra suggest that some upper Tanezzuft samples contain pyrite (Figure 4.7; Plate III; Figure A- 2). Several SEM images of sample in C1 was also obtained (sample C1-S5, 9282 ft.). The organic-rich residue from lowest Tan III (Figure 4.9) samples often contains pyrite framboids, typically 20 – 40 μm in diameter, which encrust some of the chitinozoan vesicles (Figure 4.10, Figure 4.11, Figure 4.12).

Six of the 15 palynofacies samples from Tan III contain chitinozoans. Tan III has a terrestrial phytoclasts in the C1, although the palynomorphs include marine chitinozoans and *Tasmanites* sp., a marine prasinophyte alga, as well as terrestrial spores, and phytoclasts.

Chitinozoans recovered from Tan III samples are relatively dark in color, suggesting greater thermal maturation than in overlying sediments. Tan III samples (n=9) contain on average; 30.7% terrestrial kerogen, 42.5% phytoclasts, and 26.8% AOM (Table Reference).

In our study area, Tan III occurs between 8910 -10215 ft (2716 - 3114 m) based on well-logs in the C1 core, for a thickness of 360 m. In the B1 well, it occurs between 8952-9883 ft (2729-3013 m), for a thickness of 284 m. In the H1 well, the logged interval does not appear to cover the entire upper Tanezzuft unit, however, the interval from 8967-10206 ft (2734-3112 m) belongs to Tan III. Based on the well-log stratigraphic picks, only samples from the C1 well come from the Tan III (Figure 4.4).

4.6.2. Boundary between the Akakus and Tanezzuft formations

Whereas a sharp contact exists between the Mamuniyat and Tanezzuft formations, Daniels et al. (1990) viewed the Tanezzuft/Akakus boundary as gradational. These authors placed the Tanezzuft/Akakus boundary at the first occurrence of coarse blocky sandstone as indicated by a bell shape in the well log (gamma-ray or SP). Using this marker, we place this boundary at 8867 ft (2733 m) in the H1 core, 8952 ft (2729 m) in the B1 core, and 8910 ft (2754 m) in the C1 core (Figure 4.4). Overall, the Akakus Formation contains more terrestrial palynodebris than the Tanezzuft Formation. Ongoing investigation into the spore flora of the Tanezzuft and Akakus formations may reveal a biostratigraphic marker for the Tanezzuft/Akakus boundary. Several cryptospores species identified in this study may serve as biostratigraphic markers for the Silurian of the Ghadamis Basin.

4.6.2.1. Lower Akakus Unit

The lower Akakus unit consists of interbedded siltstone, mudstone, and sandstone. While siltstone and mudstone predominate, this unit contains more sand than Tan III. Based on the available samples, the lower Akakus unit consists of a series of well-sorted, fine-grained lithologies, including argillaceous siltstone, red calcareous mudstone, and micaceous mudstone that alternate with small quartz sandstone lenses.

We have 25 hand specimens for palynodebris analysis from the lower Akakus unit 15 for which have XRD analyses. Of these 25 hand specimens, 21 come from the B1 well, 4 from the H1 well, and none from the C1 well. The mineral assemblage of the lower Akakus unit contains quartz, muscovite, and kaolinite, and in relative terms has a higher percentage of quartz than upper Tanezzuft (Tan III), which agrees with the general observation that the lower Akakus has more sandstone than upper Tanezzuft (Tan III). Siderite occurs in many of the samples. However, we could not confirm the common occurrence of chlorite in the lower Akakus Formation, reported by Taktek and Shebli (2019).

Five of the 22 palynological samples of the lower Akakus unit, all from the B1 well, contain chitinozoans, which are lighter in color than chitinozoans from Tan III. The lower Akakus Formation samples (n=7) from B1 contain on average 35.2% palynomorphs and 42.7% phytoclasts and the remainder is AOM, which is 22.1%. These proportions are rather similar to those for the Tan III (n=9): 30.7% palynomorphs, 42.5% phytoclasts, and 26.8% AOM. In addition, we observed oil residue in processed palynological samples from the B1 well. Almost all the observed chitinozoans from the Akakus Formation have a translucent amber to light

brown color, suggesting low levels of thermal maturation than in Tan III (Cole, 1994; Obermajer et al., 1996).

Based on well-logs, the lower Akakus Formation lies between 8560-8910 ft (2610-2716 m) with a thickness of 106 m in the C1 well. The lower Akakus Formation is between 8691-8967 ft (2650-2734 m) with a thickness of 84 m in the B1 well, and between 8440-8952 ft (2573-2729 m) with a thickness of 84 m in the H1 well (see Figure 4.4).

4.6.2.2. Middle Akakus Unit

The middle Akakus unit differs from the lower Akakus Formation in having a greater proportion of shale and consists of mudstone interbedded with medium to coarse-grained sandstone. For the middle Akakus unit, we have 22 hand specimens for palynodebris analysis and palynological analysis, 15 of which have XRD analyses. We have 11 hand samples for the B1 well, seven of which have XRD analyses. For the C1 well, we have four hand samples, all with XRD analyses, and for the H1 well, we have seven hand samples, four of which have XRD analyses. The XRD results suggest that the middle Akakus consists primarily of clean quartz sandstone; however, well logs indicate more shale in the middle Akakus. Because AGOCO collected cores to sample sandstone layers, the XRD results may reflect a bias in the selection of cored intervals. The XRD results show very high quartz content, low to no siderite, low to no illites, some kaolinite, and apparently more pyrite than the lower or upper Akakus unit.

Unfortunately, only three of seven of the middle Akakus unit samples, all from the H1 well, yield identifiable palynomorphs, and only one of the three contains chitinozoans. Based on these three samples, palynomorphs range from 40% to 36.0%; phytoclasts range from 44.0 to

79.6% and AOM ranges from 8.2%to 25.0%. It appears that phytoclasts dominate the middle Akakus samples while palynomorphs are comparatively rare (Table 4.1).

Based on well-logs, the middle Akakus unit occurs from 7726-8560 ft (2355-2610 m) with a thickness of 255 m in the C1 well. This Formation occurs from 7900-8691 ft (2409-2650 m) with a thickness of 241 m in the H1 well, and from 7490-8440 ft (2284-2573 m) with a thickness of 948.16 ft (289 m) in the B1 well.

4.6.2.3. Upper Akakus Unit

The upper Akakus unit consists of sandstones, often coarse-grained, with thin shale layers (Elfigih, 1991). We have four hand samples and only one XRD analysis, all from the H1 core, from this Formation. The XRD result suggests a return to the quartz-muscovite-kaolinite mineral assemblage observed in the Tan III unit and lower Akakus unit.

The four upper Akakus samples from B1 contain on average 28.8% terrestrial palynodebris and 47.8% phytoclasts and the remainder is AOM, which is 23.4%. This assemblage of spores implies that the upper Akakus accumulate in a near-shore environment. The four palynomorph samples from the upper Akakus unit each contain a different chitinozoan species (Table 4.23).

The upper Akakus occurs from 7259-7726 ft (2213-2355 m), with a thickness of 142 m in the C1 well, and from 6764-7490 ft (2062-2284 m) with a thickness of 222 m in the B1 well. In the H1 well, the base of upper Akakus occurs at 7900 ft (2408 m) but the logged interval records only 130 m of the upper Akakus unit.

Table 4.1 The average marine organic debris percentage and terrestrial palynofacies of the Ghadamis Basin wells in this study. Tan III = Tanezzuft, l. Akakus = lower Akakus, m. Akakus = middle Akakus and u. Akakus = upper Akakus.

All Samples with Chitinozoans Data																			
unit	Sample	number of marine palynomorphs	Number Spores	Total Palynorph count	% marine Palynomorph	% of terrestrial palynomorphs	Number phytoclasts	Number AOM clumps	total of phytoclasts plus AOM clusters	% phytoclast	% AOM	% marine	% terrestrial	marine %	average marine %	T/M index Prauss, 2000	Average T/M Index	phyto/AOM Index	aveage phyto/AOM Index
u. Akakus	H1_S23	11	9	20	55%	45%	26	4	30	87%	13%	68%	70%	30%		0.82		6.50	
u. Akakus	H1_S25	26	28	54	48%	52%	16	17	33	48%	52%	100%	51%	49%		1.08		0.94	
u. Akakus	H1_S27	9	17	26	35%	65%	5	11	16	31%	69%	103%	52%	48%		1.89		0.45	
u. Akakus	H1_S28	56	38	94	60%	40%	38	37	75	51%	49%	109%	45%	55%	46%	0.68	1.12	1.03	2.23
m. Akakus	H1_S15	6	11	17	35%	65%	39	4	43	91%	9%	45%	83%	17%		1.83		9.75	
m. Akakus	H1_S19	2	12	14	14%	86%	37	13	50	74%	26%	40%	77%	23%		6.00		2.85	
m. Akakus	H1_S21	9	25	34	26%	74%	11	5	16	69%	31%	58%	72%	28%	23%	2.78	3.54	2.20	4.93
l.Akakus	B1_S15	22	18	40	55%	45%	37	19	56	66%	34%	89%	57%	43%		0.82		1.95	
l.Akakus	B1_S17	9	14	23	39%	61%	11	4	15	73%	27%	66%	66%	34%		1.56		2.75	
l.Akakus	B1_S19	32	31	63	51%	49%	94	55	149	63%	37%	88%	59%	41%		0.97		1.71	
l.Akakus	B1_S21	16	14	30	53%	47%	11	8	19	58%	42%	95%	51%	49%		0.88		1.38	
l.Akakus	B1_S37	55	39	94	59%	41%	43	19	62	69%	31%	89%	53%	47%	43%	0.71	0.99	2.26	2.01
Tan III	C1_S3	40	33	73	55%	45%	24	26	50	48%	52%	107%	46%	54%		0.83		0.92	
Tan III	C1_S5	51	28	79	65%	35%	35	63	98	36%	64%	129%	36%	64%		0.55		0.56	
Tan III	C1_S7	31	34	65	48%	52%	29	26	55	53%	47%	95%	53%	48%		1.10		1.12	
Tan III	C1_S9	90	47	137	66%	34%	134	37	171	78%	22%	87%	59%	41%		0.52		3.62	
Tan III	C1_S11	45	65	110	41%	59%	120	74	194	62%	38%	79%	61%	39%		1.44		1.62	
Tan III	C1_S13	69	55	124	56%	44%	109	19	128	85%	15%	70%	65%	35%		0.80		5.74	
Tan III	C1_S15	37	17	54	69%	31%	65	34	99	66%	34%	103%	54%	46%		0.46		1.91	
Tan III	C1_S17	43	16	59	73%	27%	89	57	146	61%	39%	112%	51%	49%	47%	0.37	0.76	1.56	2.13

4.7. Results – Palynology

4.7.1. The Silurian palynoflora of Tan III unit and the Akakus Formation in the Ghadamis Basin (Table 4.2, 4.3, 4.4, 4.5, 4.6, and 4.7).

Table 4.2 through Table 4.7 show the distribution of chitinozoans (Figure 4.13; Figure 4.14), acritarchs and spores recovered from the Tan III unit and Akakus Formation samples. Our most diverse samples, C1-S7 and B1-S19 contained 7 and 9 chitinozoan species respectively.

Table 4.2 Distribution chart of chitinozoans recovered from Tan III and the Akakus Formation in this study.

Formations		Tanezzuft & Akakus formations																					
	Period/Age	Silurian																					
		Llandovery - Wenlock - Ludlow																					
Units	List of Taxa / Depths ft.	*Ancyrochitina ancyrea*	*Ancyrochitina camilleae sp.*	*Ancyrochitina gutnica*	*Ancyrochitina fragilis*	*Ancyrochitina laevaensis*	*Anthochitina radiate*	*Cingulochitina bouniensis*	*Ancyrochitina primitiva*	*Fungochitina spinifera*	*Cingulochitina convexa*	*Plectochitina cf. longispina*	*Sphaerochitina concava*	*Ramochitina sp.*	*Eisnackitina cylindrica*	*Euconochitina moussegoudaensis*	*Plectochitina sp.*	*Fungochitina sp.*	*Ancyrochitina ramosaspina*	*Cingulochitina cf. sp.*	*Pseudoclathrochitina sp*	*Sphaerochitina sphaerocephala*	*Sphaerochitina concava*
U. Akakus	8123 (H1-S28)	•																					
	8126 (H1-S27)																						
	8134.3 (H1-S25)																					•	•
	8138.4 (H1-S23)																				•		
M. Akakus	8285 (H1-S21)												•										
L. Akakus	8313.7 (B1-S23)	•																					
	8402 (B1-S21)	•											•		•		•	•		•			
	8409.5 (B1-S19)	•									•		•		•	•	•	•	•	•			
	8541.5 (B1-S17)												•										
	8544 (B1-S15)	•											•										
Tan III	9106 (C1-S11)	•		•									•		•		•						
	9112.2 (C1-S9)	•	•		•								•		•		•						
	9118.3 (C1-S7)	•				•									•		•						
	9282 (C1-S5-S5')	•						•				•	•	•	•		•						
	9289 (C1-S3)	•					•		•	•													

Table 4.3 Range chart of chitinozoans recovered from Tan III and the Akakus Formation in this study. Eur = Europe and AF = Africa.

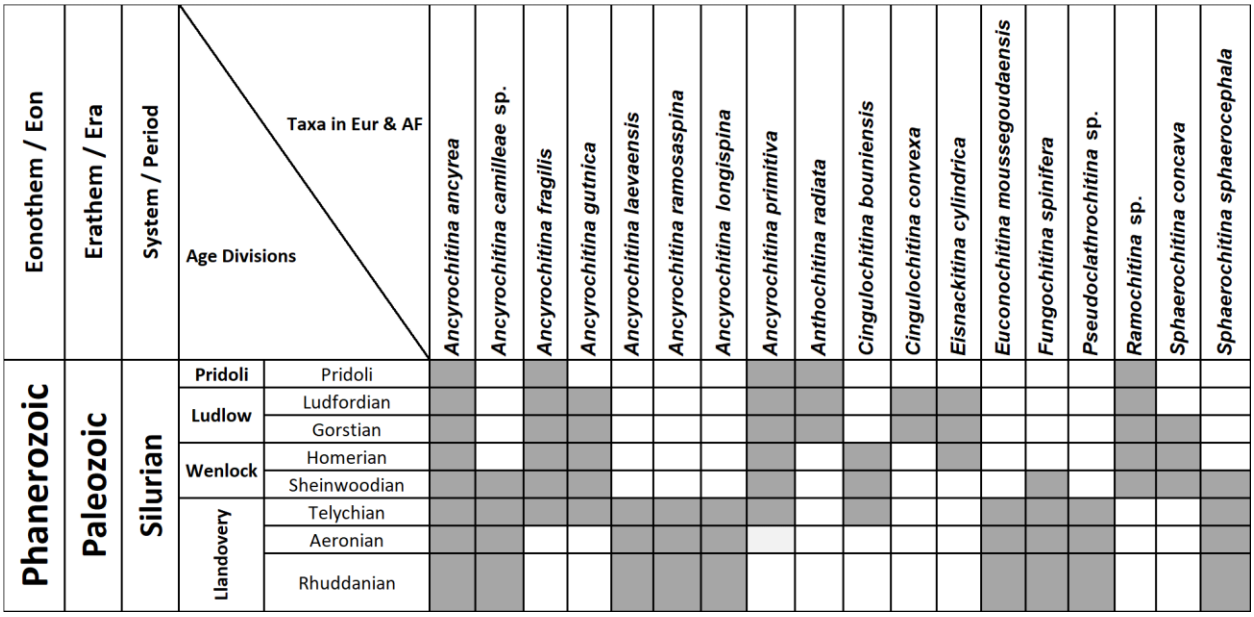

Table 4.4 Distribution chart of acritarchs recovered from Tan III and the Akakus Formation in this study.

Formations		Tanezzuft & Akakus formations															
	Period / Age	Silurian															
		Llandovery - Wenlock - Ludlow															
Units	Depths ft. \ List of Taxa	*Veryhachium europaeum*	*Leiosphaeridia wenlockia*	*Micrhystridium stellatum*	*Veryhachium lairdii*	*Leiofusa estrecha*	*Onondagella asymmetrica*	*Visbysphaera bonita*	*Multiplicisphaeridium ramuscufosum*	*Veryhachium trispinosum*	*Diexallophasis denticulate*	*Deflandrastrum millepiedii*	*Veryhachium. sp.*	*Cymbosphaeridium pilaris*	*Neoveryhachium carminae*	*Actipilion druggii*	*Visbysphaera microspinosa*
U. Akakus	8123 (H1-S28)														•		
	8126 (H1-S27)															•	
	8134.3 (H1-S25)																•
	8138.4 (H1-S23)													•			
M. Akakus	8285 (H1-S21)												•				
L. Akakus	8313.7 (B1-S23)																
	8402 (B1-S21)											•					
	8409.5 (B1-19)																
	8541.5 (B1-17)																
	8544 (B1-S15)																
Tan III	9106 (C1-S11)	•							•	•							
	9112.2 (C1-S9)																
	9118.3 (C1-S7)																
	9282 (C1-S5)		•														
	9283 (C1-S5')																
	9289 (C1-S3)			•	•	•	•	•			•						

Table 4.5 Range chart of acritarchs recovered from Tan III and the Akakus Formation in this study. Eur = Europe and AF = Africa.

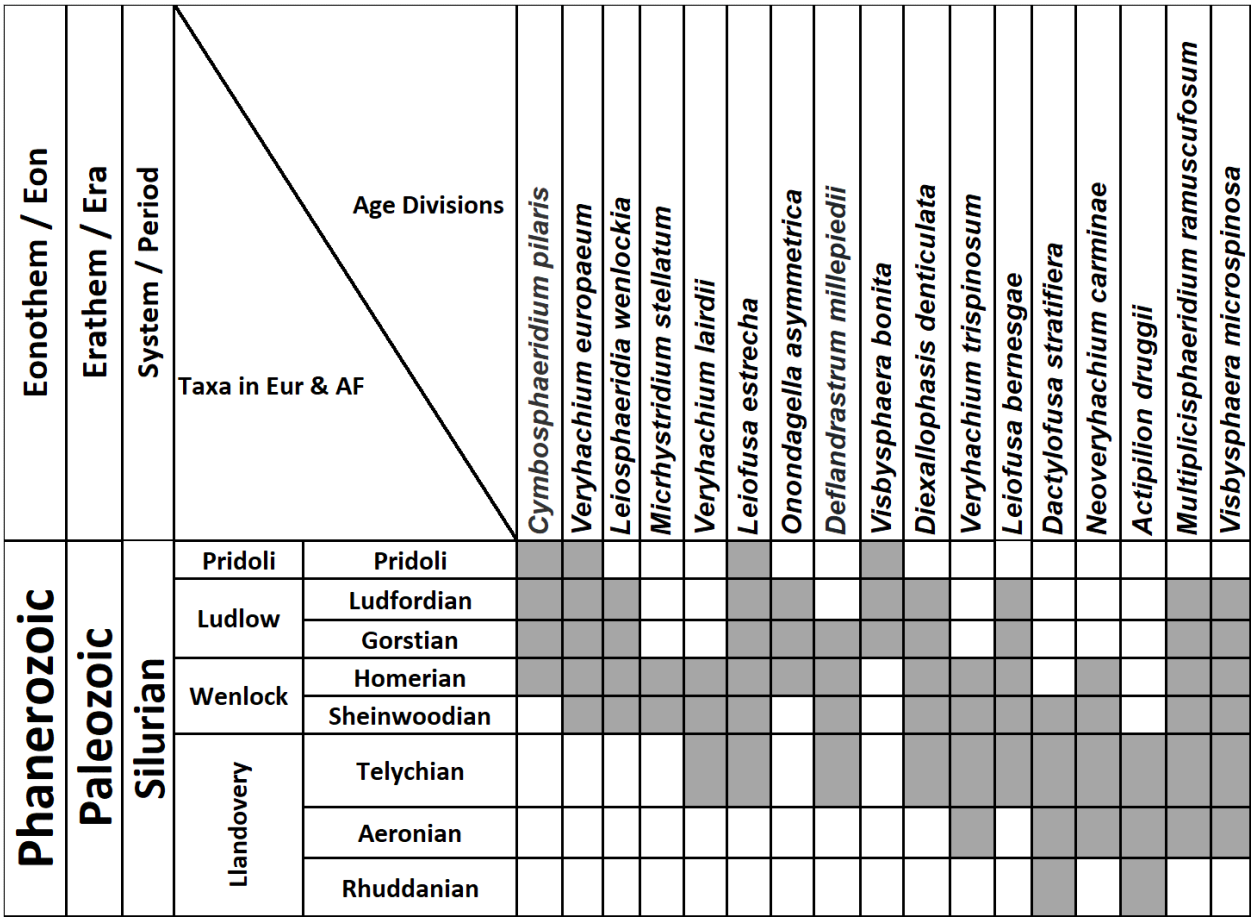

Table 4.6 Distribution chart of spores recovered from Tan III and the Akakus Formation in this study.

Formations		Tanezzuft & Akakus formations															
	Period / Age	Silurian															
		Llandovery - Wenlock - Ludlow															
Units	Depths ft. / List of Taxa	*Archaeozonotrilete cf. chulus*	*Ambitisporites dilutus*	*Retusotriletes warringtonii*	*Rugosphaera tuscarorensis*	*Retusotriletes sp.*	*Emphanisporites protophanus*	*Ambitisporites avitus*	*Pseudodyadospora sp.*	*Archaeozonotriletes cf., chulus*	*Brochotriletes sp.*	*Chelinospora textilis*	*Gneudnaspora divellomedium*	*Dyadospora murusattenuata*	Emphanisporites rotatus	*Tetrad sp.*	*Lophozonotriletes sp.*
U. Akakus	8123 (H1-S28)														●		●
	8126 (H1-S27)															●	
	8134.3 (H1-S25)												●				
	8138.4 (H1-S23)											●		●			
M. Akakus	8285 (H1-S21)								●	●	●						
L. Akakus	8616.3 (H1-S13)							●									
	8313.7 (B1-S23)																
	8402 (B1-S21)																
	8409.5 (B1-19)																
	8541.5 (B1-17)																
	8544 (B1-S15)																
Tan III	9030 (C1-S25)						●										
	9106 (C1-S11)	●															
	9112.2 (C1-S9)																
	9118.3 (C1-S7)			●													
	9289 (C1-S3)		●		●	●											

Table 4.7 Range chart of spores recovered from Tan III and the Akakus Formation in this study. Eur = Europe and AF = Africa.

Eonothem / Eon	Erathem / Era	System / Period	Age Divisions / Taxa in Eur & AF		*Archaeozonotrilete chulus*	*Emphanisporites protophanus*	*Pseudodyadospora* sp.	*Ambitisporites avitus*	*Retusotriletes* sp.	*Gneudnaspora divellomedium*	*Dyadospora murusattenuata*	*Retusotriletes warringtonii*	*Emphanisporites rotatus*	*Archaeozonotriletes* cf. *chulus*	*Tetrad* sp.	*Rugosphaera tuscarorensis*	*Ambitisporite dilutus*	*Brochotriletes* sp.	*Chelinospora textilis*	*Lophozonotriletes* sp.
Phanerozoic	Paleozoic	Silurian	Pridoli	Pridoli		■	■	■		■					■			■		■
			Ludlow	Ludfordian	■	■	■	■	■	■		■		■	■	■	■	■	■	■
				Gorstian	■	■		■	■	■		■	■	■	■	■	■		■	■
			Wenlock	Homerian	■				■		■	■	■	■	■	■	■		■	
				Sheinwoodian					■		■	■	■	■	■	■	■			
			Llandovery	Telychian					■		■	■	■		■	■				
				Aeronian							■				■	■				
				Rhuddanian							■				■	■				

4.7.2. Tan III palynology and organic debris (Table 4.8, 4.9, 4.10, 4.11, 4.12, 4.13).

All of the Tan III samples available for this study come from the C1 well. Of the 15 palynological samples from Tan III, nine contain chitinozoans. These nine samples have an average t/m index of 0.76 (range 0.37 – 1.44), an average phyto/AOM index of 2.13 (range: 0.56 – 5.74) and an average marine percentage of 47% (range 35 -64%; Table 4.1). Sample C1-S5 is the most diverse in terms of chitinozoan taxa at 7 species and 18 specimens. We report the presence/absence for acritarchs and spores from splits of the same samples. The chitinozoans,

acritarchs and spores identified in Tan III samples appear in Table 4.8, Table 4.9, Table 4.10, Table 4.11, Table 4.12, and Table 4.13.

Chitinozoans in Tan III might suggest a Telychian (late Llandoverian, early Silurian) age based on the presence of *Ancyrochitina camilleae* and *A. longispina*, which co-occur in the Qusaiba Member of the Qalibah Formation of Saudia Arabia, which (Paris et al., 2015) assigned to the Telychian (late Llandovery, early Silurian). This is the first report of *A. camilleae* outside of Saudia Arabia; likewise, our *A. longispina* specimens resemble those of Paris et al. (2015) from the same sediments in Qusaiba Member of the Qalibah Formation (Saudia Arabia). However, Bassett (1989) reported *A. laevaensis*, which co-occurs with *A. camilleae* and *A. longispina* in the Qusaiba Member in Saudia Arabia and in our Tan III samples, from the Wenlock of Estonia, which formed part of the paleocontinent, Laurussia (formerly Baltica), in mid-Silurian (Paris et al., 2015).

Likewise, the presence of *Cingulochitina bouniensis*, *Anthochitina radiata*, and *Eisenackitina cylindrica* suggest a younger age. *Cingulochitina bouniensis* occurs in Wenlock (mid-Silurian) strata from Avalonia microcontinent (Mullins, 2000), although Paris et al. (2015) listed *C. bouniensis* in the Telychian Qusaiba Member of the Qalibah Formation without further discussion. *Eisenackitina cylindrica* occurs in the Homerian through Ludfordian (Jansonius, 1978). *A. radiata* does not occur below the Gorstian (early Ludlow, early part of the late Silurian: on Baltica which was part of Laurussia (Wrona, 1980).

Assigning Tan III to the Telychian would entail an earlier range extension for *Cingulochitna bouniensis, Eisenackitina cylindrica,* and *Anthochitina radiata*. Assigning Tan III to the

Wenlock would require a later range extension for *Ancyrochitina camilleae*, and *A. longispina.* The following taxa would support either age designation (Telychian or Wenlock): *A. ancyrea, A. fragilis, A. gutnica, A. primitiva, Fungochitina spinifera, Ramochitina* sp., and *Sphaerochitina* sp. (Table 4.2 and 4.8).

The acritarchs, *Veryhachium europaeum*, *Leiosphaeridia wenlockia*, and *Micrhystridium stellatum*, all of which have their earliest occurrence in the Sheinwoodian (early Wenlock, Middle Silurian: Downie, 1963) support a Sheinwoodian or later age for all Tan III samples (Table 4.10, Table 4.11). This age designation is consistent with the presence of *V. lairdii, V. trispinosum, Leiofusa estrecha, Diexallophasis denticulata* and *Multiplicisphaeridium ramuscufosum* in Tan III (Table 4.11). However, assigning Tan III to the Sheinwoodian would represent an earlier range extension for *Onondagella asymmetrica* from the Homerian (late Wenlock) and for *Visbysphaera bonita* from the Gorstian (early Ludlow; Thusu, 1973; Table 4.11).

The presence of the spore, *Emphanisporites protophanus*, in the uppermost Tan III sample, C1-S11, supports the assignment of the uppermost Tan III to the Homerian (late Wenlock, late in the middle Silurian: Table 4.11). This spore first appears in the Homerian of Great Britain and the Late Wenlock of Argentina (Burgess and Richardson, 1995; Cesari et al., 2020). Taken together, chitinozoans, acritarchs and spores suggest an early Wenlock (Sheinwoodian) age for most of Tan III, and a late Wenlock (Homerian) age for the uppermost Tan III.

Table 4.8 Distribution chart of Chitinozoans recovered from Tan III of the Tanezzuft Formation in this study.

Formations		Tanezzuft Formation													
Period / Age		Silurian													
		Llandovery - Wenlock													
Units	Depths ft. / List of Taxa	*Ancyrochitina ancyrea*	*Ancyrochitina camilleae sp.*	*Ancyrochitina gutnica*	*Ancyrochitina fragilis*	*Ancyrochitina laevaensis*	*Anthochitina radiate*	*Cingulochitina bouniensis*	*Ancyrochitina primitiva*	*Fungochitina spinifera*	*Plectochitina cf. longispina*	*Sphaerochitina sp.*	*Ramochitina sp.*	*Eisnackitina cylindrica*	*Plectochitina sp.*
Tan III	9106 (C1-S11)	●		●								●		●	●
	9112.2 (C1-S9)	●	●		●							●		●	●
	9118.3 (C1-S7)	●				●								●	●
	9282 (C1-S5)	●						●				●	●	●	●
	9283 (C1-S5')										●				
	9289 (C1-S3)	●					●		●	●					

Table 4.9 Range chart of chitinozoans recovered from Tan III of the Tanezzuft Formation in this study.

Eonothem / Eon	Erathem / Era	System / Period	Age Divisions / Taxa in Eur & AF		*Ancyrochitina ancyrea*	*Ancyrochitina camilleae sp.*	*Ancyrochitina fragilis*	*Ancyrochitina gutnica*	*Ancyrochitina laevaensis*	*Ancyrochitina longispina*	*Ancyrochitina primitiva*	*Anthochitina radiata*	*Cingulochitina bouniensis*	*Eisnackitina cylindrica*	*Euconochitina moussegoudaensis*	*Fungochitina spinifera*	*Ramochitina sp.*	*Sphaerochitina concava*
Phanerozoic	Paleozoic	Silurian	Pridoli	Pridoli	■							■				■	■	
			Ludlow	Ludfordian	■							■		■		■	■	
				Gorstian	■		■	■				■		■				■
			Wenlock	Homerian	■		■	■			■		■	■				■
				Sheinwoodian	■	■	■	■			■		■					■
			Llandovery	Telychian	■	■	■	■	■	■	■		■		■			
				Aeronian	■	■			■	■	■				■			
				Rhuddanian	■	■			■	■					■			

Table 4.10 Distribution chart of acritarchs recovered from Tan III of the Tanezzuft Formation in this study.

Units	Depths ft. \ List of Taxa	*Veryhachium europaeum*	*Leiosphaeridia wenlockia*	*Micrhystridium stellatum*	*Veryhachium lairdii*	*Leiofusa estrecha*	*Onondagella asymmetrica*	*Visbysphaera bonita*	*Multiplicisphaeridium ramuscufosum*	*Veryhachium trispinosum*	*Diexallophasis denticulate*
Tan III	9106 (C1-S11)	●							●	●	
	9118.3 (C1-S7)										
	9282 (C1-S5)		●								
	9289 (C1-S3)			●	●	●	●	●			●

Table 4.11 Range chart of acritarchs recovered from Tan III of the Tanezzuft Formation in this study.

Eonothem / Eon	Erathem / Era	System / Period	Age Divisions \ Taxa in Eur & AF		*Veryhachium europaeum*	*Leiosphaeridia wenlockia*	*Micrhystridium stellatum*	*Veryhachium lairdii*	*Leiofusa estrecha*	*Onondagella asymmetrica*	*Visbysphaera bonita*	*Diexallophasis denticulata*	*Veryhachium trispinosum*	*Multiplicisphaeridium ramuscufosum*
Phanerozoic	Paleozoic	Silurian	Pridoli	Pridoli										
			Ludlow	Ludfordian										
				Gorstian										
			Wenlock	Homerian										
				Sheinwoodian										
			Llandovery	Telychian										
				Aeronian										
				Rhuddanian										

Table 4.12 Distribution chart of spores recovered from Tan III of the Tanezzuft Formation in this study.

Units	List of Taxa / Depths ft.	*Archaeozonotrilete sp.*	*Ambitisporite dilutus*	*Retusotriletes warringtonii*	*Rugosphaera tuscarorensis*	*Retusotriletes sp.*	*Emphanisporites protophanus*
Tan III	9030 (C1)						●
	9106 (C1-S11)	●					
	9118.3 (C1-S7)			●			
	9289 (C1-S3)		●		●	●	

Table 4.13 Range chart of spores recovered from Tan III of the Tanezzuft Formation in this study.

System / Period	Age Divisions / Taxa in Eur & AF		*Archaeozonotriletes sp.*	*Ambitisporite dilutus*	*Retusotriletes warringtonii*	*Rugosphaera tuscarorensis*	*Retusotriletes sp.*	*Emphanisporites protophanus*
Silurian	Pridoli	Pridoli						
	Ludlow	Ludfordian						
		Gorstian						
	Wenlock	Homerian						
		Sheinwoodian						
	Llandovery	Telychian						
		Aeronian						
		Rhuddanian						

4.7.3. Lower Akakus palynology and organic debris (Table 2.013, 2.014).

Of the 21 samples available for palynofloral analysis from the lower Akakus Formation, five yielded chitinozoans, all from the B1 well. These five samples have an average t/m index of 0.99 (range 0.71 – 1.56), an average phyto/AOM index of 2.01 (range: 1.38 – 2.75) and an average marine percentage of 43% (range 34 -49%; Table 4.1). Sample B1-S19 is the most diverse in terms of chitinozoan taxa with 9 species and 9 specimens. We report the occurrence of acritarchs and spores from splits of the same samples. The chitinozoans, acritarchs and spores identified in lower Akakus samples appear in Table 4.14, Table 4.15.

Chitinozoans in the lower Akakus appear to indicate a Wenlock or later age based on presence of *Cingulochitina convexa* (range: Sheinwoodian, early Wenlock - Gorstian, early Ludlow) and *Eisenackitina cylindrica* (range: Homerian, late Wenlock - Ludlow: Table 4.2: Jansonius, 1978. However. *E. cylindrica* appears to range into the early Wenlock (Sheinwoodian) in Tan III. Assigning the lower Akakus Formation to the Wenlock or later would require a later range extension for *Euconochitina moussegoudaensis* and *Ancyrochitina ramosaspina*, from the Telychian to the Sheinwoodian or Homerian (Table 4.4; 4.14).

Only one acritarch, *Deflandrastrum millepiedii*, and one spore, *Ambitisporites avitus*, occur in our lower Akakus samples. The range of *Deflandrastrum millepiedii* (Telychian – Gorstian: (Richardson and Lister, 1969) is consistent with a Wenlock or later age for the lower Akakus. Likewise, *Ambitisporites avitus* ranges from late Llandoverian of Libya (Deunff et al., 1975) to the early Devonian of France (Le Hérissé, 1981).

Table 4.14 Distribution chart of chitinozoans, acritarchs, and spores recovered from lower Akakus unit in this study.

Formation		L. Akakus Formation											
		Silurian											
Period / Age			Ludlow										
Units	List of Taxa / Depths ft.	*Ancyrochitina ancyra*	*Cingulochitina convexa*	*Sphaerochitina sp.*	*Ramochitina sp.*	*Eisnackitina cylindrica*	*Euconochitina moussegoudaensis*	*Plectochitina sp.*	*Fungochitina sp.*	*Ancyrochitina ramosaspina*	*Cingulochitina cf. sp.*	*Deflandrastrum millepiedii*	*Ambitisporites avitus*
	8616.3 (H1-S13)												●
L. Akakus	8313.7 (B1-S23)	●											
	8402 (B1-S21)			●		●		●	●		●	●	
	8409.5 (B1-S19)		●	●		●	●	●	●	●	●		
	8541.5 (B1-S17)			●									
	8544 (B1-S15)			●									

Table 4.15 Range chart of Chitinozoans, acritarchs, and spores recovered from lower Akakus unit in this study. Light grey blocks indicate range extensions based on the results of this study.

Eonothem / Eon	Erathem / Era	System / Period	Age Divisions / Taxa in Eur & AF		*Ancyrochitina ancyra*	*Cingulochitina convexa*	*Sphaerochitina sp.*	*Eisnackitina cylindrica*	*Euconochitina moussegoudaensis*	*Plectochitina sp.*	*Fungochitina sp.*	*Ancyrochitina ramosaspina*	*Cingulochitina sp.*	*Deflandrastrum millepiedii*	*Ambitisporites avitus*
Phanerozoic	Paleozoic	Silurian	Pridoli	Pridoli											
			Ludlow	Ludfordian											
				Gorstian											
			Wenlock	Homerian											
				Sheinwoodian											
			Llandovery	Telychian											?
				Aeronian											?
				Rhuddanian											?

4.7.4. Middle Akakus palynology and organic debris (Table 2.16, 2.17).

Of the 22 Middle Akakus samples available for palynofloral analysis, only one sample from the H1 well (H1-S21) yielded identifiable palynomorphs, although two additional samples contained palynomorphs and organic debris. We report the presence/absence for acritarchs and spores from splits of the H1-S21 sample. The chitinozoan, acritarchs, and spores identified in the middle Akakus sample appear in Table 4.15. The three middle Akakus unit samples that contain palynomorphs have an average t/m index of 3.54 (range 1.83 – 6.00), an average phyto/AOM index of 4.93 (range: 2.20 – 9.75) and an average marine percentage of 23% (range 17 -28%; Table 4.1).

None of the palynomorphs recovered from the middle Akakus Formation in this study enable us to determine its age (Table 4.17 ranges in middle Akakus). The chitinozoan, acritarch, and cryptospore genera, respectively *Sphaerochitina* sp., *Veryhachium* sp., and *Pseudodyadosporites* range from the early Silurian through the early Devonian. The spore, *Brochotriletes*, ranges from the Ordovician through the Cenozoic (Deunff, 1961; Fradkina, 1967); *Archaeozonotriletes* cf. *chulus*, ranges from the late Ordovician to middle Devonian in Europe (Richardson et al., 1986; Vavrdovy, 1988), and the early Silurian (Rhuddanian) - early Devonian (Emsian) in North Africa (Tekbali et al., 1991; Steemans et al., 2000). Nonetheless, because this unit overlies Tan III and the lower Akakus, it must be Wenlockian or younger in age.

Table 4.16 Distribution chart of chitinozoans, acritarchs and spores recovered from middle Akakus unit in this study.

Units	Depths ft. \ List of Taxa	*Sphaerochitina sp.*	*Veryhachium. sp.*	*Pseudodyadospora sp.*	*Archaeozonotriletes cf. chulus*	*Brochotriletes sp.*
M. Akakus	8285 (H1-S21)	●	●	●	●	●

Table 4.17 Range chart of chitinozoans, acritarchs, and spores recovered from middle Akakus unit in this study.

Eonothem / Eon	Erathem / Era	System / Period	Age Divisions \ Taxa in Eur & AF		*Sphaerochitina sp.*	*Veryhachium. sp.*	*Pseudodyadospora sp.*	*Archaeozonotriletes cf. chulus*	*Brochotriletes sp.*
Phanerozoic	Paleozoic	Silurian	Pridoli	Pridoli					
			Ludlow	Ludfordian					
				Gorstian					
			Wenlock	Homerian					
				Sheinwoodian					
			Llandovery	Telychian					
				Aeronian					
				Rhuddanian					

4.7.5. Upper Akakus palynology and organic debris (Table 4.18, 4.19, 4.20, 4.21, 4.22, 4.23).

Of the 15 samples available for palynofloral analysis from the upper Akakus samples, three yielded chitinozoans (Figure 4.8), all from sediments close to the base of the unit in the H1 well (Figure 4.4). These three samples have an average t/m index of 1.12 (range 0.82 – 1.89), and average phyto/AOM index of 2.23 (range 0.45 – 6.5) and an average marine percentage of 46 (range 30 - 55%; Table 4.1). The most diverse upper Akakus sample (H1-S25) contains two chitinozoan species. We report acritarchs and spores from splits of these samples and two additional samples (H1-S27, H1-29), which contain a single acritarch species and a spore tetrad, but no chitinozoans. The chitinozoans, acritarchs, and spores identified in upper Akakus samples appear in Table 4.15, Table 4.16, Table 4.17.

Chitinozoans in the upper Akakus indicate a Wenlock - Ludlow age based on the presence of *Sphaerochitina concava* (range: Wenlock - Ludlow), consistent with the presence of *Sphaerochitina sphaerocephala* (range: Aeronian, early Silurian - Ludlow: Table 4.19 upper Akakus range). The cryptospore, *Dyadospora murusattenuata* (range: Llandovery - Gorstian, early Ludlow), and the acritarch, *Cymbosphaeridium pilaris* (range Homerian - Pridoli) further constrain the age of the upper Akakus Formation to the Homerian (late Wenlock) - Gorstian (early Ludlow). The range of *Chelinospora textilis* (Sheinwoodian - Ludfordian) is consistent with a Wenlock - Ludlow age for the upper Akakus unit (Libya: Spina et al., 2015). Within this age range, we favor a Ludlow (late Silurian) age for the base of the lower Akakus unit; previous studies placed the uppermost Akakus Formation in the Pridoli (Rubinstein and Steemans, 2002).

Table 4.18 Distribution chart of Chitinozoans recovered from upper Akakus unit in this study.

Formation		Akakus Formation			
Period / Age		Silurian			
		Wenlock - Ludlow			
Units	Depths ft. / List of Taxa	*Ancyrochitina ancyra*	*Pseudoclathrochitina sp*	*Sphaerochitina sphaerocephala*	*Sphaerochitina concava*
U. Akakus	8123 (H1-S28)	●			
	8134.3 (H1-S25)			●	●
	8138.4 (H1-S23)		●		

Table 4.19 Range chart of Chitinozoans, recovered from upper Akakus unit in this study.

Eonothem / Eon	Erathem / Era	System / Period	Age Divisions / Taxa in Eur & AF		*Ancyrochitina ancyrea*	*Sphaerochitina concava*	*Pseudoclathrochitina sp*	*Sphaerochitina sphaerocephala*
Phanerozoic	Paleozoic	Silurian	Pridoli	Pridoli				
			Ludlow	Ludfordian				
				Gorstian				
			Wenlock	Homerian				
				Sheinwoodian				
			Llandovery	Telychian				
				Aeronian				
				Rhuddanian				

Table 4.20 Distribution chart of acritarchs recovered from upper Akakus unit in this study.

Units	List of Taxa / Depths ft.	*Cymbosphaeridium pilaris*	*Neoveryhachium carminae*	*Diexallophasis denticulata*	*Visbysphaera microspinosa*
U. Akakus	8123 (H1-S28)		•		
	8134.3 (H1-S28)				
	8138.4 (H1-S23)	•		•	•

Table 4.21 Range chart of acritarchs recovered from upper Akakus unit in this study.

Eonothem / Eon	Erathem / Era	System / Period	Age Divisions / Taxa in Eur & AF		*Cymbosphaeridium pilar*	*Diexallophasis denticulata*	*Neoveryhachium carminae*	*Visbysphaera microspinosa*
Phanerozoic	Paleozoic	Silurian	Pridoli	Pridoli				
			Ludlow	Ludfordian				
				Gorstian				
			Wenlock	Homerian				
				Sheinwoodian				
			Llandovery	Telychian				
				Aeronian				
				Rhuddanian				

Table 4.22 Distribution chart of spores recovered from upper Akakus unit in this study.

Formation		Akakus Formation					
Period / Age		Silurian					
		Wenlock - Ludlow					
Units	Depths ft. / List of Taxa	*Chelinospora textilis*	*Gneudnaspora divellomedium*	*Dyadospora murusattenuata*	Emphanisporites rotatus	*Tetrad sp.*	*Lophozonotriletes sp.*
U. Akakus	8123 (H1-29)				•		•
	8126 (H1-27)					•	
	8134.3 (H1-25)		•				
	8138.4 (H1-23)	•		•			

Table 4.23 Range chart of spores recovered from upper Akakus unit in this study.

Eonothem / Eon	Erathem / Era	System / Period	Age Divisions	Taxa in Eur & AF	*Gneudnaspora divellomedium*	*Dyadospora murusattenuata*	Emphanisporites rotatus	*Tetrad sp.*	*Chelinospora textilis*	*Lophozonotriletes sp.*
Phanerozoic	Paleozoic	Silurian	Pridoli	Pridoli						
			Ludlow	Ludfordian						
				Gorstian						
			Wenlock	Homerian						
				Sheinwoodian						
			Llandovery	Telychian						
				Aeronian						
				Rhuddanian						

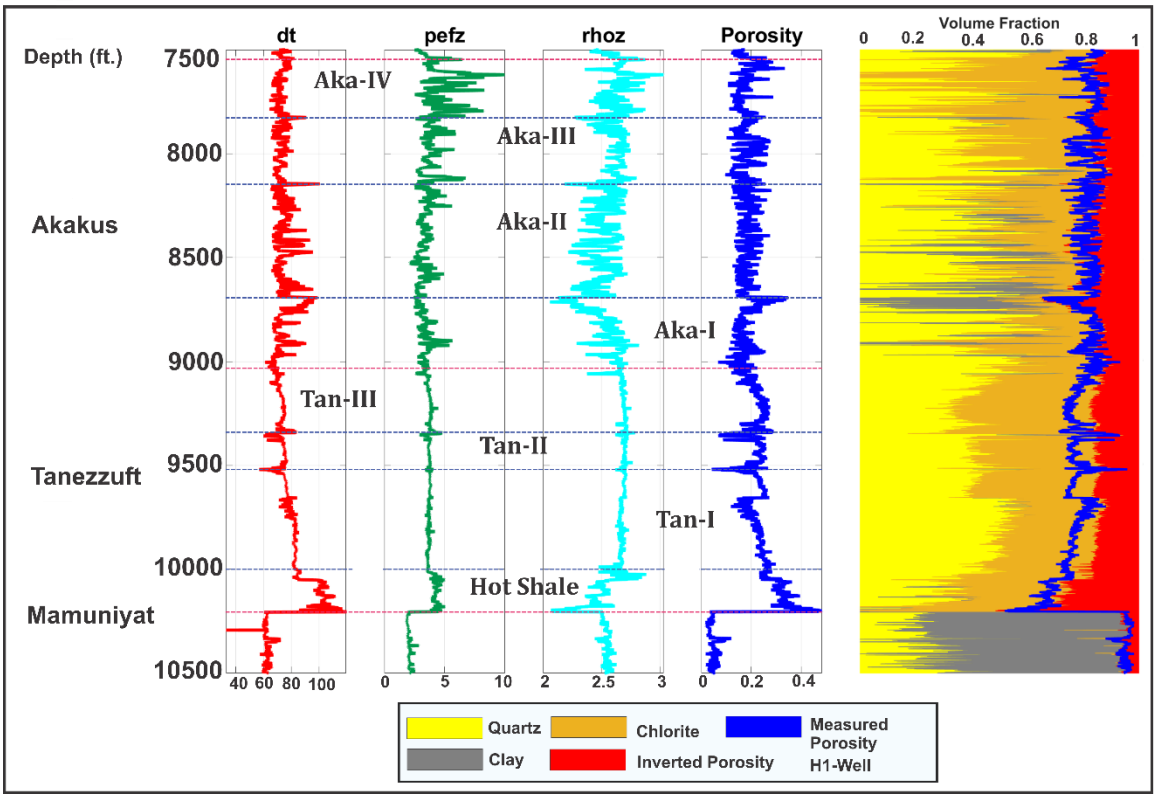

Figure 4.5: Petrophysical log and interpreted composition of the upper part of the Mamuniyat, the Tanezzuft and the Akakus formations in the H1 well made using MinInversion. Petrophysical tools: dt (µs/ft) = sonic log; pefz (b/e) = photoelectric log; rhoz (g/cc) = density log (modified from Amosu and Sun, 2018).

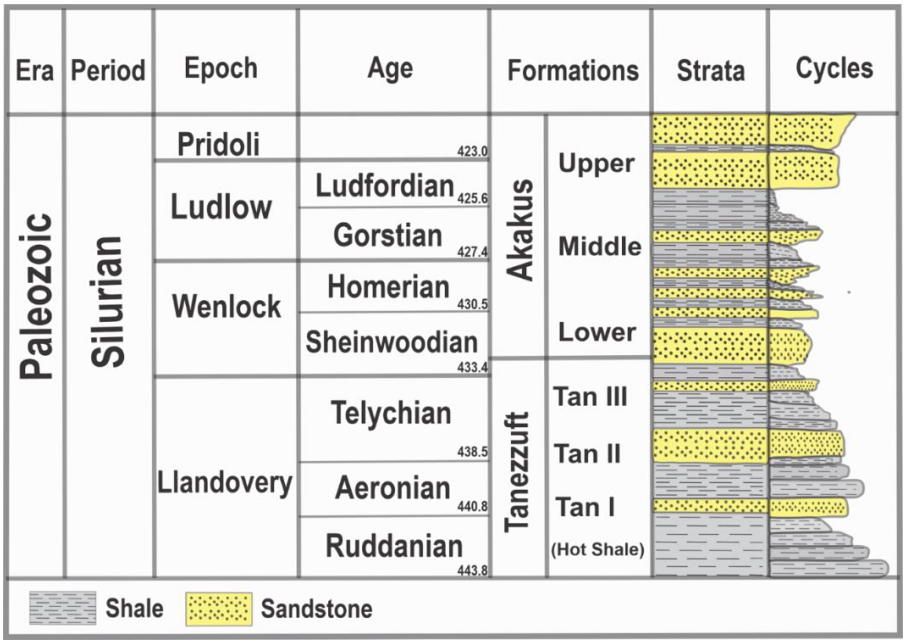

Figure 4.6: Chronostratigraphic column of units in the Tanezzuft and Akakus formations defined by Daniels et al. (1990) for the Silurian in Ghadamis Basin and used in this study. Lithostratigraphy and cycles from Daniels et al. (1990). Absolute ages from Ogg et al. (2016).

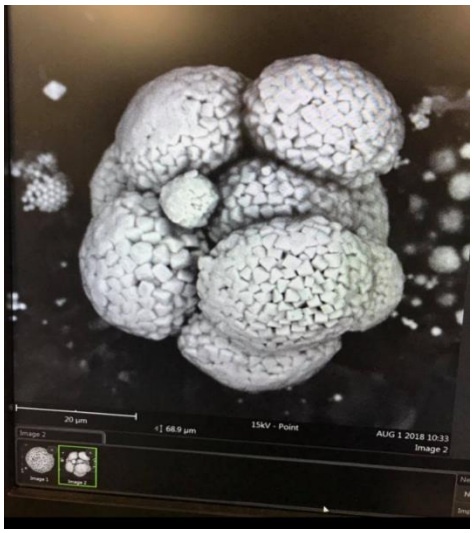

Figure 4.7: SEM image of framboidal pyrite (scale is 20 μm) from C1 S5 (9282 ft) in the Tan III unit.

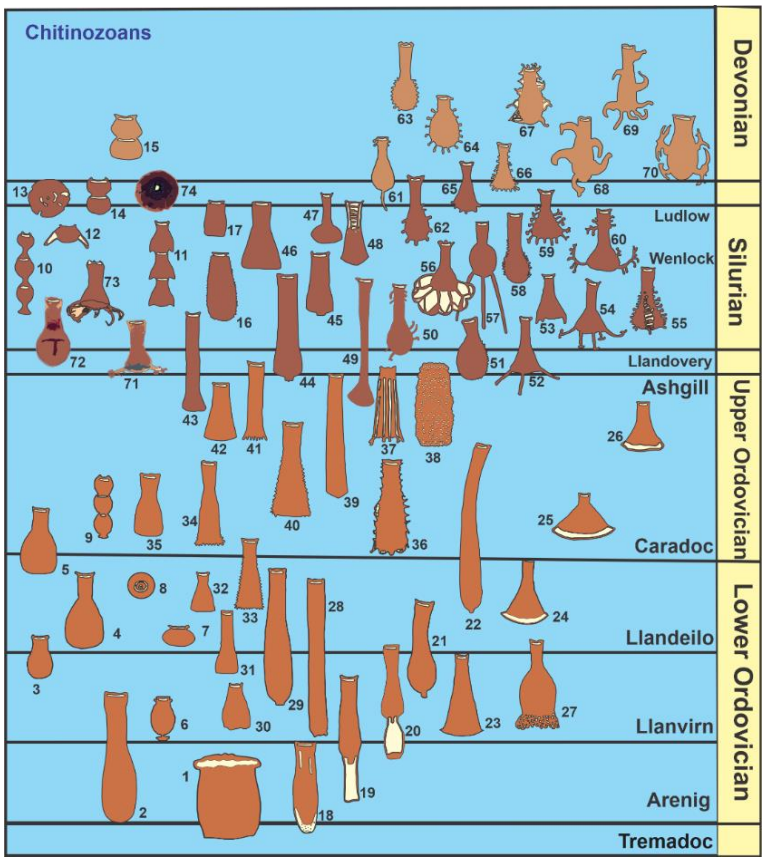

Figure 4.8: Exemplifying schematic drawing some of the major improvements in chitinozoan Palynostratigraphic succession in the Ordovician- Silurian division and Devonian Modified from (Haq and Boersma 1998). Figure numbers refer to the following species: Revised from Jansonius and Jenkins (1978) 1. *Ollachitina ingens Poumot.* 2. *Lagenochitina maxima* Taugourdeau and De Jekhowsky. 3. *Lagenochitina brevicollis* Taugourdeau and De Jekhowsky. 4. *Lagenochitina esthonica* Eisenack. 5. *Lagenochitina baltica* Eisenack. 6. *Desmochitina minor* Eisenack. 7. *Hoegisphaera complanata* (Eisenack). 8. *Hoegisphaera bransoni* Wilson and Dolly. 9. *Desmochitina nodosa* Eisenack. 10. *Margachitina margaritana (*Eisenack*).* 11. *Linochitina cingulata serrata* Taugourdeau and De Jekhowsky. 12. *Pterochitina perivelata (*Eisenack*).* 13. *Hoegisphaera glabra Staplin.*14. *Eisenackitina sphaerica (Taugourdeau and De Jekhowsky).* 15. *Eisenackitina bursa (*Taugourdeau and De Jekhowsky). 16. *Eisenackitina. oblonga (*Taugourdeau and De Jekhowsky*).* 17. *Eisenackitina cylindrica (*Taugourdeau and De Jekhowsky*).* 18. *Siphonochitina veligera* (Poumot). 19. *Siphonochitina copulata (*Poumot*).* 20. *Siphonochitina fornwsa* Jenkins. 21. *Ereniochitina niucronata* Taugourdeau and De Jekhowsky. 22. *Conochitina niinnesotensis* (Stauffer). 23. *Cyathochitina calix* (Eisenack). 24. *Cyathochitina campanulaeforniis* (Eisenack). 25. *Cyathochitina kuckersiana forma brevis* Eisenack. 26. *Cyathochitina kuckersiana* (Eisenack). 27. *Sagenachitina striata* (Benoit and Taugourdeau). 28. *Rhabdochitina magna* Eisenack. 29. *Ereniochitina baculata* Taugourdeau and De Jekhowsky. 30. *Conochitina simplex* Eisenack. 31. *Conochitina primitiva* Eisenack. 32. *Conochitina conulus* Eisenack. 33. *Belonechitina wesenbergensis* (Eisenack). 34.

Belonechitina micracantha* (Eisenack). 35. *Conochitina aculeata* Taugourdeau. 36. *Hercochitina downiei* Jenkins. 37. *Hercochitina crickmayi* Jansonius. 38. *Acanthochitina barbata* Eisenack. 39. *Rhabdochitina hedlundi* Taugourdeau. 40. *Belonechitina robusta (Eisenack).* 41. *Coronochitina coronata (Eisenack).* 42. *Conochitina turris Taugourdeau.* 43. *Conochitina elegans* Eisenack. 44. *Conochitina proboscifera* Eisenack. 45. *Conochitina tuba* Eisenack. 46. *Conochitina communis* Taugourdeau. 47. *Sphaerochitina pistilliformis* (Eisenack). 48. *Sphaerochitina vitrea* Taugourdeau. 49. *Sphaerochitina longicollis* Taugourdeau and De Jekhowsky. 50. *Angochitina filosa* Eisenack. 51. *Angochitina eisenacki* Bachmann and Schmid. 52. *Aficyrochitina longicornis* Taugourdeau and De Jekhowsky. 53. *Ancyrochitina diabolo* (Eisenack). 54. *Ancyrochitina ancyrea* (Eisenack). *55. Gotlandochitina martinssoni* Laufeld. 56. *Plectochitina carmijiae* Cramer. 57. *Ancyrochitina nodosa* Taugourdeau and De Jekhowsky. 58. *Angochitina capillata* Eisenack. 59. *Gotlandochitina spiriosa* (Eisenack). 60. *Ancyrochitina desmea* Eisenack. 61. *Urochitina simplex* Taugourdeau and De Jekhowsky. 62. *Ajigochitina crassispina* Eisenack. 63. *Ajigochitina comosa* Taugourdeau and De Jekhowsky. 64. *Angochitina mourai* Lange. 65. *Ancyrochitina primitiva* Eisenack. 66. *Ancyrochitina* sp. 67. *Angochitina* sp. 68. *Ramochitina magnifica* Lange. 69. *Cladochitina biconstricta* (Lange). 70. *Angochitina devonica* Eisenack. 71. *Ancyrochitina ramosaspina.* 72. *Sphaerochitina sphaerocephala.* 73. *Ancyrochitina ancyrea.* 74. *Anthochitina radiata.

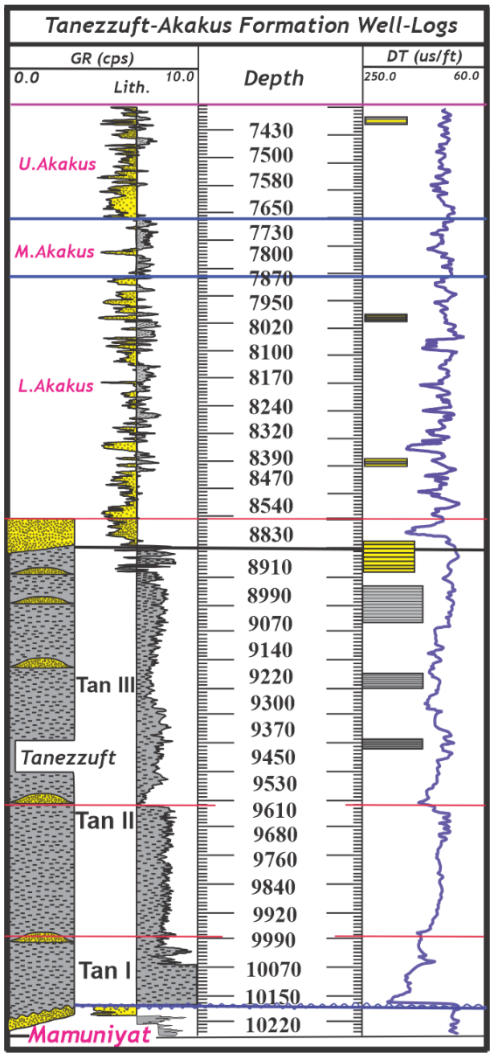

Figure 4.9: Stratigraphic column and well logs for the C1 Well. The well logs available are gamma-ray (GR) and acoustic (DT). The shaded boxes (yellow, gray, and dark gray) in the acoustic log column show the cored intervals for C1 from which we sampled for the study. In this figure, gray is for shale and yellow is for sandstone. The gamma-ray log was reported in units of counts per second (cps) because it was acquired by an old style of gamma-ray detector that was not calibrated.

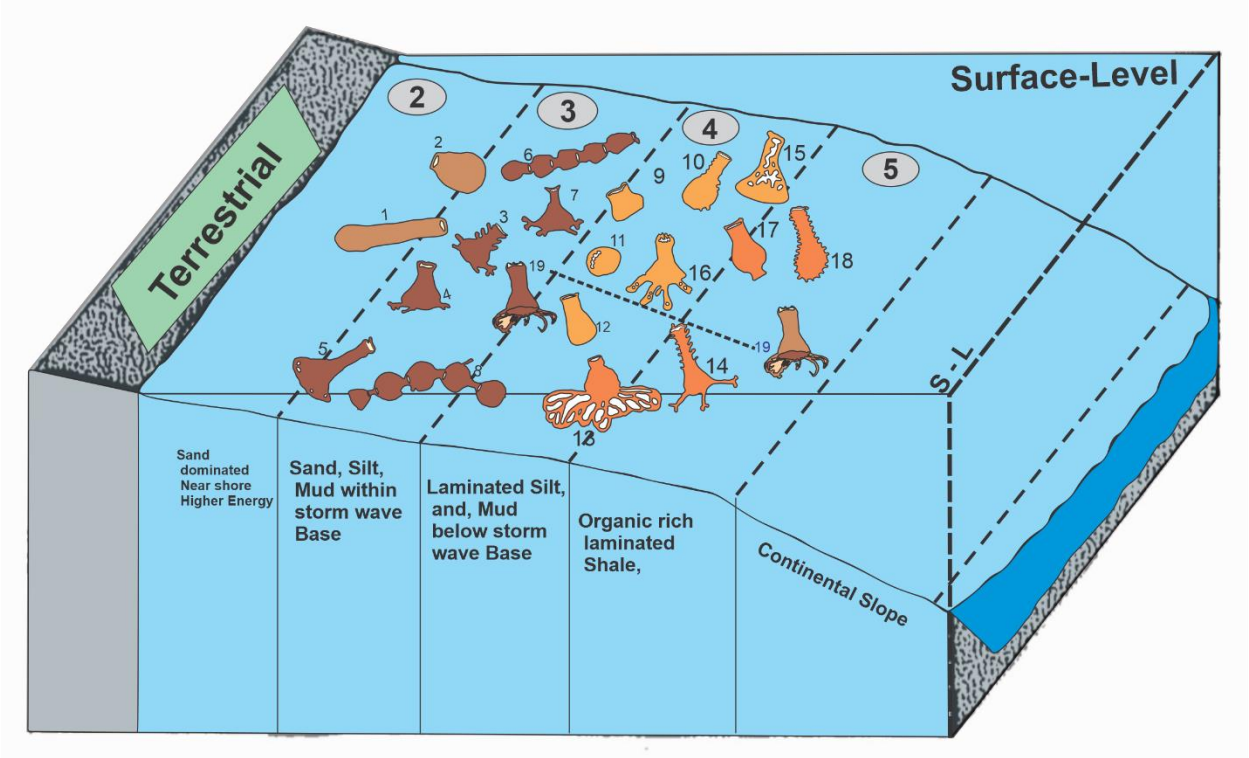

Figure 4.10: Schematic three-dimensional diagram displaying the distribution and connections between selected wall-resistant Chitinozoans and varieties of palynofacies (Modified from Al-Ameri 1983). Key to taxa: 1 = *Chonochitina decipiens; 2 = Conochitina* sp.*;* 3 = *Gotlandichitina* sp.*;* 4 = *Ancyrochitina* sp.*;* 5 = *Clathrochitina clathrata;* 6 = *Linochitina cingulata;* 7 = *Ancyrochitina fragillis;* 8 = *Margachitina* sp.*;* 9, 12 = *Bursachitina* ssp.; 10 = *Sphaerochitina* ssp.*;* 11 = *Petrochitina vitrea;* 13 = *Plectochitina carminae;* 14 = *Ancyrochitina gutnica;* 15 = *Lagenochitina vitrea;* 16 = *Plectochitina pseudoaglutinans;* 17 = *Linochitina erratica*; 18 = *Angochitina* ssp.*;* 19 = *Ancyrochitina ancyrea* in C1 well from Ghadamis Basin northwestern Libya.

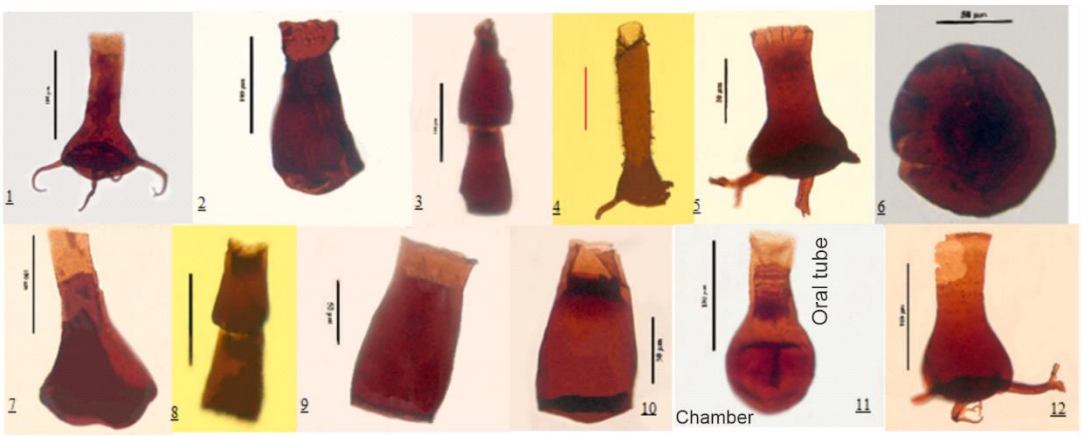

Figure 4.11: Key to taxa: Chitinozoans: All scale bar = 50 µm and 100 µm, 1: *Ancyrochitina fragilis.* C1-S9, [V15\4]; 2: *Euconochitina moussegoudaensis,* B1-S19, [Z21\4]; 3: *Cingulochitina convexa,* B1-S19, [T14\1]; 4: *Ancyrochitina* cf. *longispina,* C1-S5, 100 µm, [42\74]; 5: *Ancyrochitina gutnica,* C1-S11, [N29\2]; 6: *Anthochitina radiata*, C1-S3, [O43\3]; 7: *Sphaerochitina concava,* H1-S25, [W21\2]; 8: *Cingulochitina bouniensis,* C1-S5, 100 µm, 20x, [40\77]; 9: *Eisenackitina cylindrica.*, B1-S19, [R11\2]; 10: *Eisenackitina* sp., B1-S19, [T31\3]; 11: *Sphaerochitina sphaerocephala*, H1-S25, [R12\1]; 12: *Ancyrochitina primitive*, C1-S3, [D28\2].

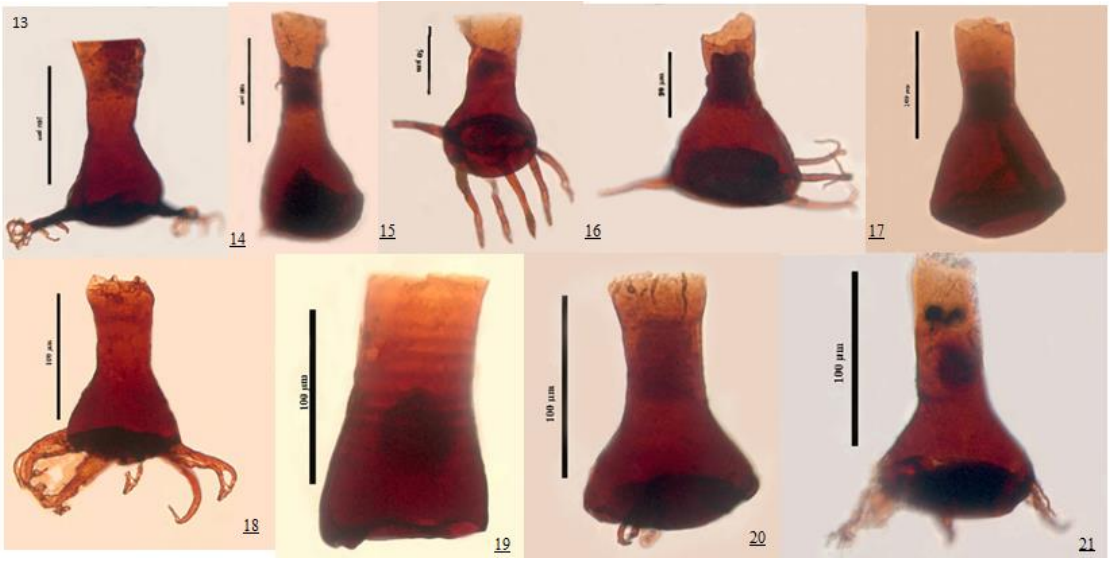

Figure 4.12: Key to taxa: Chitinozoans: All scale bar = 50 µm and 100 µm, 13: *Ancyrochitina ramosaspina* C1-S3, [O43\3]; 14: *Ancyrochitina ramosaspina,* B1-S19, [R36\3]; 15: *Ancyrochitina camilleae,* C1-S9, [N27\3]; 16: *Ancyrochitina camilleae,* B1-S19, [T28\3]; 17: *Fungochitina spinifera,* C1-S3, [T40\2]; 18: *Ancyrochitina ancyrea,* C1-S3, [N42\1]; 19: *Pseudoclathrochitina* sp., C1-S3, *[S12\2];* 20: *Ancyrochitina gutnica,* C1-S11, [W11\4]; 21*: Ancyrochitina laevaensis*, C1-S7, [J40\].

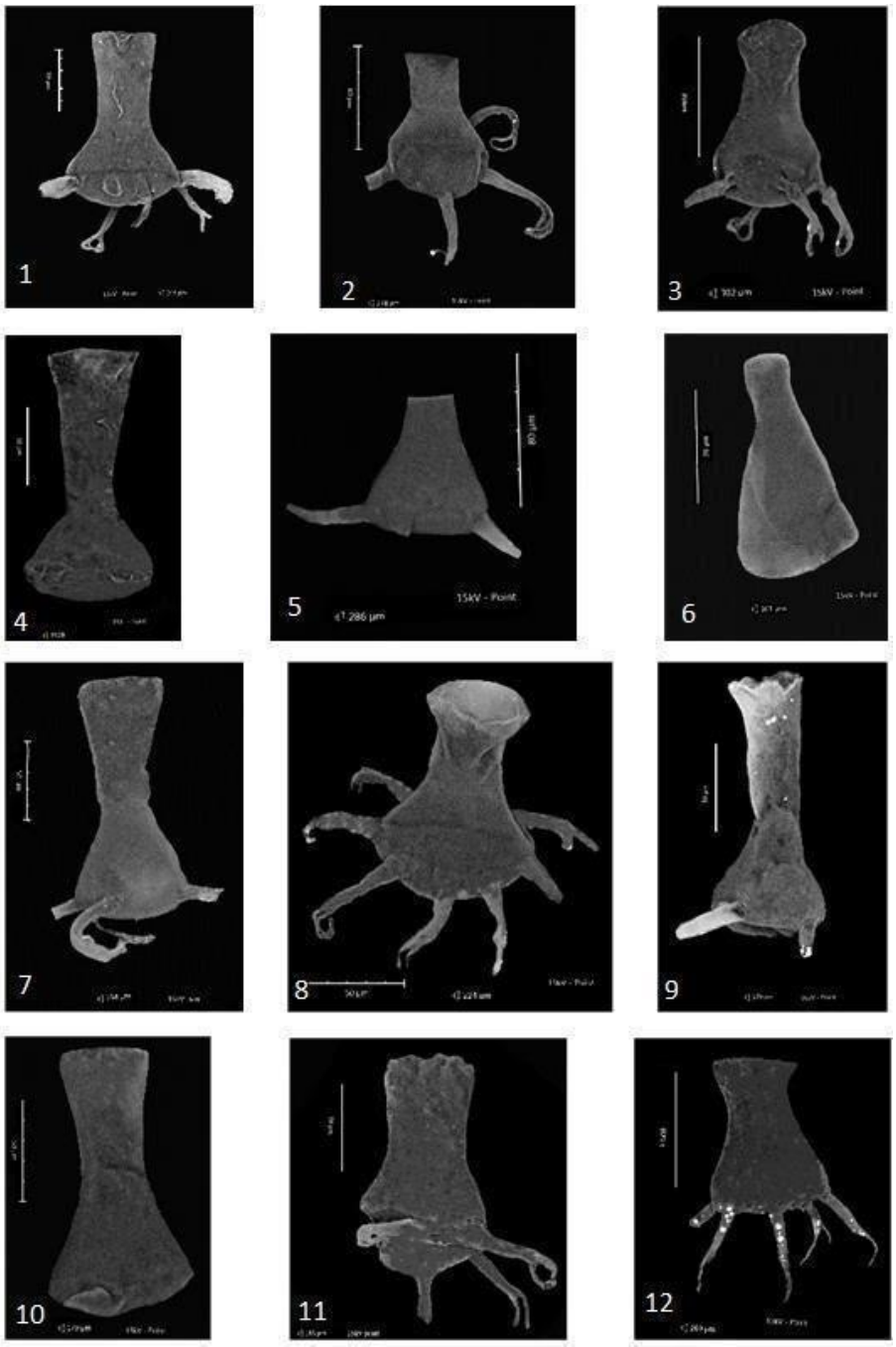

Figure 4.13: Key to taxa: Chitinozoans: All scale bar = 50 µm and 100 µm, 1: *Ancyrochitina ramosaspina*, 2- *Ancyrochitina camilleae* sp., 3: *Ancyrochitina camilleae* sp., 4: *Sphaerochitina concave,* 5*: Ancyrochitina fragilis,* 6: *Euconochitina moussegoudaensis,* 7*: Ancyrochitina ramosaspina,* 8: *Ancyrochitina ancyrea,* 9: *Ancyrochitina ramosaspina,* 10*: Ancyrochitina gutnica,* 11: *Ancyrochitina camilleae* sp., 12: *Ancyrochitina ancyrea*.

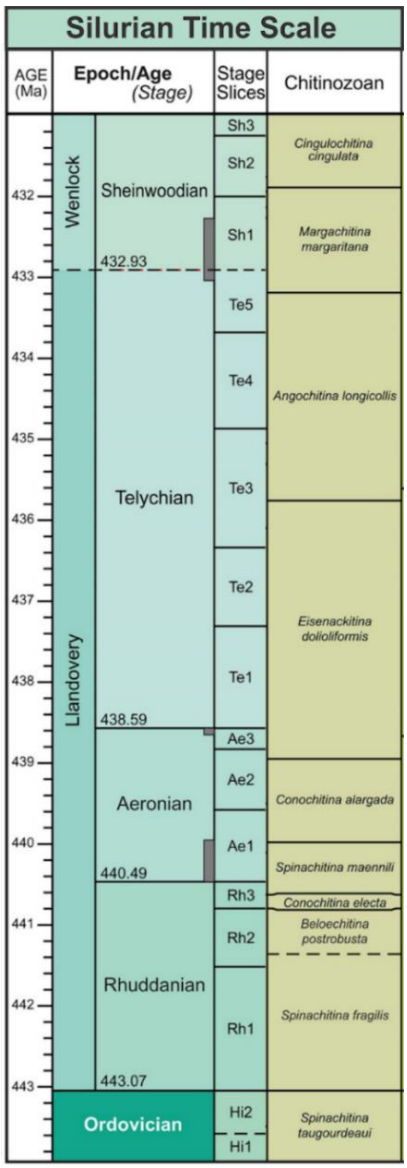

Figure 4.14: Silurian epochs and geologic time scale (modified from Gradstein et al., 2020), stage slices, chitinozoan zoning schemes. Stage slices from Cramer et al. (2011); chitinozoan zoning from Verniers et al. (1995), updated based on Nestor (2012). Gray boxes at the boundary of the stage indicate the interval of uncertainty in the correlation between the stratotype points. Dashed lines at the zone boundary indicate significant uncertainties in the placement or correlation of the zone boundary relative to the composite scale.

4.8. Discussion

4.8.1. Paleoenvironmental distribution of chitinozoans.

The distribution of chitinozoans is primarily affected by the depth and the temperature of the water, current energy, availability of oxygen, salinity, and to a lesser extent, substrate (Al-Ameri, 1983; Dorning, 1981). We recovered the chitinozoans species *Ancyrochitina ancyrea* from siltstone lenses in the sand-dominated upper Akakus unit and the interbeded shale-sand dominated middle Akakus unit (palynofacies 3 of Al-Ameri, 1983), from laminated mud and siltstone in Tan III (palynofacies 4 of Al-Ameri, 1983) from laminated mudstones in Tan III (palynofacies 5 of Al-Ameri, 1983: Table 4.2; Figure 4.10). Likewise, we recovered *Sphaerochitina concava* from all four units investigated in this study, which range from the siltstone lenses in the sand-dominated upper Akakus unit (Al-Ameri palynofacies 3) to pyritic, laminated mudstones of Tan III (Al-Ameri palynofacies 5: Table 4.2; Figure 4.10), indicating a possible epiplanktonic life habit for this species. Although neither *Eisenackitina cylindrica* nor *Plectinochitina* sp. occurred in the sand-dominated upper Akakus unit, both these taxa occurred in the lower Akakus unit, composed of sandstone, siltstone and shale (Al-Ameri palynofacies 3), in the laminated siltstones and mudstones of Tan III (Al-Ameri palynofacies 4), and in the pyritic, laminated mudstones of Tan III (Al-Ameri palynofacies 5), suggesting that these taxa may have been epiplanktonic as well.

Following Al-Ameri (1983) we interpret chitinozoans with anastomosing appendices as indicative of quiet water depositional settings, below storm-wave base (palynofacies 4 and 5). This effect is probably not taphonomic because we would expect to find broken branching appendices in samples from higher energy terrestrially-influenced deposits even if complete chitinozoans with anastomosing appendices were absent under microscope. We sampled two

environments below storm wave base in our study, the laminated, pyritic mudstones from samples C1-S3 and C1-S5 in Tan III (Al-Ameri palynofacies 5), and laminated mud- and siltstones from Tan III (Al-Ameri palynofacies 4). The pyritic, laminated mudstones of Tan III contain a mix of chitinozoan taxa assigned to quiet water and more energetic settings. As discussed above, *Ancyrochitina ancyrea, Eisenackintina cylindrica, Sphaerochitina concava,* and *Plectochitina* sp. occur in a wide range of depositional environments and may be epiplanktonic. In this study, *A. longispina, A. primitiva, Anthochitina radiata, Cingulochitina bouniensis* and *Fungochitina spinifera* occur only in pyritic laminated mudstones and may be adapted to quiet, deep-water, low oxygen environments. A group of *Ancyrochitina* species, *A. camilleae, A. gutnica* and *A. laevaensis* occur only in laminated mudstones and siltstones of Tan III (Al-Ameri palynofacies 4). Al-Ameri (1983) also placed *A. gutnica* in palynofacies 4.

Five taxa, *Ancyrochitina ramosaspina, Cingulochitina convexa,* cf. *Cingulochitina* sp. *Fungochitina* sp. and *Euconochitina moussegoudaensis,* occur only in the mixed sandstone, siltstone and shale facies of the lower Akakus unit (Al-Ameri palynofacies 3). Finally, two taxa occurred only in the sand-dominated upper Akakus unit (Al-Ameri palynofacies 2), *Sphaerochitina sphaerocephala* and *Pseudoclathrochitina* sp. Confirmation of these paleoecological hypotheses will require additional studies of chitinozoans in the Tanezzuft and Akakus formations.

4.8.2. Comparison with Other Assemblages from Northern Africa.

Ghadamis Basin - Tanezzuft Formation: Much of the palynological work on the Ghadamis Basin has focused on cryptospores and spores (Hoffmeister, 1959; Richardson and Ioannides, 1973; Loboziak and Streel, 1988; Rubinstein and Steemans, 2002; Vecoli and

Riboulleau, 2008; Spina and Vecoli, 2009; Paris et al., 2012; Le Hérissé et al., 2013; Paris, 2015).

Richardson and Ioannides (1973) described the spores and acritarchs of the Tanezzuft and Akakus formations from the B2-34 and C1-34 cores in the Ghadamis Basin. Their C1-34 core lies in the NC4 concession, as do our B1, C1 and H1 wells (Imsalem, 2018). Richardson and Ioannides (1973) placed the Tanezzuft/Akakus boundary in the Wenlock or early Ludlow and the upper part of the Akakus Formation in the late Silurian or early Devonian. Because they reported the depth of their samples in each core, we can place their results from the C1-34 core in the stratigraphic framework of this contribution (Daniels et al., 1990; Elfigih 2000). Further, assuming that the Tanezzuft Formation has the same approximate thickness in both cores as implied in Text-Figure 2 of Richardson and Ioannides (1973), we can extrapolate from the C1-34 to the B2-34 core to provisionally identify the Tanezzuft/Akakus boundary in the B2-34 core, allowing us to tentatively place their samples 23 through 19 in units of the Tanezzuft Formation.

In core C1-34, the Tanezzuft/Akakus boundary of Richardson and Ioannides (1973) lies approximately 39 m below the AGOCO preferred boundary (Elfigih 2000). Their sample 19 from B2-34, which lies approximately 17 m below AGOCO Tanezzuft/Akakus boundary and 56 m below the extrapolated AGOCO boundary in the B2-34 core, almost certainly belongs to the Tan III unit, which is approximately 100 m thick in the C1-34 core. The acritarchs present in sample 19 include: *Baltisphaeridium* spp., *Buedingiisphaeridium* sp. *A, Bued.* sp. *B, Diexallophasis caperoradiola,* cf. *Diexallophasis denticula, Micrhystridium* spp., *Multiplicasphaeridium* spp., *Tunisphaeridium* cf. *venosum, Neoveryhachium carminae, Onangadella deunffi, Triangulina* sp. *A, Veryhachium trispinosa, Leiofusa bernesga, L. cantabrica, L. estrecha, L.* cf. *estrecha, L. irroratipellis, L. stratifera*. The spores in this sample

include*: Retusotriletes warringtonii, R.* cf. *warringtonii, R. minor, R.* sp. *C, Ambitisporites avitus, A. dilutus, Synorisporites* cf. *verrucatus,* cf. *Synorisporites verrucatus, Archeozonotriletes chulus var. chulus, A. chulus var. nanus, Archeozonotriletes*? cf. *divellomedium*, spore type C and *Retialetes* cf. *legionis.* The acritarchs and spores in Sample 19 have relatively broad stratigraphic ranges (Tables 4.4 and 4.6). Richardson and Ioannides (1973) assigned sample 19 to the Homerian (late Wenlock) or early Ludlovian. We favor a Homerian age for the top of Tan III based on the occurrence of *Emphanisporites* cf. *protophanus,* placed by Wellman (1993) placed in *Artemopyra brevicosta,* in samples 20 and 21 of the B2-34 core, which lie below sample 19. Most occurrences of *A. brevicosta* are Homerian through early Pridolian (Burgess, 1991; Steemans, 1996), with the exception of a late Llandovery – early Wenlock occurrence in Ireland (Williams, 1996). We note that Richardson and Ioannides (1973) assigned a similar age range (late Wenlock - Pridoli) to both *E. protophanus* and *E.* cf. *protophanus*.

Samples 20 and 21 in the C1-34 core lie approximately 88 m below the Tanezzuft/Akakus boundary of Richardson and Ioannides (1973) and 127 m below the extrapolated AGOCO boundary, close to the Tan II/Tan III boundary, assuming that Tan III has the same approximate thickness in both the C1-34 and B1-34 cores. The acritarchs present in samples 20 and 21 of the B2-34 core include: *Baltisphaeridium* spp., *Buedingiisphaeridium* sp. *B, Diexallophasis caperoradiola,* cf. *Diexallophasis denticulata, Geron* spp., *Microsphaeridium* spp., *Multiplicasphaeridium* spp., *Neoveryhachium carminae, Onangadella deunffi, Triangulina* sp. *A, Veryhachium trispinosa, Leiofusa bernesga, L. cantabrica, L. estrecha, L.* cf. *estrecha, L. irroratipellis, L. striatifera, Deunffia monospinosa.* The spores present in samples 20 and 21 in the B2-34 core include: *Retusotriletes* cf. *warringtonii, Emphanisporites* cf. *protophanus*

(*Artemopyra brevicosta* of Wellman, 1993), *Ambitisporites avitus*, *Ambitisporites dilutus*, cf. *Synosporites verrucatus. Archeozonotriletes chulus var. chulus, Archeozonotriletes chulus var. nanus, Archeozonotriletes*? cf. *divellomedium, Retialetes* cf. *legionis, Verrucate tetrad.* As previously discussed, both samples 20 and 21 contain *Artemopyra brevicosta* (formerly *Emphanisporities* cf. *protophanus)*, consistent with assigning Tan III to the Wenlock. We assign most of our Tan III samples from the C1 well to the early Wenlock (Sheinwoodian) to minimize the later range extensions of the chitinozoan taxa, *Ancyrochitina camilleae*, and *A. longispina*. If most of the Tan III unit belongs to the Homerian as suggested by this analysis of the results of Richardson and Ioannides (1973), these taxa would extend into the Homerian.

Samples 22 and 23 lie 83 m above the Mamuniyat/Tanezzuft boundary, very close to the extrapolated Tan I/Tan II boundary, which lies at approximately 76 m in the B2-34 core (Figure 4.15). Acritarchs in samples 22 and 23 of Core B2-34 include: *Baltisphaeridium* spp., ?*Cymbosphaeridium pilaris, Diexallophasis denticulata* cf. *Microsphaeridium* spp. *Multiplicasphaeridium* spp., *Tunisphaeridium* cf. *venosum, Carminella maplewoodensis, Neoveryhachium carminae, Onangadella deunffi, Triangulina* sp. *A, Veryhachium trispinosa, Domasia* cf. *trispinosa, Leiofusa bernesga, L. cantabrica, L. estrecha, L. irroratipellis, L. striatifera,* and *Deunffia monospinosa.* Spores in samples 22 and 23 of Core B2-34 include: *Retusotriletes* cf. *warringtonii*, *Ambitisporites avitus*, *Ambitisporites dilutus*, *Ambitisporites* sp., and *Retialetes* cf. *legionis.* The spores and acritarchs in these samples have long stratigraphic ranges and could be late Llandovery (late in the early Silurian) or Wenlock (middle Silurian) in age.

Vecoli and Riboulleau (2008) reported chitinozoans, acritarchs and spores from the Tanezzuft Formation in the middle of Ghadamis Basin on the border between Tunisia and Libya, to the west of our sample localities (Figure 4.1). These authors provisionally placed the upper part of the Tanezzuft Formation, which is approximately equivalent to our Tan III, in the Ludlow (Late Silurian). However, all of the chitinozoans they used to make this determination range into the late Wenlock in western Gondwana or the peri-Gondwanan terranes: *Ancyrochitina primitiva* occurs throughout the Silurian; *Cingulochitina convexa* ranges from the Sheinwoodian (early Wenlock; Figure 4.13) to the Gorstian (early Ludlow); *Angochitina echinata* occurs in the Wenlock of Romania, the Czech Republic, Spain and Brazil (Givulescu, 1978; Schweineberg, 1987; Dufka, 1992; Grahn et al., 1992); and *Sphaerochitina acanthifera* appears in the Wenlock of France (Moreau-Benoit, 1972). Likewise, most of the acritarchs and all of the spores reported from Tanezzuft samples which Vecoli and Riboulleau (2008) assigned to the Ludlow, range into the Wenlock in Africa and the peri-Gondwanan terranes. The exception is *Deflandrastrum leonardii*, known only from the late Ludlow of Spain. The presence of this acritarch in the upper portion of the Tanezzuft Formation may be an earlier range extension into the Homerian (late Wenlock) for this taxon.

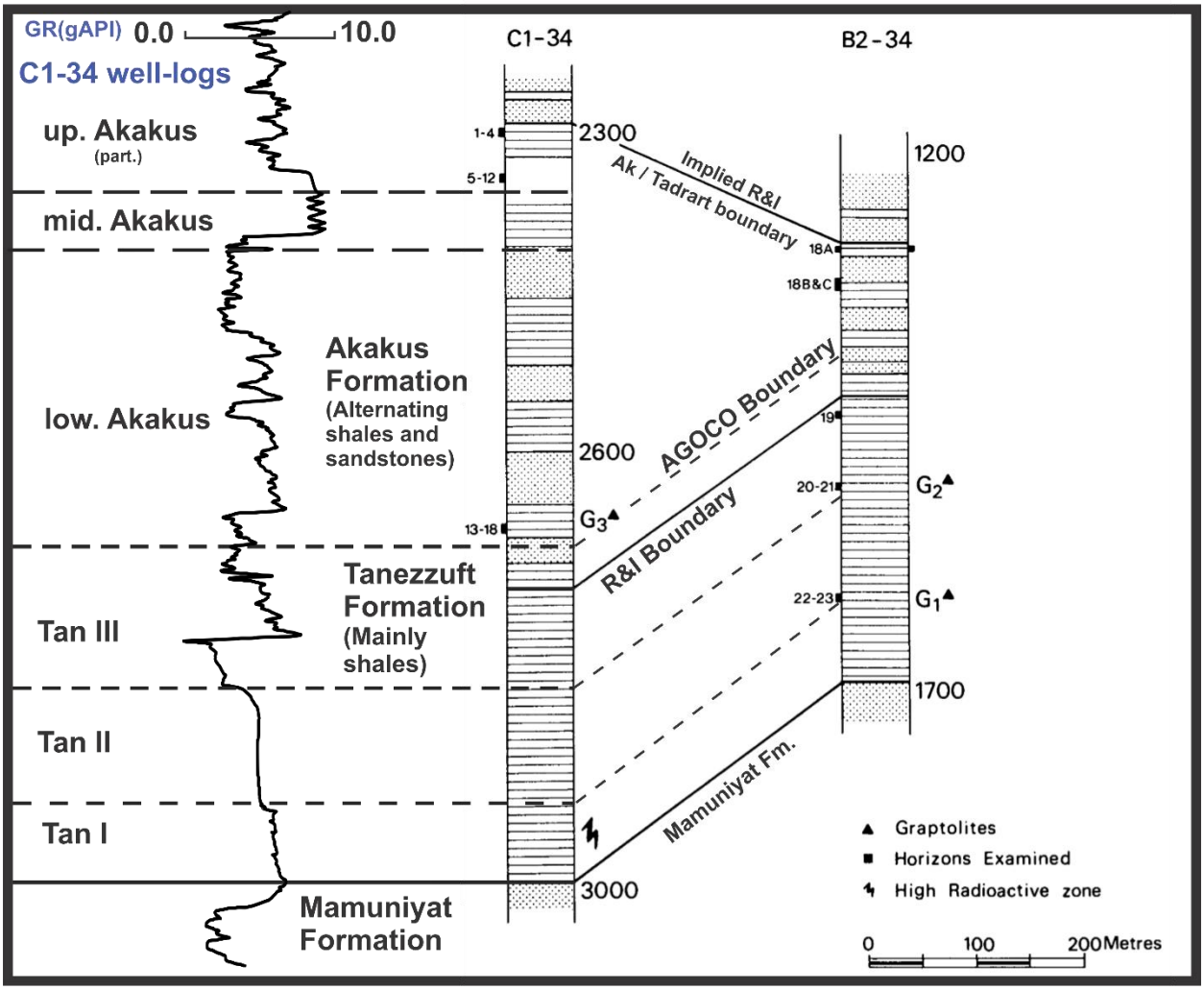

Figure 4.15: Postion of the Tanezzuft and Akakus formation units in the C1-34 core based on the AGOCO (formerly British Petroleum) well log, showing the Tanezzuft /Akakus boundary of Richardson and Ioannides (1973) and AGOCO (El-Mehdawi, 2004). Dashed lines between the C1-34 and B2-34 cores indicate the estimated position of Tanezzuft and Akakus formation units in the B2-34 ccore. Solid lines indicate the correlations of Richardson and Ioannides (1973). Tan I is a 'hot shale', Tan II has a silty shale lithology and Tan III has a very fine sandstone. Low. Akakus has a medium to coarse sandstone, mid. Akakus has more shaly sandstone. Up. Akakus has fine to medium sandstones.

Spina and Vecoli (2009) reported chitinozoans, and spores from the same locality studied by Vecoli and Riboulleau (2007). These authors assigned these shale sediments from the Tanezzuft Formation to the late Gorstian (early Ludlow) – Ludfordian (late Ludlow), based on the presence of *Angochitina echinata*. However, as discussed above, this taxon occurs in the

Wenlock in western Gondwana and the peri-Gondwanan terranes (Givulescu, 1978; Schweineberg, 1987; Dufka, 1992; Grahn et al., 1992), consistent with a Wenlock age for Tan III. Assigning Tan III to the Wenlock would not require a downward range extension for *Synorisporites libycus*, reported by Spina and Vecoli (2009) from the Tanezzuft Formation. Richardson and Ioannides (1973) recovered this species from the Akakus Formation, but not the Tanezzuft Formation. However, *S. libycus* has been reported from the late Homerian (late Wenlock) of Great Britain (Richardson et al., 1986; Burgess et al., 1991).

Ghadamis Basin - Akakus Formation: Samples 13 through 18 from the C1-34 core of Richardson and Ioannides (1973) come from a depth of about 2674 m, about 20 m above the Akakus/Tanezzuft boundary, which lies at 2694.4 m in the C1-34 core (Figure 4.15). Thus, the palynoflora of these samples contributes new information concerning the age of the Lower Akakus unit. The acritarchs in these samples include: *Baltisphaeridium* spp., *Buedingiisphaeridium* sp. *A, Cymbosphaeridium* sp. *A, Diexallophasis caperoradiola*, cf. *Diexallophasis denticula, Geron* sp., *Micrhystridium spp, Multiplicasphaeridium* spp., *Visbysphaera* sp. *A.*, *Lophosphaeridium* sp. *A.*, *Neoveryhachium carminae, Veryhachium lairdii V. trispinosa, Leiofusa estrecha, L. irroratipellis, L. stratifera*, and *Deunffia monospinosa.* The spores in this sample include*: Retusotriletes warringtonii, R.* cf. *warringtonii, R. minor, Emphanisporites protophanus, E.* cf. *protophanus* (*Artemopyra brevicosta* of Wellman, 1993), *E. neglectus, E. cf micronatus, E.* sp. *B, E.* sp. *C,* cf. *Brochotriletes, Ambitisporites avitus, A. dilutus, A.* sp. *A, Synorisporites* cf. *verrucatus*, cf. *S. verrucatus S.*? *libycus, S.* sp. *B, S.* sp. *C, Lophozonotriletes*? *poicilomorphus, L.*? sp. *A, Archeozonotriletes chulus var. nanus (Wenlock Ged), Archeozonotriletes*? cf. *divellomedium*, spore type A, *Tetraletes variabilis*, and *Retialetes*

cf. *legionis*. Richardson and Ioannides (1973) referred to these samples as the 'middle assemblage', and did not identify their age, although they placed the underlying Tanezzuft Formation in the Wenlock or Ludlow, and the overlying 'upper assemblage" in the Ludlow – Gedinnian (late Silurian – early Devonian). The presence of *Emphanisporites protophanus* indicates a late Wenlock or later age (Burgess and Richardson, 1995; Cesari et al., 2020); *E. neglectus* indicates a Wenlock or later age (Marshall, 1991). Moreau-Benoit (1988) reported *E. neglectus* in the Pridoli of Ghadamis basin, but source was Richardson and Ioannides (1973). Because our samples from the lower Akakus unit contain a mix of taxa elsewhere confined to the Telychian, as well as taxa that occur in the Wenlock through Gorstian (early Ludlow, late Silurian), we favor a late Wenlock – early Ludlow (Gorstian) age for the middle assemblage of Richardson and Ioannides (1973).

Richardson and Ioannides (1973) suggested that samples 1 through 12 of Core C1-34 and samples 18 a –c of B2-34 came from near the top of the Akakus Formation, close to the boundary with the overlying Tadrart Formation (Figure 4-15). However, well-log data from the C1-34 core indicates that the Akakus/Tadrart boundary lies many meters above samples 1-12 of the C1-34 core (Elfigih 2000: Figure 4-15). Based on well-log data, these samples may come from the base, rather than the top of the upper Akakus unit, and the position of samples 18 a-c relative to the Akakus/Tadrart boundary remains unknown.

Because of the uncertainty of correlation, we discuss the biostratigraphy of Samples 1-12 from the C1-34 core and samples 18 a-c from the B2-34 core separately. The acritarchs in samples 1-12 from the C1-34 core include: *Ammonidium* sp. *A, Ammonidium* sp. *B, Baltisphaeridium* spp., *Buedingiisphaeridium* sp. *A, Buedingiisphaeridium* sp. *B, Cymbosphaeridium pilaris, C.* sp. *A, Diexallophasis caperoradiola,* cf. *Diexallophasis denticula,*

Filisphaeridium sp. *A, Geron* spp., *Microsphaeridium* spp., *Microsphaeridium*? sp. *A, Multiplicasphaeridium* spp., *Visbysphaera dilatispinosa, V.* sp. *A, Lophosphaeridium* sp. *A, Estiastra* cf. *barbata, Neoveryhachium carminae, Oonondagella deunffii, Veryhachium lairdii, V. octoaster, V. trispinosum, Domasia* cf. *trispinosa, Leiofusa bernesga, L. cantabrica, L. estrecha, L. striatifera, Metaleiofusa* sp. *A, Deunffia monospinosa, Cymatiosphaera* sp. *A, Cymatiosphaera*? sp. *B, Cymatiosphaera*? sp. *C,* and *Quadraditum fantasticum* (Richardson and Ioannides, 1973). The spores from these samples include: *Retusotriletes* cf. *goensis, R. warringtonii, R.* cf. *warringtonii, R.* cf. *dubius, R.* cf. *frivolus, R. minor, R.* cf. *minor, Retusotriletes* sp. *A, Retusotriletes* sp. *B, Retusotriletes* sp. *D, Apiculiretusispora spicula, A. synorea, Apiculiretusispora* sp. *A, Apiculiretusispora* sp. *B, Emphanisporites protophanus, Emphanisporites* cf. *protophanus* (*Artemopyra brevicosta* of Burgess and Richardson 1991), *E. rotatus, E.* cf. *rotatus, E. neglectus, E.* cf. *micronatus, E. pseudoerraticus* (*E. splendens* of Richardson et al., 1979*), Emphanisporites* sp. *D,* cf. *Brochotriletes* sp. *A, Ambitisporites avitus, A. dilutus, Ambitisporites* sp. *B, Synorisporites* cf. *verrucatus,* (renamed *Hispanaediscus verrucatus*? of Wellman, 1993), cf. *Synorisporite verrucatus, S.? libycus, Synorisporite* sp. *A, Synorisporite* sp. *C, Lophozonotriletes*? *poicilomorphus, Lophozonotriletes* sp. *A, Archeozonotriletes chulus var. chulus, A. chulus var. nanus, A.*? cf. *divellomedium, Cymbosporites* sp. *A, Chelinospora* sp. *A, Chelinospora* sp. *B, Spore Type A, Spore Type B, Spore Type D, Tetraletes variabilis, T. granulatus, Retialetes* cf. *legionis.* Most of these taxa have relatively broad stratigraphic ranges and wide paleogeographic distributions. However, the spore, *E. splendens,* has a relatively restricted paleogeographic distribution (Libya, Saudia Arabia, Great Britain, Canada, and China: (Moreau-Benoit, 1988; Stump, 1995; Burden, 2002; Lianda, 1981) and first appears in the Ludlovian (late Silurian), which would suggest a

Ludlovian age for samples 1 - 12 in core C1-34, and for the base of the lower Akakus unit, which is consistent with the age of the base of the lower Akakus unit based on our samples.

Samples 18 a-c in the B2-34 core contain fewer taxa than upper Akakus unit samples from the C1-34 core of Richardson and Ioannides (1973). The acritarchs in these samples include: *Baltisphaeridium* spp., *Buedingiisphaeridium* sp. *B, Cymbosphaeridium* sp. *A, Diexallophasis caperoradiola,* cf. *Diexallophasis denticula, Geron* sp., *Micrhystridium* spp., *Micrhystridium* spp.? sp. *A, Multiplicasphaeridium* spp., *Visbysphaera dilatispinosa, Visbysphaera* sp. *A.*, *Lophosphaeridium* sp. *A.*, *Deflandrastum* sp. *A, Neoveryhachium carminae, Onangadella deunff, Triangulina* sp. *A, Veryhachium lairdii, V. trispinosum, Leiofusa bernesga, L. estrecha, L. irroratipellis, L. stratifera, Metaleiofusa* sp. A, *Deunffia monospinosa,* and *Quadraditum fantasticum.* The spores in these samples include*: Retusotriletes warringtonii, R.* cf. *warringtonii, R.* cf. *dubius, R. minor, R.* sp. *A, Emphanisporites protophanus, E.* cf. *protophanus* (renamed *Artemopyra brevicosta* of Wellman, 1993), *E. neglectus, E.* cf. *micronatus, E* sp. *A, E.* sp. *D,* cf. *Brochotriletes* sp. *A, Ambitisporites avitus, A. dilutus, Synorisporites* cf. *verrucatus* (*Hispanaediscus verrucatus*? of Wellman, 1993), cf. *S. verrucatus S.*? *libycus, Lophozonotriletes*? *poicilomorphus, L.*? sp. *A, Archeozonotriletes chulus var. chulus, Archeozonotriletes chulus var. chulus nanus, Archeozonotriletes*? cf. *divellomedium, Cymbosporites* sp. *A.* spore type A, *Tetraletes variabilis, T. granulatus,* and *Retialetes* cf. *legionis.* The presence of *Artemopyra brevicosta* (*Emphanisporiites* cf. *protophanus* of Richardson and Ioannides, 1973) suggests a late Wenlock (Homerian) – Pridolian, or mid to late Silurian age for these samples.

Based on spores, Rubinstein and Steemans (2002) placed the Akakus Formation from the MG-1 borehole of the Ghadamis Basin in the Ludlow – Pridoli. This locality lies close to the

Tunisian/Libyan boundary and to the west of our study locality. These authors did not report the position the lower, middle and upper units of the Akakus Formation in the MG-1 borehole, although their C14 and C15 samples, which they placed in the middle Pridoli (late Silurian), come from the top of the Akakus Formation, close to the Akakus/Tadrart Boundary. This age assignment for the uppermost Akakus Formation suggests that the upper Akakus unit may range into the Pridoli.

Le Hérissé et al. (2013) used acritarchs and chitinozoans to place the upper 400 m of the Akakus Formation in the A161 well in the Ludlow - Pridoli. This location lies close to our C1 well (Figure 4.1). Many of the taxa used to place the earliest biozone (biozone 1) of Le Hérissé et al. (2013) into the Ludlow - Pridoli (Late Silurian) also occur in Wenlock (mid Silurian). These taxa include: *Anthochitina superba, Baltisphaeridium gordonense, Leoniella carminae, Onondagella cylindrica, Schizocystia saharica, Veryhachium scabratum, V. bonitum, V. jardinei*. The uppermost Akakus Formation (Figure 4.4) may range into the Pridoli (Late Silurian).

Murzuq Basin - Tanezzuft: Paris et al. (2012) studied the lower Tanezzuft Formation on the east edge of the Murzuq Basin of Libya, where the Tanezzuft Formation is condensed. These authors used chitinozoans to place the lower Tanezzuft Formation in the Rhuddanian (early Llandovery, early Silurian) to Wenlock (mid Silurian). This age for the lower part of the Tanezzuft Formation (possibly equivalent to our Tan I and Tan II) is consistent with our age assignment of Tan III to the Sheinwoodian (early Wenlock, mid Silurian).

Saudia Arabia - Qalibah Formation: Paris et al. (2015) studied the Qusaiba Member of the Qalibah Formation in Saudia Arabia, which correlates to the Tanezzuft Formation of Libya and Tunisia. These authors assigned the Qusaiba Member to the Rhuddanian (early Llandoverian, early Silurian) through Aeronian (mid Llandoverian, early Silurian), and the

overlying Sharawra Member to the Sheinwoodian and lower Homerian. They correlated sediments in the lower Qusaiba Member to the 'hot shale' of the Tanezzuft Formation (Tan I in part) and assigned these samples to the Rhuddanian (early Llandoverian, early Silurian). They correlated the overlying sediments in the Qusaiba Member to the Rhuddanian through Aeronian (early to mid-Llandoverian, early Silurian). These sediments contain the chitinozoan *Ancyrochitina camilleae*, which also occurs in our Tan III samples, assigned here to the Sheinwoodian. In the Qusaiba Member, Paris et al. (2015) used *A. camilleae* to define a local sub-biozone at the top of the hemeri biozone, known only from Saudia Arabia. These authors assigned the *camilleae* sub-biozone to the late Aeronian.

Paris et al. (2015) did not comment on the correlation of the overlying Sharawra Member. However, Rahmani et al. (2019) suggested that the early Silurian 'hot shale' and overlying 'cold shales' of Northern Africa accumulated in former tunnel valleys formed during glacial melting. They further suggested that, as the shales of the Qusaiba Member accumulated in these old tunnel valleys, the overlying Sharawra Member accumulated on the Arabian shelf, which would make the Sheinwoodian Sharawra Member equivalent in age with the upper part of the Tanezzuft Formation (i.e., Tan III). Resolution of the correlation between the Tanezzuft Formation of the Ghadamis Basin and the Qusaiba and Sharawra members of the Qalibah Formation will require study of the palynoflora of Tan I and II from the Ghadamis Basin.

4.8.3. Depositional environments of the Tanezzuft and Akakus formations in the Ghadamis Basin.

Tan I and II - The deposition of the Tanezzuft Formation began in the early Rhuddanian (early Llandovery, early Silurian), with the accumulation of organic-rich shales (the 'hot shale'

of Tan I) in former tunnel valleys, carved as Late Ordovician glaciers melted (Le Héron et al., 2018; Rahmani et al., 2019). Based on well-log data from this study and the literature, the distinctive 'hot shale' unit at the base of the Tanezzuft appears in southern Jordan (Mudawwara Shale) as well as northeast Libya (Butcher, 2009; Loydell et al., 2009). The high TOC content of the 'hot shale' (up to 17% TOC) and the presence of heavy minerals (U) suggest that these sediments accumulated in a marine, anoxic setting (Lüning et al., 2000; Butcher, 2013). 'Hot shale' palynofloras contain abundant chitinozoans and marine acritarchs also indicating deposition in a deep-water marine environment (Butcher, 2013). Sediments from the upper part of Tan I and all of Tan II lack Ur and have lower TOC values (1 – 5% TOC), consistent with deposition in quiet water on an open marine shelf.

The fine-grained laminated sediments of Tan III, which may contain pyrite framboids, suggest deposition in a low-energy setting, supported by the presence of chitinozoan with long, branching appendices in Tan III samples, for example *A. fragilis, A. gutnica* and *Plectochitina* sp. Al-Almeri (1983) placed chitinozoans such as *A. ancyrea, A. fragilis,* and *A. gutnica*, which have long, branching appendices, in marine shelf environments: *A. ancyrea* in shallow, *A. gutnica* in intermediate shelf environments and *A. fragilis* on the boundary between the two. In our samples, *Ancyrochitina ancyrea* occurs in a broad range of depositional environments, from pyritic laminated mudstones in Tan III (Al-Ameri palynofacies 5) to siltstone lenses in the very fine sand-dominated upper Akakus (Al-Ameri palynofacies 2) and may be epiplanktonic. *Plectochitina* sp., another chitinozoan in Tan III samples, also indicates an intermediate shelf environment (Al-Almeri, 1983).

Machado (pers com. 2020) defined the marine percentage of a unit or sample as the percentage of all palynomorphs derived from marine groups (in this case, acritarchs,

chitinozoans and scelecodonts) plus the percentage of all palynodebris consisting of AOM clusters. Tan III samples have a high average marine percentage (47%), which is consistent with the presence of chitinozoans from deep, shallow and intermediate shelf environments in these samples. Tan III samples have relatively low t/m and phyto/AOM indices, respectively 0.76 and 2.13 (Table 4.1).

Although no Tan III sample has the high TOC and U content of the 'hot shale', the growth of pyrite framboids inside chitinozoans from the lowest two Tan III samples (C1-S3 and C1-S5) indicates the presence of anoxic pore water in Tan III sediments for short intervals of time. Tan III deposition probably began in the Sheinwoodian (early Wenlock, middle Silurian) and continued into the Homerian (late Wenlock, middle Silurian), although this age designation requires extending the ranges of some early Silurian chitinozoans into the middle Silurian.

Lower Akakus unit – Daniels et al. (1990) identified the base of the Akakus Formation as the lowest, coarse, blocky sandstone. During the deposition of the lower Akakus unit, the shelf became progressively shallower as deltaic sediments prograded from the southeast to northwest (Turner, 1991; Gindre et al., 2012; Aimen et al., 2020). Aimen et al. (2020) interpreted herringbone cross-stratification in the lower Akakus unit as evidence of tidal sedimentation. Hallett and Clark-Lowes (2016) also interpreted the lower Akakus unit as progradational.

Despite evidence of tidal sedimentation in this unit, the chitinozoans recovered from interbedded shales suggest shallow and intermediate open shelf environments. For example, Al-Almeri (1983) placed the following chitinozoan genera from the lower Akakus uint in intermediate shelf environments, *Sphaerochitina* and *Plectochitina*. Another chitinozoan from the lower Akakus unit, *Ancyrochitina ramosaspina*, has long, branching appendices like *A. ancyrea*, *A. gutnica* and *A. fragilis*, species which Al-Almeri (1983) placed in shallow and

intermediate shelf environments. The average marine percentage and t/m and phyto/AOM indices of the lower Akakus unit, respectively 43%, 0.99% and 2.01% are similar to those of the Tan III.

Middle Akakus unit – In our study area, the middle Akakus unit contains more mud and less sandstone than the underlying lower Akakus unit. Although most workers have viewed the middle Akakus unit as part of a progradational sequence (Gindre et al., 2020), Hallet and Clark-Lowes (2016) interpreted the middle Akakus as a transgressive unit sandwiched between the progradational lower and upper Akakus units.

Palynofloral analysis of the middle Akakus unit supports the Gindre et al. (2020) progradational interpretation. The middle Akakus samples have the lowest average marine percentage (23%) and the highest T/M and phyto/AOM indices (respectively 3.54 and 4.93) of any unit in the Tanezzuft or Akakus formations. We recovered only one chitinozoan, *Sphaerochitina* sp., which Al-Almeri (1983) placed in intermediate shelf environments below storm wave base (Palynofacies 4). However, the presence of *Sphaerochitina* sp. in the middle Akakus unit may indicate quiet water conditions, rather than quiet, deep water.

Upper Akakus unit – The upper Akakus unit contains more sandstone than the lower and middle units. Hallet and Clark-Lowes (2016) interpreted the upper Akakus unit as a progradational unit, and Hallet (2002) reported land-plant macrofossils near the top of this Formation. Nonetheless, Gindre et al. (2012) interpreted the upper Akakus unit as transgressive.

Our only palynofloral samples in the upper Akakus unit come from the base of the Formation. However, the palynoflora of these samples indicates a return to marine, open shelf conditions. Two upper Akakus chitinozoans *Ancyrochitina ancyrea* and *Sphaerochitina concava*, *Sphaerochitina sphaerocephala* and *Pseudoclathrochitina* sp. have long, branching appendices

indicative of shallow and intermediate marine shelf environments (Al-Almeri, 1983). Likewise, Al-Almeri (1983) placed the chitinozoan genus, *Sphaerochitina* sp., which also occurs in our upper Akakus unit samples, in intermediate shelf environments, although its presence in the middle Akakus unit suggests that some sphaerochitinids lived in near-shore, low-energy settings. The average marine percentage of upper Akakus unit samples (46%) is slightly lower than the average marine percentage of Tan III samples (47%), which also contain chitinozoans indicative of marine shelf environments. The t/m and phyto/AOM indices of upper Akakus samples (respectively 1.12 and 2.23) are similar to those of Tan III and lower Akakus samples (respectively 0.76 - 0.99 and 2.01 - 2.13). Although palynofloral analysis supports a transgressive interpretation for the base of the upper Akakus unit, we have no palynofloral data for the top of the upper Akakus unit, which could be progradational.

4.8.4. Systematics

Reference slides are housed at the Paleontological Laboratory, Texas A&M University, College Station, TX and were processed at The University of Texas of the Permian Basin (UTPB), Odessa, TX. Slide numbers and alphabetical letters are England Finder's reference position (Figure 4.11; Figure 4.12). Chitinozoans are described alphabetically in the order below.

1. ***Ancyrochitina ancyrea* Eisenack, 1931**

   Description: *A. ancyrea* shows a finely spinose ornamentation on the upper part of the chamber and on the neck (Ghavidel-Syooki, 2011). It has the long, branching appendices.

   Size: Vesicle length 126.8 -147.9 µm

   Total appendices: length including branches 46.5–78.9 µm.

Stratigraphic range: middle Llanvirn (Llandeilian) - late Ludlovian (late Ordovician to late Silurian worldwide; Ghavidel-Syooki, 2011).

Remarks: Processes on our specimens are often broken distally, but, when intact, they possess all characteristics of *A. ancyrea*.

2. *Ancyrochitina camilleae* Paris, 2015

Description: *A. camilleae* has a tiny overall size, a deltoid-shaped body chamber with virtually straight flanks, a psilate wall, and a short neck. The collarette on the neck is well-developed, with serrate lips. Six different appendages are affixed to the body chamber's basal border. Appendices are lengthy, hollow, and branch distally (Paris et al., 2015).

Size: Vesicle length 134.2-144.7 µm.

Total appendices: length including branches 39.5–65.8 µm.

Stratigraphic range: Rhuddanian – Sheinwoodian (early – middle Silurian; Paris et al., 2015; this study).

Remarks: The second recorded occurrence of *A. camilleae* is in Tan III from the C-1 well (this study). These specimens differ slightly from those described by Paris et al. (2015) in lacking well-developed distal branching which we attribute to taphonomic factors. *A. camilleae* co-occurs with *A. longispina* and *A. laevaensis* in the early Silurian Qusaiba Member of the Qalibah Formation of Saudia Arabia (Paris et al., 2015).

3. *Ancyrochitina longispina* Achab, 1978

Description: *P.* cf. *longispina* is almost as tall as it is wide with an irregular wall line. Usually conoid, sometimes semi conoid. Vasant with a translucent collar and a cylindrical shape. The prosome joins at the base of the neck. Spongy appendages, usually simple, are attached to a flat or slightly convex base (Achab, 1978).

Size: Vesicle length 139.7-146.8 µm.

Total appendices: length including branches 7.4 - 23.4 µm.

Stratigraphic range: Ashgill - Sheinwoodian (late Ordovician – middle Silurian; Achab, 1978; Paris, 1996; Nestor, 2012; this study).

Remarks: Our specimens are comparable in shape, size and appendage appearance to those found in the upper part of the Vaureal Formation of Quebec (Achab, 1978). *A. longispina* co-occurs with *A. camilleae* and *A. laevaensis* in the Qusaiba Member of the Qalibah Formation (early Silurian) of Saudia Arabia (Paris et al., 2015). Paris (1996) reported *A. longispina* in the early Sheinwoodian of Baltica and Gondwana. We extend its range thoughout the Sheinwoodian (early Wenlock, middle Silurian).

4. *Ancyrochitina fragilis* Eisenack, 1955

Description: *A. fragilis* is sac-bearing shape with internal spongy section, central appendages attached at the base of the test. It has chitinozoan assemblages with many different shapes and with different types of appendices (Nestor, 2011).

Size: Vesicle length 161.8 - 167.4 µm.

Total appendices: length including branches 38 - 42.5 µm.

Stratigraphic range: Telychian – Early Devonian (early Silurian – early Devonian; Taugourdeau et al., 1960; Nestor, 2011).

Remarks: *A. fragilis* displays variation in its shape and appendices. Nestor (2011) reported *A. fragilis* from a short interval just above the base of the *E. kerria* and *A. tomentosa* Biozone in East Baltic location. I used the *A. fragilis* range in Gondwana of Algeria (Taugourdeau et al., 1960).

5. *Ancyrochitina gutnica* Laufeld, 1974

Description: *A. gutnica* has a convex base and cylindro-conical vesicle. The basal edge is bluntly to widely rounded. The neck is nearly half the length of the whole fossil, and widens as it approaches the aperture, which is smooth and infringed. The shoulder is rounded bluntly. Most specimens have a broadly rounded shoulder; however, it can be absent. In the aboral region of the neck, the spines are long and well-developed, but shrink in size as they approach the aperture (Laufeld, 1974).

Size: Vesicle length 127.5-148.7 µm.

Total appendices: length including branches 11.8-13.2 µm.

Stratigraphic range: Telychian – Ludfordian (early – late Silurian; this study).

Remarks: *A. gutnica* first appears in the Katrinelund Limestone of the Slite Beds and is then encountered in all lithologies of the Slite Beds, where it is a characteristic element most abundant in the marly facies. It is common in the Mulde Beds (Laufeld, 1974).

6. *Ancyrochitina laevaensis* Nestor, 1980

Description: In cross section, the vesicle chamber is conical in shape, with a convex base and a convex basal edge. The basal edge is rounded from blunt to broadly rounded (Nestor, 1994).

Size: Vesicle length 142.1-153.7 µm.

Total appendices: length including branches 22.4 - 49.2 µm.

Stratigraphic range: Rhuddanian - Wenlock (early – middle Silurian; Bassett et al., 1989; Nestor, 1994; Vernier et al., 1995).

Remarks: *A. laevaensis* co-occurs with *A. camilleae* and *A. longispina* in the Qusaiba Member of the Qalibah Formation (early Silurian) of Saudia Arabia (Paris et al., 2015).

7. *Ancyrochitina primitiva* Eisenack, 1964

Description: *A. primitiva* has a flat to slightly convex base and a conical chamber. The surface has slight ornamentation "consisting of curved spines" and ramified appendices attached to the base (Askew, 2019).

Size: Vesicle length 146.5-159.8 µm.

Total appendices: length including branches 18.6-50.7 µm.

Stratigraphic range: Telychian - Pridoli (Silurian; this study).

Remarks: Although deterioration often prevents assessment of its size, *A. primitiva* can be identified if the flexure is visible and the aperture flares (Askew, 2019). The specimens recovered in this study are damaged, but can identified as *A. primitiva* due to their flaring aperture and the shape of their appendices.

8. *Ancyrochitina ramosaspina* Nestor, 1994

Description: *A. ramosaspina* has a big vesicle characterized by multiple branching processes roughly half of the overall length of the vesicle, with each subsequent branch more robust (Paris et al., 2015).

Size: Vesicle length 191.8 – 211.2 µm.

Total appendices: length including branches 59.8 – 60.8 µm.

Stratigraphic range: Rhuddanian – Homerian or possibly Ludlow (early – middle or late Silurian; Nestor, 1994; this study).

Remarks*:* The neck of *A. longispina* is longer and the branching structure of its long processes differs slightly from those figured in Paris et al. (2015). In the Ghadamis Basin, *A. ramosaspina* occurs in the lower Akakus unit, which could be Homerian (late Wenlock, middle Silurian) or Gorstian (early Ludlow, late Silurian) in age.

9. *Anthochitina radiata* Wrona, 1980

Description: The vesicle of *A. radiata* is identical in form and size are to that of *A. superba* Eisenack. Like *A. radiata*, our specimens resemble wheels with spokes in aboral view under transmitted light, with the vesicle base in the center and the spongy membrane of the carina at the periphery. The radial processes are solid at the base. The proximal sections of the radial processes, on the other hand, may have little hollows that widen toward the outer edge (Wrona, 1980).

Size: Vesicle length 110.0-115.2 µm.

Total appendices: No appendices in this taxon.

Stratigraphic range: Sheinwoodian – early Devonian (middle Silurian – early Devonian; this study).

Remarks: *A. radiata* differs from *A. superba* Eisenack in the shape of the caraina (Wrona, 1980). In the Ghadamis Basin, *A. radiata* occurs in Tan III, which could be Sheinwoodian (early Wenlock, middle Silurian) in age.

10. *Cingulochitina bouniensis* Vernier, 1999

Description: Cono-ovoid *Cingulochitina* with a tapering neck that is very short. The shoulders are amorphous, and the flanks are convex or straight. A ridge-like carina or

folding occurs beneath the vesicle's maximum width. The carina can be seen within the vesicle chain. The surface is perfectly smooth without decoration (Vernier, 1999).

Size: Vesicle length 175.5-199.2 µm.

Total appendices: No appendices in this taxon.

Stratigraphic range: Telychian - Homerian (early - middle Silurian: Van Grootel and Vernier et al., 1998).

Remarks: *C. bouniensis* is shorter and wider than *C. angusta.* Most of our *C. bouniensis* specimens lack longitudinal folds. Some foldss occur but are randomly distributed and not parallel to the longitudinal axis.

11. *Cingulochitina convexa* Laufeld, 1974

Description: *C. convexa* can be distinguished from other *Cingulochitina* taxa by its characteristic convex base. *C. convexa* was identified in the Akakus lower unit. However, compared to other *Cingulochitina* taxa, *C. convexa* differs slightly in length and diameter and in the absence of fine rugose ornamentation on the vesicle surface. The original diagnosis of the *C. convexa* compared this species to *C. crassa*, which has a fully smooth surface (Nestor, 1994). Laufeld (1974, p.99, fig. 58b) clearly shows a *C. convexa* chitinozoan specimen with fine rugose ornamentation.

Size: Vesicle length 236.8-253.6 µm.

Total appendices: No appendices in this taxon.

Stratigraphic range: Gorstian – Ludlow (middle – late Silurian; Verniers et al., 1995; Nestor, 2007). *Cingulochitina convexa* has been recorded on Gotland only from the Ludlow (Hemse and Eke beds); however, in the Ventspils and Pavilosta sections of Latvia this species appears in the late Wenlock (Siesartis Formation; Nestor, 2007).

Remarks: In the Ghadamis Basin, *C. convexa* occurs in the lower Akakus unit, which could be Homerian (late Wenlock, middle Silurian) or Gorstian (early Ludlow, late Silurian).

12. *Eisenackitina cylindrica* (*Eisenackitina clunensis*, Miller, 1997)

Description: *E. cylindrica* has a cylindrical and conical vesicle with convex flanks. The aboral margin is distinct. The broadly rounded shoulder is positioned at mid-point. Granules may show a slight increase in size and concentration on the aboral margin where they can reach 2 mm in diameter and take on a more spinose character (Miller, 1997)

Size: Vesicle length 130.4-133.8 µm.

Total appendices: No appendices in this taxon.

Stratigraphic range: Sheinwoodian – Pridoli (middle – late Silurian; Miller, 1997; This was found in Tan III in this study).

Remarks: This species is similar to *E. barrandei* (Paris, 1984) from Bohemia. Both of these chitinozoans demonstrate similar vesicular dimensions and aexure and shoulder (Miller, 1997). In the Ghadamis Basin, *A. radiata* occurs in Tan III, which could be Sheinwoodian (early Wenlock, middle Silurian) in age.

13. *Eisenackitina* sp. (like *Eisenackitina kerria*, Miller, 1997)

Description: This species has vesicle that is cylindrical or conical in shape. describe vesicle. It has a distinct aboral margin. The mid-point of the shoulder is broad and rounded. Ornamentation consists of spines that can be 5 mm long, and that frequently

shrink in size and density approaching the aperture. Specimens that have been poorly preserved may appear to have a granular rather than spinose decoration. There were no twins or chains of individuals found. The base is spine-free, but greater magnification may reveal a subtle rugose structure. The base is frequently slightly convex.

Size: Vesicle length 126 - 138.7 µm.

Total appendices: No appendices in this taxon.

Stratigraphic range: lower Akakus unit, Homerian – Gorstian (middle – late Silurian; this study).

Remarks: *Eisnackitina sp.* from the lower Akakus unit ressembles *E. kerria* Miller, 1997. Both Miller's (1997) *E. kerria* and E. sp. from the lower Akakus unit are similar to *E. bohemica* Eisenack, 1934 from the Lochkovian of Armorica as figured by Paris (1981), but lack the oviform vesicle of *E. bohemica*.

14. *Euconochitina moussegoudaensis* Paris, 2013

Description: *E. moussegoudaensis* has an elongate conical vesicle with a glabrous wall surface, a straight aperture, and a rounded edge, as well as minor constriction of the flanks in the lower third of the chamber (Paris, 2013). It was identified from the middle Akakus unit.

Size: Vesicle length 152.5-181.5 µm.

Total appendices: No appendices in this taxon.

Stratigraphic range: Rhuddanian – Homerian wenlock (early – middle Silurian) Late Ordovician-earliest Silurian palynomorph. *Euconochitina moussegoudaensis* dominates the rather poor chitinozoan assemblage recovered from a siltstone dominated sequence.

These strata are regarded as latest Hirnantian or earliest Rhuddanian in age (Paris, 2013).

Remarks: The original range of this species was Rhuddanian – Telychian (early Silurian). The occurrence of this form in the lower Akakus unit suggests that its range extends into the Homerian. Because of its glabrous vesicle, *Euconochitina moussegoudaensis* like most of the *Euconochitina* species, lacks clear and fully discriminating features (Paris et al., 2013), however our specimens appear to be *E. moussegoudaensis*.

15. *Fungochitina spinifera* Eisenack, 1962

Description: *F. spinifera* characterized by a very small spine. It doee not have any appendices. It has several folds on the vesicle and the neck. It has a maximum vesicle length of 174 μm and maximum chamber length of 70 μm (Verniers, 2006).

Size: Vesicle length 188.8-205.8 μm.

Total appendices: No appendices in this taxon.

Stratigraphic range: Ashgill – Sheinwoodian (late Ordovician – middle Silurian; Zalasiewicz et al. 1995; Van Nieuwenhove et al., 2006)

Remarks: *F. spinifera* Biozone chitinozoan assemblages, found in sections in northern England, are assigned between the late Onnian and early Cautleyan (Late Ordovician to Early Silurian). This is according to data from the Onnian and Pusgillian of Pus Gill (Cross Fell Inlier), the Pusgillian to lowermost Cautleyan of the Type Ashgill area (north

of Sedbergh: Zalasiewicz, Rushton & Owen, 1995) and the Greenscoe road cutting in the Lake District (Van Nieuwenhove, Vandenbroucke & Verniers, 2006).

16. *Pseudoclathrochitina* sp. Cramer, 1964

Description: In terms of size, form, and the growth of its outer layer, the species is quite variable. The shape of the vesicle is mostly influenced by the collarette, which is typically short with a narrow base and distinctly flaring oral ward. Minorities have a broad cylindrical collarette of varying lengths, occasionally rather long. The conical chamber is shaped like a cylinder (Priewalder, 1997).

Size: Vesicle length 154.4-161.3 µm.

Total appendices: No appendices in this taxon.

Stratigraphic range: lower part of the upper Akakus unit, Ludlovian in this study.

Remarks: Cramer 1964 described a "perforated cingulum" as the periderres aboral expansion over the vesicles basal border. Investigations using a light microscope showed that this occurrence is related to a condition known as optical illusion, induced by the flattening of the vesicles (Vernier et al., 1995).

17. *Sphaerochitina concava* Laufeld, 1974

Description: The neck is narrowest at the flexure and widens as it approaches the fringed aperture. The base is consistantly concave, not due to diagenesis. The ornamentation is closely spaced throughout the vesicle, and descreses in size as it approaches the aperture and aboral pole (Laufeld, 1974).

Size: Vesicle length 191.7-203.8 µm.

Total appendices: No appendices in this taxon.

Stratigraphic range: Wenlockian – Ludlow (middle to late Silurian; Laufeld, 1974).
Remarks: The vesicle wall is composed of two layers and the inner layer has a lamellar structure. *S. concava* is distinguished from other *Sphaerochitina* species by its concave base and by its characteristic, very dense ornamentation.

18. *Sphaerochitina sphaerocephala* Eisenack, 1932

Description: This species has vesicle that is spherical in shape. describe vesicle. It has a distinct aboral margin. Light brownish grey, coarse-grained crinoid limestone rich in stromatoporoids, about 5.5 m a.s.l. Chitinozoa (Laufeld, 1974).

Size: Vesicle length 155.9-169.8 µm.

Total appendices: No appendices in this taxon.

Stratigraphic range: Llandovarian – Famennian (early Silurian – late Devonian: Taugourdeau, 1962).
Remarks: *S. sphaerocephala* is distinguished from similar *S. impia* species by its large size and *S. impia* had verrucae and granulate ornamentation (Laufeld, 1974). It was identified in the upper Akakus unit in this study.

4.9. Conclusion.

Based on chitinozoans, acritarchs and spores, we provisionally place Tan III in the Wenlock (middle Silurian). The occurrence of *E. protophanus* in sample C1-S25 supports a Homerian (late Wenlock) age for the top of the Tan III unit (Richardson and Ioannides, 1973; Burgess and Richardson 1991). This age assignment for the Tan III requires an earlier range extension for *Anthochitina radiata* from the Ludlow to the Sheinwoodian (early Wenlock, mid-Silurian), and for *Eisenackitina cylindrica* from the Homerian (late Wenlock, mid-Silurian) to

the Sheinwoodian (early Wenlock, mid-Silurian). It also requires a later range extension for *Ancyrochitina camilleae* from the Telychian (late Llandovery, early Silurian) to the Sheinwoodian (early Wenlock, mid-Silurian). However, this is the second recorded occurrence of *A. camilleae*, thus the range extension of this taxon may not be surprising. Bassett et al. (1989) reported *A. laevaensi*s, which co-occurs with these two species in the Qusaiba Member, in the middle Silurian of Saudi Arabia (Paris et al., 2015).

We provisionally assign the lower Akakus Formation to the late Wenlock or later. Once again, this age assignment requires a later range extension for the following Telychian (late Llandovery, early Silurian) chitinozoans to the Wenlock (middle Silurian) or later: *Euconochitina moussegoudaensis* and *Ancyrochitina ramosaspina*. We provisionally assign the Upper Akakus Formation to the Ludlow (late Silurian).

Based on established depth gradients for chitinozoan species and genera, Tan III sediments likely accumulated in an open marine shelf environment of intermediate depth. The presence of pyrite framboids and pyrite inside chitinozoan appendices from samples C1-S3 and C1-S5 of Tan III suggests anoxic intervals during the accumulation of this unit.

Sandstone layers in the lower Akakus unit contain tidal sedimentary features (Lüning 2000) suggesting deposition in shallow water. Nonetheless, chitinozoans from interbedded shales in this unit suggest deposition in an open marine setting, in relatively deep, quiet water. The presence of these 'intermediate' shelf taxa in shale samples from the lower Akakus unit may indicate that some chitinozoans, reconstructed by Al-Almeri (1983) as open shelf, relatively deep-water taxa, lived in shallow quiet-water habitats.

The middle Akakus unit has been reconstructed both as transgressive (Gindre et al., 2012) and as progradational (Hallet and Clark-Lowes, 2016). The palynoflora of the middle

Akakus suggests a transgressive sequence, with a high average phytoclast (terrestrial palynodebris) percentage and a low average marine percentage. Likewise, the upper Akakus has been reconstructed both as transgressive (Gindre et al., 2012) and prograding (Hallet and Clark-Lowes 2016). Palynofloral analysis suggests a marine, open-shelf environment for the base of the upper Akakus, which has the highest average marine percentage, and the lowest average phytoclast percentage of Tan III and the units of the Akakus Formation.

Keywords — Silurian; Palynomorphs; Chitinozoans; Ghadamis Basin; Tanezzuft; Akakus formations.

4.10. References

Achab, A., 1978, Sur Quelques Chitinozoaires de la formation de Vauréal et de la formation de macasty (Ordovicien Supérieur), Ile d'anticosti, Québec, Canada: Review of Palaeobotany and Palynology, v. 25, no. 3-4, p. 295–314, doi:10.1016/0034-6667(78)90032-5.

Al-Ameri, T. K., 1983, Acid-resistant microfossils used in the determination of Palaeozoic Paaeoenvironments in Libya: Palaeogeography, Palaeoclimatology, Palaeoecology, v. 44, no. 1-2, p. 103–116, doi:10.1016/0031-0182(83)90007-x.

Amosu, A., and Y. Sun, 2018a, Mininversion: A program for petrophysical composition analysis of geophysical well log data: Geosciences, v. 8, no. 2, p. 65, doi:10.3390/geosciences8020065.

Amosu, A., and H. Mahmood, 2018, Pylogfinder: A python program for graphical geophysical log selection: Research Ideas and Outcomes, v. 4, doi:10.3897/rio.4. e23676.

Arduini, M., M. Barassi, A. Golfetto, A. Ortenzi, E. Serafini, E. Tebaldi, E. Trincianti, C. Visentin, 2003, Silurian–Devonian sedimentary geology of the Libyan Ghadamis Basin: example of an Integrated Approach to the Acacus Formation Study. In: Salem, M.J., Oun, K.M. (Eds.), Symposium on the Sedimentary Basins of Libya II.

Askew, A. J., and E. Russell, 2019, A new Middle Devonian chitinozoan assemblage from Northern Iberia: Review of Palaeobotany and Palynology, v. 268, p. 72–87, doi: 10.1016/j.revpalbo.2019.06.007.

Beicip, 1973, Evaluation and geology study of the western part of Libya (Ghadames Basin): Final Report for NOC, 197p.

Burden, E. T. 2002, Palynology, and micropaleontology of the clam Bank Formation (Lower Devonian) of Western newfoundland, canada. *Palynology*, *26*(1), 185–215. https://doi.org/10.2113/0260185.

Butcher, A., 2009, Early Llandovery chitinozoans from jordan: Palaeontology, v. 52, no. 3, p. 593–629, doi:10.1111/j.1475-4983.2009.00862. x.

Butcher, A., 2013, Chitinozoans from the Middle Rhuddanian (Lower Llandovery, Silurian) 'hot' shale in the E1-NC174 Core, Murzuq basin, SW Libya: Review of Palaeobotany and Palynology, v. 198, p. 62–91, doi: 10.1016/j.revpalbo.2012.11.009.

Césari, S. N., S. Marenssi, C. O. Limarino, P. L. Ciccioli, F. C. Bello, L. C. Ferreira, and L. R. Scarlatta, 2020, The first Upper Silurian Land-Derived Palynological Assemblage from South America: Depositional Environment and Stratigraphic Significance: Palaeogeography, Palaeoclimatology, Palaeoecology, v. 559, p. 109970, doi: 10.1016/j.palaeo.2020.109970.

Cocks, L. R., and T. H. Torsvik, 2020, Ordovician palaeogeography and climate change. Gondwana Research: p. 20, https://doi.org/ 10.1016/j.gr.2020.09.008.

Cole, G. A., 1994, Graptolite-Chitinozoan reflectance and its relationship to Other Geochemical maturity indicators in the Silurian Qusaiba Shale, Saudi Arabia: Energy & Fuels, v. 8, no. 6, p. 1443–1459, doi:10.1021/ef00048a035.

Combaz, A. and G. Peniguel, 1972, Étude palynostratigraphique de l'Ordovicien dans quelques sondages de Bassin de Canning (Australie Occidentale). Bull. Centre Rech. Pau - SNPA, 6 : 121- 167.

Cramer, BD, CE. Brett, MA. Melchin, P. Mannik, MA. Kleffer, PI. McLaughlin, DK. Loydell, A. Munnecke, L. Jeppsson, C. Corradini, and FR. Bruton, 2011, Revised chronostratigraphic correlation of the Silurian System of North America with global and regional chronostratigraphic units and $\delta^{13}C_{carb}$ chemostratigraphy. Lethaia 44:185–202.

Daniels, HJ, B. Thusu, and S. Abushaala, 1990, Sedimentological and palynological facies analysis of Acacus and Tanezzuft formations in Concession NC7A, northwest Libya: AGOCO internal report.

Dardour, A. M., D. R. D. Boote, and A. W. Baird, 2004, Stratigraphic controls on Palaeozoic petroleum systems, Ghadames Basin, Libya: Journal of Petroleum Geology 27 (2): 141-162.

Doher, LI., 1980, Palynomorph preparation procedures currently used in the paleontology and stratigraphy laboratories: Washington (DC): U.S. Geological Survey. USGS Circular 830.

Domeier, M. 2016, A plate tectonic scenario for the Iapetus and Rheic oceans. Gondwana Research: 36:275-295.

Dorning, J. K., 1981b, Silurian acritarchs distribution in the Ludlovian shelf sea of South Wales and the Welsh Borderland. in: Microfossils from Recent and Fossils Shelf Seas (eds J.W. N. Neale and M.D. Brasier). Ellis Horwood, Chichester, 31-36.

Downie, C., 1963, Hystrichosheres', (acritarchs), and spores of the Wenlock Shales, (Silurian), of Wenlock, England. Palaeontology v. 6, no. 4, p. 625- 652.

Echikh, K., 1998, Geology and hydrocarbon occurrences in the Ghadames Basin, Algeria, Tunisia, Libya. In: MacGregor DS, Moody RTJ, Clark-Lowes DD, editors. Petroleum Geology of North Africa. Geological Society London, Special Publication 132:109-129.

Eisenack, A., 1931, Neue Mikrofossilien des baltischen Silurs I: Paläontologische Zeitschrift 13:74–118.

Eisenack, A., 1932, Neue Mikrofossilien des baltischen Silurs. II. Palaeontol. Z. 14, 257–277.

Eisenack, A., 1955a, Chitinozoan, Hystrichospharen und andere Mikrofossilien aus dem Beyrichia-Kalke: Senckenbergiana Lethaea 36:157–188.

Eisenack, A., 1964, Mikrofossilien aus dem Silur Gotlands phosphatische reste: Paläontologische Zeitschrift, v. 38, no. 3-4, p. 170–179, doi:10.1007/bf02988846.

Eisenack, A., 1955b, Neue Chitinozoen aus dem Silur des Baltikums und dem Devon der Eifel: Seckenbergiana Lethaea 36:311–319.

El-Arnauti, A. Owens B., Thusu B., 1988, Subsurface Palynostratigraphy of Northeast Libya: A research project: Benghazi: Garyounis University Publications.

Elfigih, OB., 2000, Regional diagenesis and its relation to facies change in the Upper Silurian, Lower Acacus Formation, Hamada (Ghadames) Basin, northwestern Libya [dissertation]: St. John's (NL, Canada): Memorial University of Newfoundland.

Elfigih, OB., 2017, Determination of reservoir play fairway of the Lower Acacus Formation in the Ghadames Basin, NW Libya: International Journal of Petroleum and Petrochemical Engineering 3(1):60-69.

El-Kelani, MMA., GJ. Reichart, SJ. Sinninghe Damsté, B. Van De Schootbrugge, and Z. Smeenk, 2014, Stable carbon isotope and palynological records from the Silurian "hot" shale in Libya: In: Silurian and Devonian rocks and crude oils from the western part of Libya. Organic geochemistry, palynology, and carbon isotope stratigraphy. Utrecht; p. 21–69. (Utrecht Studies in Earth Sciences 71, LPP Contributions Series No. 42).

El-Mehdawi, A. D., 2004, Palynological analysis of the lower Acacus Member in wells Al-NC1 and Al-NC3A, Ghadāmis Basin, NW Libya: Second symposium on the sedimentary basin of Libya, the geology of northwest Libya, Vol. 1. (M. J. Salem and A. M. Oun), Earth Science Society of Libya Tripoli.

Finnegan, S., K. Bergmann, J. M. Eiler, D. S. Jones, D. A. Fike, I. Eisenman, N. C. Hughes, A. K. Tripati, and W. W. Fischer, 2011, The magnitude and duration of Late Ordovician-Early Silurian Glaciation: Science, v. 331, no. 6019, p. 903–906, doi:10.1126/science.1200803.

Fischer, WW., 2011, The magnitude and duration of Late Ordovician-Early Silurian glaciation: Science 331:903-906.

Ghavidel-Syooki, M., 2001, Biostratigraphy and palaeogeography of Late Ordovician and Early Silurian chitinozoans from the Zagros Basin, Southern Iran. Historical Biology. 15:29–39.

Ghavidel-Syooki, M., J. Hassanzadeh, and M. Vecoli, 2011, Palynology and isotope geochronology of the Upper Ordovician–Silurian successions (Ghelli and Soltan Maidan formations) in the khoshyeilagh area, eastern alborz range, northern Iran; stratigraphic and paleogeographic implications: Review of Palaeobotany and Palynology, v. 164, no. 3-4, p. 251–271, doi: 10.1016/j.revpalbo.2011.01.006.

Gradstein, FM, JG. Ogg, MD. Schmitz, and GM. Ogg, 2020, Geologic Time Scale 2020: Elsevier.

Grahn, Y., 1995, Lower Silurian Chitinozoa and biostratigraphy of subsurface Gotland: GFF. 117:57–65.

Hallett, D., 2016, Petroleum Geology of Libya. Kidlington (UK): Elsevier.

Haq, BU, Boersma A, 1998, Introduction to Marine Micropaleontology. Singapore: Elsevier.

Hodairi, TA, 2012, Organic geochemical characterization of the Silurian Tanezzuft Formation and crude oils from the Murzuq Basin, S.W. Libya [dissertation]. Norman (OK): University of Oklahoma.

Imsalem, M, T. Olszewski, A. Raymond, 2018a, Pollen and Multivariate Analysis from Ecological and latitudinal gradients in Morocco. Poster presented at: 52nd Annual Meeting of the Geological Society of America; March 12-13; Little Rock Marriott, Arkansas, AR.

Imsalem, M, M. K. Zobaa, A. Raymond, 2018b, Palynomorph identification and Preliminary Palynostratigraphy of the Silurian Tanezzuft and Akakus Formations in the Libyan Ghadames Basin: Poster presented at: 130th Annual Meeting of the Geological Society of America; 2018; 4-7 November; Indianapolis, IN.

Imsalem, M, A. Amosu, M. Wehner, A. Raymond, and Y. Sun, 2018c, Reservoir Quality Assessment of the Lower Acacus and Tannezuft Formations in the NC4 Block, Ghadames Basin, Libya: Gulf Coast Association of Geologic Societies Transactions 68:255-268.

Jansonius, J, WAM. Jenkins, 1978, Chitinozoa. In: Haq BU, Boersma A, editors. Introduction to marine micropalaeontology: Elsevier, New York, pp. 341–357.

Klitzsch, E., 1970, Die Strukturgeschichte DER ZENTRALSAHARA: Geologische Rundschau, v. 59, no. 2, p. 459–527, doi:10.1007/bf01823806.

Laufeld, S., 1977, Paleoecology of Silurian chitinozoans. Abstracts of Coloquio International de Palinologia; Leon, Spain. p. 23-24.

Laufeld, S., 1974, Silurian Chitinozoa from Gotland. Fossils Strata, 5, 130 pp.

Le Héron, DP, HA. Armstrong, C. Wilson, JP. Wilson, L. Gindre, 2010, Glaciation and deglaciation of the Libyan Desert: The Late Ordovician record. Sedimentary Geology 223:100-125.

Le Héron, DP, G. Meinhold, A. Page, A. Whitham, 2013, Did lingering ice sheets moderate anoxia in the Early Palaeozoic of Libya?: Journal of the Geological Society 170(2):327-339.

Le Héron, DP, S. Tofaif, J. Melvin, 2018, The Early Palaeozoic Glacial Deposits of Gondwana. In: Menzies J, van der Meer JJM, editors. Past Glacial Environments. Elsevier. Chapter 3; p. 47-73.

Lianda, G., 1981, Devonian spore assemblages of China. Review of Palaeobotany and Palynology, 34 (1), 11–23. https://doi.org/10.1016/0034-6667(81)90063-4.

Loboziak, S., and M. Streel, 1989, Middle-Upper Devonian Miospores from the Ghadamis Basin (Tunisia-Libya): Systematics and stratigraphy. Review of Palaeobotany and Palynology 58 (2-4): 173–196.

Loydell, DK, A. Butcher, J. Frýda, S. Lüning, and M. Fowler, 2009, Lower Silurian "hot shales" in Jordan: a new depositional model. Journal of Petroleum Geology 32(3):261–270.

Lüning, S, Craig J, Loydell DK, Storch P, Fitches B. 2000. Lower Silurian 'hot shales' in North Africa and Arabia: regional distribution and depositional model. Earth-Science Reviews 49:121-200.

Lüning, S., and N.M. Fello, 2006, Silurian 'hot shales' in the Murzuq and Al Kufrah bains (S. Libya): improved predictability of source rock distribution based on gamma ray spectrometry in surface exposures. In: Salem MJ, Oun KM, Essed AS, editors. Third Symposium on the Sedimentary Basins of Libya, Geology of East Libya; vol. 4. Tripoli (Libya): Earth Science Society of Libya. p. 3–12.

Lyle, P., 2019, Introducing Stratigraphy. Edinburgh and London (UK): Dunedin Academic Press.

Mabillard, J. E., and R. J. Aldridge, 1985, Microfossil distribution across the Base of the Wenlockian series in the type area. Palaeontology v. 28, no. 1, p. 89- 100.

McDougall, ND. I. Polonio, H. Abdallah, and K. Tawengi, 2006, Late Ordovician palaeovalleys in the Sahara: a new perspective. Proceedings of the 10th Tunisian Petroleum Exploration and Production Conference; Tunis, ETAP Memoir 26, p. 217-231.

Meinhold, G., DP. Le Héron, M. Elgadry, and Y. Abutarruma, 2016, The search for 'hot shales' in the western Kufra Basin, Libya: geochemical and mineralogical characterization of outcrops, and insights into latest Ordovician climate. Arabian Journal of Geosciences 9:62.

Massa, D., H. Jaeger, 1971, Données stratigraphiques sur le Silurien de l'Ouest de la Libye. In. Colloque Ordovicien-Silurien, Brest. Mémoires du Bureau des Recherches Géologiques et minéralogiques 73 :313-321.

Moreau, J., 2011, The late Ordovician deglaciation sequence of the SW Murzuq Basin (Libya). Basin Research 23(4):449-477.

Nestor, V., 2012, A summary and revision of the East Baltic Silurian chitinozoan biozonation. Estonian Journal of Earth Sciences 61:242–260.

Nestor, V., 1980, New chitinozoan species from the Lower Llandoverian of Estonia. Eesti NSV Tead. Akad. Toim. Koide Geol., 29(3): 98 107.

Nestor, V., 2007, Chitinozoans in the Wenlock-Ludlow boundary beds of the East Baltic. Estonian Journal of Earth Sciences, 56 (2), 109−128.

Nestor, V., 1990, Silurian chitinozoans. In: Kaljo D, Nestor H, editors. Field meeting Estonia 1990, An Excursion Guidebook. Tallinn (Estonia): Estonian Academy of Science; p. 80-83.

Obermajer, M., MG. Fowler, F. Goodarzi, LR. Snowdon, 1996, Assessing thermal maturity of Paleozoic rocks from reflectance of chitinozoa as constrained by geochemical indicators: an example from southern Ontario, Canada. Mar. Petrol. Geol 13:907-919.

Paris, F., C. Girard, R. Feist, and T. Winchester-Seeto, 1996, Chitinozoan bio-event in the frasnian-famennian boundary beds at La Serre (Montagne Noire, southern France): Palaeogeography, Palaeoclimatology, Palaeoecology, v. 121, no. 3-4, p. 131–145, doi:10.1016/0031-0182(95)00083-6.

Paris F, B. Thusu, S. Rasul, G. Meinhold, D. Strogen, JP. Howard, Y. Abutarruma, M. Elgadry, and AG. Whitham, 2012, Palynological and palynofacies analysis of early Silurian shales from borehole CDEG-2a in Dor el Gussa, eastern Murzuq Basin, Libya. Review of Palaeobotany and Palynology 174:1–26.

Paris, F., J. Verniers, M. Miller., J. Melvin, and CH. Wellman, 2015, Late Ordovician–earliest Silurian chitinozoans from the Qusaiba-1 core hole (North Central Saudi Arabia) and their relation to the Hirnantian glaciation. Review of Palaeobotany and Palynology 212:60-84.

Pope, MC., and JB. Steffen, 2003, Widespread, prolonged late Middle to Late Ordovician upwelling in North America: a proxy record of glaciation. Geology 31(1):63-66.

Richardson, J. B., and N. Ioannides, 1973, Silurian Palynomorphs from The Tanezzuft and Acacus FORMATIONS, Tripolitania, North Africa: Micropaleontology, v. 19, no. 3, p. 257, doi:10.2307/1484881.

Richardson, J. B., and T. R. Lister, 1969, Upper Silurian and Lower Devonian spore assemblages from the Welsh Borderland and South Wales. Palaeontology, vol. 12, pt. 2, pp. 201-252, pls. 37-43, text- figs. 1-4, tables 1-7.

Rombouts, L. P., 1982, Factors controlling the distribution of chitinozoa in the Gleedon Chronozone, (Wenlockian) of northern Europe.

Sahney, S., MJ. Benton, L. Falcon, and J. Howard, 2010, Rainforest collapse triggered Pennsylvanian tetrapod diversification in Euramerica: Geology 38(12):1079–1082.

Scotese, CR., 2014, Atlas of Silurian and Middle-Late Ordovician Paleogeographic Maps (Mollweide Projection), Maps 73-80. Evanston (IL). (The Early Paleozoic, vo. 5). *Paleomap Project.* doi:10.13140/2.1.1087.2324.

Servais, T., A. Achab, and E. Asselin, 2013, Eighty years of chitinozoan research: from Alfred Eisenack to Florentin Paris. Review of Palaeobotany and Palynology 197:205–217.

Staplin, FL., SJ. Pocock, J. Jansonius, and EM. Oliphant, 1960, Palynological techniques for sediments. Micropaleontology 6(3) :329-331.

Stampfli, GM., C. Hochard, C. Vérard, C. Wilhem, and J. von Raumer, 2013, The formation of Pangea: Tectonophysics 593:1–19.

Steemans, P., A. le Hérissé, and N. Bozdogan, 1996, Ordovician and silurian cryptospores and MIOSPORES from southeastern Turkey: Review of Palaeobotany and Palynology, v. 93, no. 1-4, p. 35–76, doi:10.1016/0034-6667(95)00119-0.

Steemans, P., 2000, Annotations to the Devonian Correlation Table, b501di00: Miospore Palynology, Western Europe: Senckenbergiana lethaea, v. 80, no. 2, p. 759–760, doi:10.1007/bf03043378.

Steemans, P., T. Servais, and M. Streel, 2002, Dr. Stanislas Loboziak Retired: Review of Palaeobotany and Palynology, v. 118, no. 1-4, p. vii-viii, doi:10.1016/s0034-6667(01)00104-x.

Stump, T. E., S. Al-Hajri, and J. G. L. A. Van der Eem, 1995, Geology and Biostratigraphy of the Late Precambrian through Palaeozoic sediments of Saudi Arabia. Review of Palaeobotany and Palynology, *89*(1-2), 5–17. https://doi.org/10.1016/0034-6667(95)00038-y.

Taktek, EABM., and NMO. Shebli, 2019, Pore-lining and grain-coating chlorites in siliciclastic reservoir sandstones (Acacus Formation, Ghadamis Basin, Libya), nature and implications for their origin: Journal of Research in Environmental and Earth Sciences 7:186-197.

Tekbali, A. O., and G. D. Wood, 1991, Silurian spores, acritarchs and chitinozoans from the Bani Walid Borehole of the Ghadamis Basin, Northwest Libya. (In: The Geology of Libya. M.J. Salem et al, editors) The Geology of Libya. Third Symposium on the Geology of Libya. (M.J. Salem, O.S. Hammuda and B.A. Eliagoubi, editors). Amsterdam; New York: Elsevier Vol. 4 P. 1243- 1273.

Thusu, B., 1973, Acritarchs from the Ilion Shale (Wenlockian), Utica, New York [Acritarches provenant de l'Ilion Shale (Wenlockien), Utica, New York.] Revue de Micropaleontologie Vol. 16 # 2 P. 137- 146

Torsvik, TH., and Cocks LR, 2013, Gondwana from top to base in space and time. Gondwana Research 24(3-4):999–1030.

Taugourdeau P., and de Jekhowsky B, 1960, Répartition et description des Chitinozoaires siluro-dévoniens de quelques sondages de la C.R.E.P.S., de la C.F.P.A. et de la S.N. Repal au Sahara: Revue de l'Institut Français du Pétrole, 15: 1199– 1260.

Taugourdeau, P., 1962, Associations de Chitinozoaires dans quelques sondages de la region d'Édjelé (Sahara). Rev. Micropaléontol. 4, 229–236.

Van Grootel G., Zalasiewicz J., Verniers J., Servais and T., 1998, Chitinozoa and graptolite biozonation of the Aeronian and lower Telychian in the Brabant Massif (Belgium): 6th International Graptolite Conference (GWG-IPA) & 1998 Field Meeting, IUGS.

Verniers, J, V. Nestor, F. Paris, P. Dufka, SJE, Sutherland, G. Van Grootel, 1995, A global chitinozoa biozonation for the Silurian: Geological Magazine 132:651–666.

Verniers, J., 1999, Calibration of Wenlock Chitinozoa versus graptolite biozonation in the Wenlock of Builth Wells district (Wales, UK), compared with other areas in Avalonia and Baltica. Boll. della Soc. Paleontol. Ital. 38, 359–380.

Vodička, J., and Š. Manda, 2019, A taxonomical and statistical study of chitinozoan distribution across the Lundgreni Event (Wenlock, Silurian) from the Prague Basin, Czech Republic: a specific pattern driven by ecological changes. Marine Micropaleontology 149:44-63.

Wrona, R.M., 1980, Upper Silurian-Lower Devonian chitinozoa from the subsurface of Southeastern Poland. Górno Sylurskie i Dolodewonskie Chitinozoa z Wier Cen Południowo Wschodniej Polski, Palaeontologia Polonica no. 41, p. 103 - 165.

Underdown, R., Redfern, J. and F. Lisker 2007, Constraining the burial history of the Ghadames Basin, North Africa: an integrated analysis using sonic velocities, vitrinite reflectance data and apatite fission track ages: Basin Research, v. 19, n. 4, p. 557-578.

5. CONCLUSIONS

The Ghadamis Basin located in North West Libya contains important oil and gas producing reservoirs. It is a polycyclic intracratonic basin composed of many superimposed basins laid on top of one another, influenced by multiple tectonic events, which result in the development of regional unconformities and fault structures (Hallett 2016). Upper Ordovician sandstone belonging to the Mamuniyat Formation lies at the base of the Silurian section in the Ghadamis Basin. The Tanezzuft Formation, an Early Silurian marine transgressive shale produced by eustatic sea-level rise, overlies the Mamuniyat Formation. At the top of the section, the Lower Akakus Formation consists of northward prograding sandstones and shales of middle to upper Silurian age, deposited in shallow marine sediment. In this study, I make use of integrated data from three wells in the NC4 block of the Ghadamis basin, including well log data, core samples, and thin sections. With colleagues, I correlate the well-logs using facies identification as well as palynological markers and examine detailed structural and stratigraphic variation within the block. Multi-mineral composition analysis enables us to estimate the volume of quartz, calcite, anhydrite, kaolinite and other clay minerals. We successfully map out the variation in several components such as kaolinite, illite and lithified sediments within the Akakus and Tanezzuft Formations. We demonstrate that low lithification correlates with small volumes of kaolinite and illite. When coupled with extensive fracturing, this leads to a better reservoir quality. Reservoir facies in these formations are affected by diagenetic iron-oxides (from meteoric water), clay and pore-filling kaolinite/illite cements.

I completed a palynofloral anlaysis of the following Tanezzuft and Akakus formation units: Tan III, lower Akakus, middle Akakus, and upper Akakus. Chitinozoan, acritarch and spore distributions suggest the following ages for each unit: Tan III (Wenlock); lower Akakus

(Wenlock or later); base of the upper Akakus (Ludlow: Chapter 4). Tan III accumulated on Sheinwoodian (early Wenlock, middle Silurian) and continued into the Homerian (late Wenlock, middle Silurian), (Chapter 4).

APPENDIX A

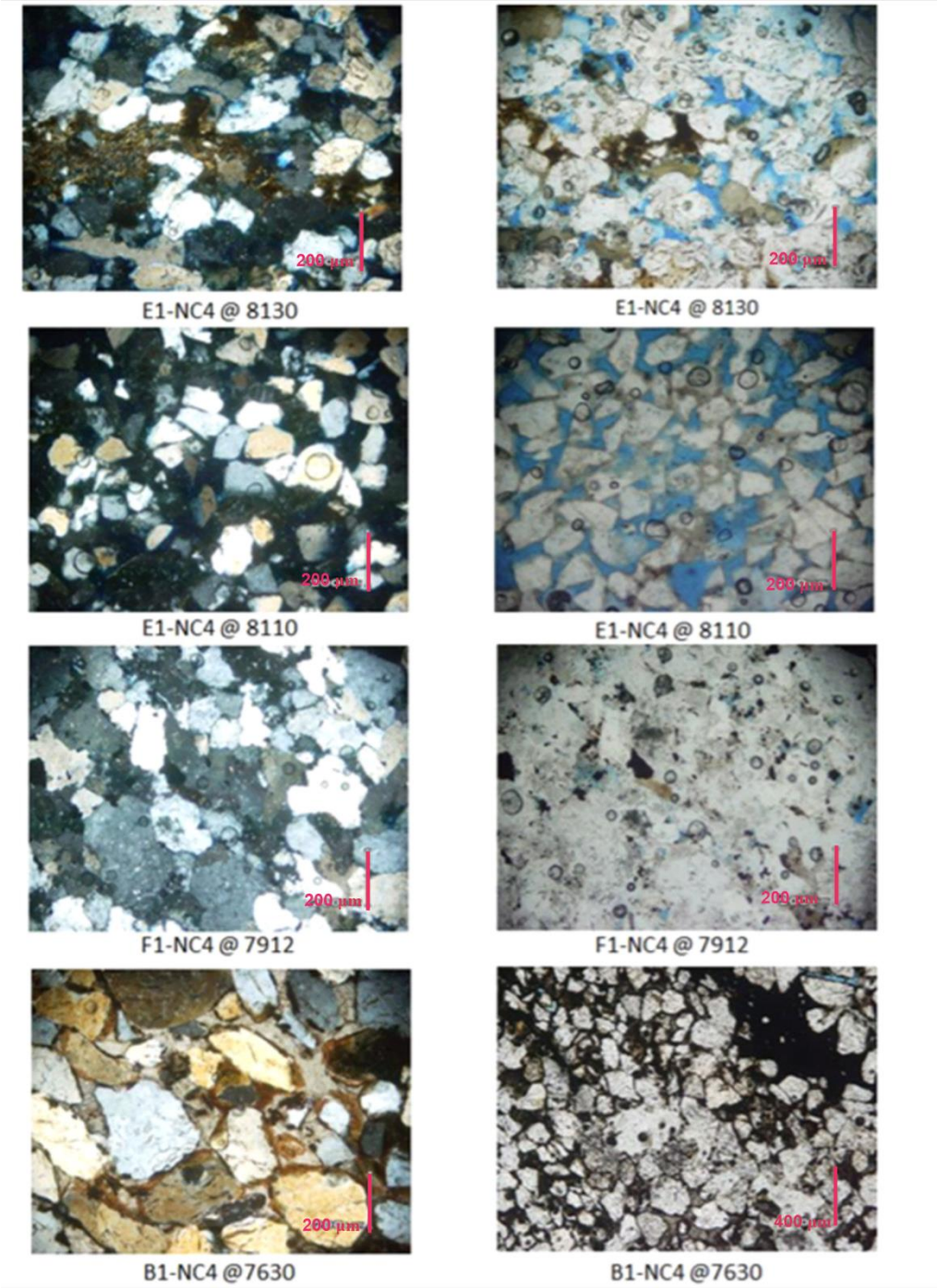

Figure A- 1: Thin section of sandstones in NC4 concession, Ghadamis Basin, Libya.

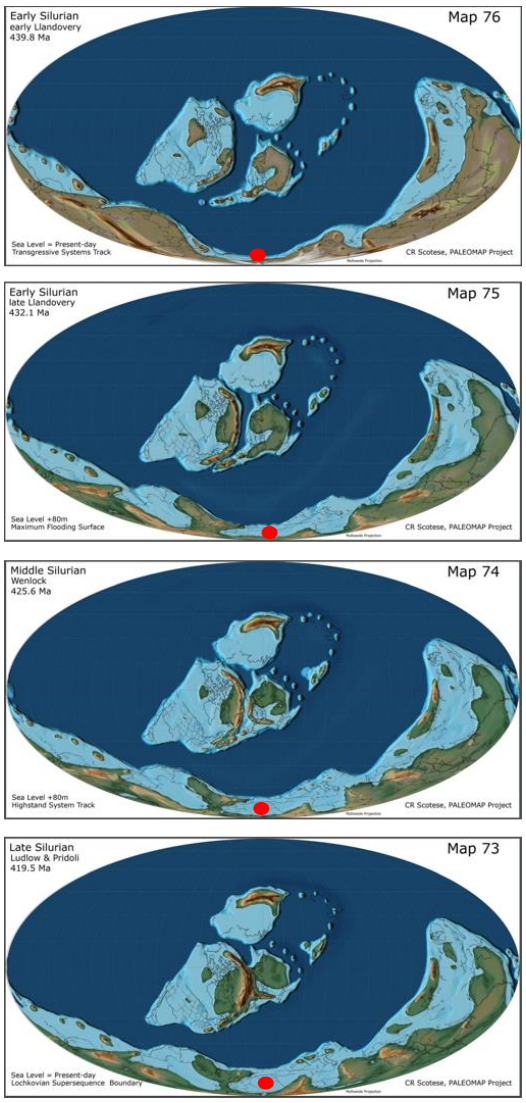

Figure A-2: Llandovery, Wenlock, and Ludlow (Pridoli) of paleogeographic maps and the position of Libya at the silurian period modified from (Scotese. C., 2014).

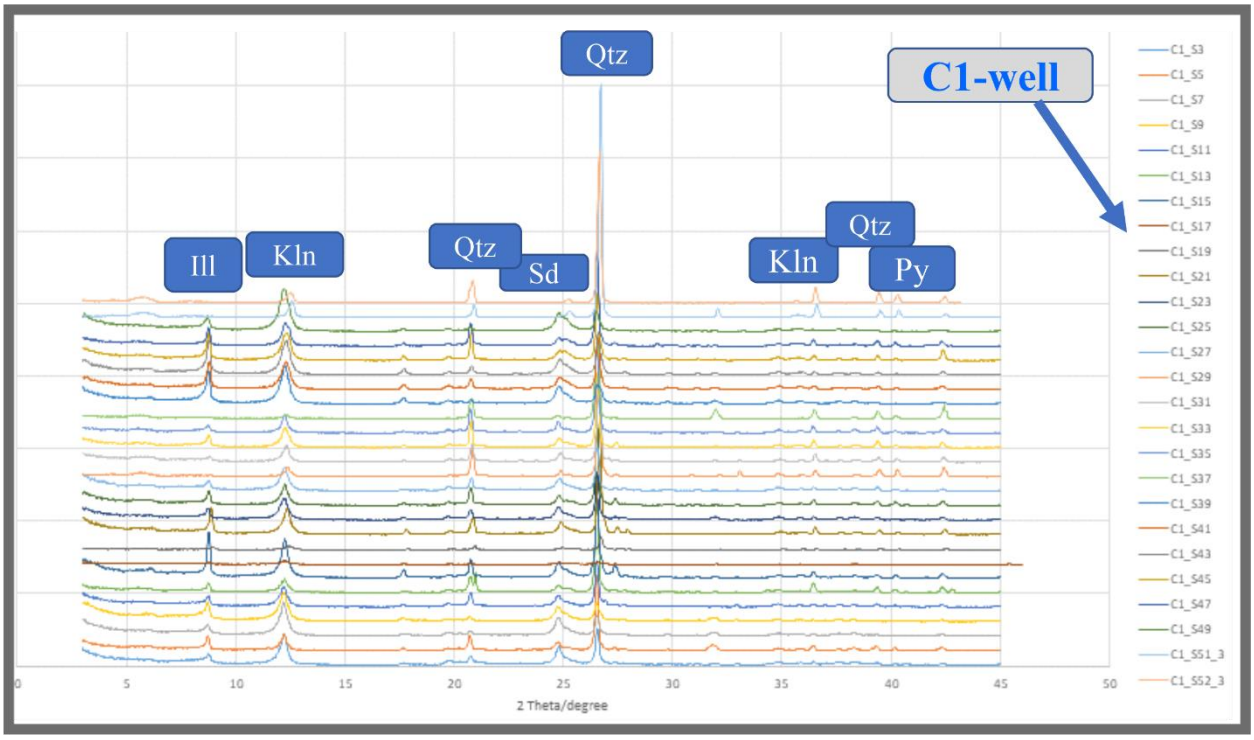

Figure A-3: XRD Stacked layered peaks C1 well in Ghadamis Basin.

Table A-1: Paleolatitudinal position of the Ghadamis Basin in different paleogeographic reconstrcutions.

Source	Late Ordovician (age in Ma - latitude)	Middle Silurian (age in Ma - latitude)
Stampfli et al. 2013	445 - 70° S	425 - 60° S
Domeier 2016	449 - 60° S	429 - 45° S
Torsvik and Cocks 2013	445 - 65° S	mid Silurian - 45° S
Cocks and Torsvik 2021	445 - 75° S	N/A
Scotese 2014	L. Ordo. - 70° S	mid Silurian - 70° S